Effect of hypoxia-inducible factor 1α (HIF-1α) deficiency in tumor cells and murine tumor stroma on radiation sensitivity and growth of tumors

Inaugural-Dissertation zur

Erlangung des Doktorgrades

Dr. rer. nat.

der Fakultät für

Biologie

an der

Universität Duisburg-Essen

vorgelegt von

Alexandra Wolf

aus Osch

Oktober, 2018

Die der vorliegenden Arbeit zugrunde liegenden Experimente wurden am Institut für Physiologie in der Arbeitsgruppe vom Prof. Dr. Metzen, Universitätsklinikum Essen, Universität Duisburg-Essen durchgeführt.

1. Gutachter:	Prof. Dr. Eric Metzen
2. Gutachter:	Prof. Dr. Anke Hinney
3. Gutachter:	Prof. Dr. Bernhard Brüne
Vorsitzender des Prüfungsausschusses:	Prof. Dr. Sven Brandau
Tag der mündlichen Prüfung:	25.01.2019

Für Erika und Valentina

Table of Contents

1 Introduction

1.1 Hypoxia and cancer

Oxygen is involved in a variety of cellular processes in eukaryotes, such as life-sustaining aerobic respiration. In vertebrates oxygen diffuses through membranes in the lungs and is transported by red blood cells, the erythrocytes, to all other organs. Oxygen acts as an electron acceptor during oxidative phosphorylation within the mitochondrial inner membrane, resulting in the synthesis of adenosine 5´-triphosphate (ATP), the coenzyme that provides energy to all active metabolic processes (Semenza et al., 1994). In the human body oxygen transport can be divided into convective and diffusive oxygen transport. Convective transport describes the bulk movement of oxygen within the blood circulation, which requires energy provided by the heartbeat. Diffusive oxygen transport refers to the passive movement down a concentration gradient, e.g. the capillary-intracellular oxygen tension (pO_2) gradient (Dunn et al., 2016; Leach and Treacher, 1992). Failure of either mechanism leads to the reduction in the normal level of oxygen tension in tissue and occurs during acute and chronic vascular disease, pulmonary disease and cancer. This state is called hypoxia (Hx) and results in cell death unless the cells can undergo genetic and adaptive changes which is characteristic for tumor cells (Harris, 2002). In solid tumors hypoxia is a result of imbalanced oxygen supply and consumption (Vaupel et al., 2002). It can be differentiated between acute, chronic and anemic hypoxia. An acute (or perfusion-limited) hypoxia is a result of the insufficient blood flow in tissue caused by structural and functional abnormalities of tumor microvasculature (Brown and Giaccia, 1998). A chronic or diffusion-related hypoxia is induced by growing distance between expanding tumors and blood vessels (> 100-200 µm), which results in inadequate oxygen supply (Harris, 2002; Helmlinger et al., 1997). Another form of hypoxia, anemic hypoxia, is a consequence of reduced oxygen transport capacity of the blood caused by tumor-associated or therapy-induced anemia (Vaupel et al., 2001). Hypoxia induces a variety of adaptive responses in organisms at systemic and cellular levels (Bunn and Poyton, 1996). On the one hand, adaptation includes inducted synthesis of certain proteins that enable cell survival. On the other hand, cells need access to an adequate supply of oxygen for long term survival. One of the most important responses to lowered oxygen tension is hypoxia-induced production of erythropoietin (Epo), a hormone that stimulates the production of erythrocytes and thereby increases the oxygen-carrying capacity of the blood (Blanchard et al., 1993). Furthermore, hypoxia often leads to neovascularization caused by factors such as

vascular endothelial growth factor (VEGF), which acts as a hypoxia-inducible angiogenic factor (Shweiki et al., 1992).

In order to survive, tumor cells use adaptation processes well-established by previous reports. The altered energy metabolism of cancer cells was first reported in 1924 by Otto Warburg, the Nobel laureate honored for discovering cytochrome c oxidase. In the presence of oxygen normal cells primarily convert glucose into pyruvate within the cytosol through the process of glycolysis and then oxidize the pyruvate in the mitochondrial tricarboxylic acid (TCA) cycle. During this reaction the reduced form of nicotinamide adenine dinucleotide (NADH) is produced which is essential for the oxidative phosphorylation with up to 36 ATPs per molecule glucose (Vander Heiden et al., 2009). However, under anaerobic conditions normal cells are limited to using only glycolysis and then converting pyruvate into lactate. This pathway generates only 2 ATPs per molecule glucose. In contrast to normal cells, many types of cancer cells mostly rely on glycolysis producing large amounts of lactate regardless of the availability of oxygen. This 'aerobic glycolysis' of cancer cells has been termed the Warburg effect (Warburg, 1956). Many tumors show an elevated expression of hypoxia-inducible lactate dehydrogenase-A (LDH-A), which is involved in interconversion between pyruvate and lactate (Firth et al., 1995). Compensation of the reduced energy results in increased glucose consumption, which is assumed to be an adaptation to intermittent hypoxia in tumors (Gatenby and Gillies, 2004). It was also shown that the increase of glucose uptake correlates with tumor aggressiveness and poor prognosis (Younes et al., 1996). As a result, increased lactate production leads to acidosis which is a hallmark of hypoxia in tissues (Seagroves et al., 2001). Furthermore, the increased glucose uptake in hypoxia is associated with increased expression of the glucose transporters GLUT-1 and GLUT-3, which are involved in glycolysis (Ebert et al., 1995; O'Rourke et al., 1996). Hypoxia also regulates cancer epigenetics and induces alteration of histone modifications associated with general transcriptional repression (Johnson et al., 2008).

The discovery of hypoxia related molecular mechanisms was honored in 2016 with the Albert Lasker Basic Medical Research Award. The recipients were William Kaelin, Peter Ratcliffe and Gregg Semenza (Hurst, 2016). In 1992 the first description of a key protein associated with hypoxia, the hypoxia-inducible factor 1 (HIF-1), was published (Semenza and Wang, 1992). It was shown that increased activity of HIF-1 is characteristic for the hypoxic microenvironment within solid tumors. Furthermore, HIF-1 acts as a master transcriptional

regulator of the adaptive response to hypoxia and is responsible for induction of glycolysis, erythropoiesis and angiogenesis (Talks et al., 2000; Wang and Semenza, 1993b).

1.2 The HIF-1α pathway

HIF is a dimer composed of two subunits: a 120 kDa oxygen-regulated α-subunit and a 91- to 94 kDa β-subunit named aryl hydrocarbon receptor nuclear translocator (ARNT, also known as HIF-1β). Both are basic-helix-loop-helix (bHLH)-PER-ARNT-SIM (PAS) proteins (Wang et al., 1995; Wang and Semenza, 1995). The bHLH and PAS domains serve as recognition motifs for other bHLH proteins and facilitate interaction with target genes via DNA binding and dimerization (Murre et al., 1994). The PAS domains are located at the carboxy-terminal (C-terminal) end of the bHLH region and can be characterized by a homology region between the protein product of the *D. melanogaster* period clock protein (PER), ARNT and a product of *D. melanogaster* single-minded locus (SIM) (Nambu et al., 1991; Reddy et al., 1986).

ARNT is constitutively expressed and also dimerizes with other HLH proteins, including PAS proteins (Rowlands and Gustafsson, 1997; Swanson and Bradfield, 1993). Three isoforms of the α-subunit were discovered: HIF-1α, HIF-2α and HIF-3α. HIF-1α was shown to be widely expressed in tissues with the highest levels in kidneys and heart, whereas nuclear accumulation of HIF-2α, which was initially called endothelial PAS protein 1 (EPAS1), is not ubiquitous and characteristic for distinct cell types, such present in kidneys, small intestines, endothelium, lungs and heart (Ema et al., 1997; Tian et al., 1997). However, both HIF-1α and HIF-2α are co-expressed in several cell types and regulate sets of target genes that partially overlap (Hu et al., 2003; Wiesener et al., 2003). HIF-3α is expressed in adult thymus, lungs, brain, heart and kidneys. However, little is known about the function of HIF-3α in tissues. The splice variants of HIF-3α mRNA contribute to either activation or inhibition of other HIF complexes. The inhibitory PER-ARNT-SIM domain protein (IPAS) is one of the alternative splicing products of the HIF-3α locus and has been reported to serve as a negative regulator of HIF-α functions (Gu et al., 1998; Makino et al., 2002).

The highly conserved structures of HIF-1α and HIF-2α are very similar (Figure 1 A). The PAS domain of HIF-1α consists of two subdomains named PAS-A and PAS-B that are responsible for target specific protein-protein interaction by dimerization with other PAS-containing proteins (Zelzer et al., 1997). The oxygen-dependent degradation domain (ODD),

which mediates proteosomal degradation, is located in the central region of HIF-1α and consists of approximately 300 amino acid residues (Huang et al., 1998). HIF-1α has two transactivation domains, the N-terminal transactivation domain (NTAD) and the C-terminal transactivation domain (CTAD). The CTAD recruits transcriptional regulatory proteins and its regulation depends on hydroxylation of an asparagine residue by the protein "factor inhibiting HIF-1" (FIH-1) (Lando et al., 2002). The NTAD overlaps with the ODD and its transcriptional activity depends on protein stability (Semenza, 2007b). The inhibitory domain (ID) which is located between NTAD and CTAD can repress the transcriptional activities of both ADs (Jiang et al., 1997).

Under normoxic conditions the HIF-α subunits have a short half-life of 5-8 min (Berra et al., 2001). In the presence of oxygen HIF is post-translationally modified at the proline residues 402 and 564 by specific prolyl hydroxylase domain proteins (PHDs), which belong to the group of dioxygenases and require oxygen, ferrous iron and 2-oxoglutarate to maintain activity (Figure 1 B). The PHD family consists of three members, PHD1, PHD2 and PHD3, whereas mainly the loss of PHD2 leads to increased HIF-1α accumulation (Berra et al., 2003; Epstein et al., 2001; Ivan et al., 2001; Jaakkola et al., 2001; Kaelin and Ratcliffe, 2008; Metzen et al., 2003; Schofield and Ratcliffe, 2004; Semenza, 2007a). The enzymatic hydroxylation of HIF-α promotes the interaction of the ODD with the ß-domain of von Hippel-Lindau protein (pVHL) (Huang et al., 1998; Masson et al., 2001; Maxwell et al., 1999). The product of the VHL gene (pVHL) acts as the recognition subunit of an ubiquitin E3 ligase complex. The pVHL complex includes elongin-C, elongin-B, Cul2 and the RING-H2 finger protein Rbx1. Rbx1 triggers the activation of E1 ubiquitin-activating and E2 ubiquitin-conjugating enzymes, which mediates the ubiquitination of HIF-1α (Cockman et al., 2000; Duan et al., 1995; Kamura et al., 2000; Lonergan et al., 1998; Ohh et al., 2000; Stebbins et al., 1999; Tanimoto et al., 2000). As a result, polyubiquitinated HIF-1α undergoes proteosomal degradation. The protein factor inhibiting HIF-1 (FIH-1) is another α-ketoglutarate-dependent dioxygenase, which hydrolyses HIF-1α at asparagine residue 803, a conserved amino acid within the CTAD of HIF-1α. This modification leads to the inhibition of interaction between HIF-1α and the coactivator protein p300 and cAMP response element-binding (CREB)-binding protein (CBP) (Peet and Linke, 2006)

During hypoxia, stabilized HIF-1α accumulates and is translocated to the cell nucleus, where it dimerizes with HIF-1ß and forms the transcriptionally active complex with CBP/ p300. This complex binds to a hypoxia-responsive element (HRE) (sequence 5´-RCGTG-3´) in the major

groove of the DNA double helix and activates transcription of HIF-1 target genes that are involved in glucose metabolism, angiogenesis, erythropoiesis and cell survival (Mole et al., 2009; Wang and Semenza, 1993b).

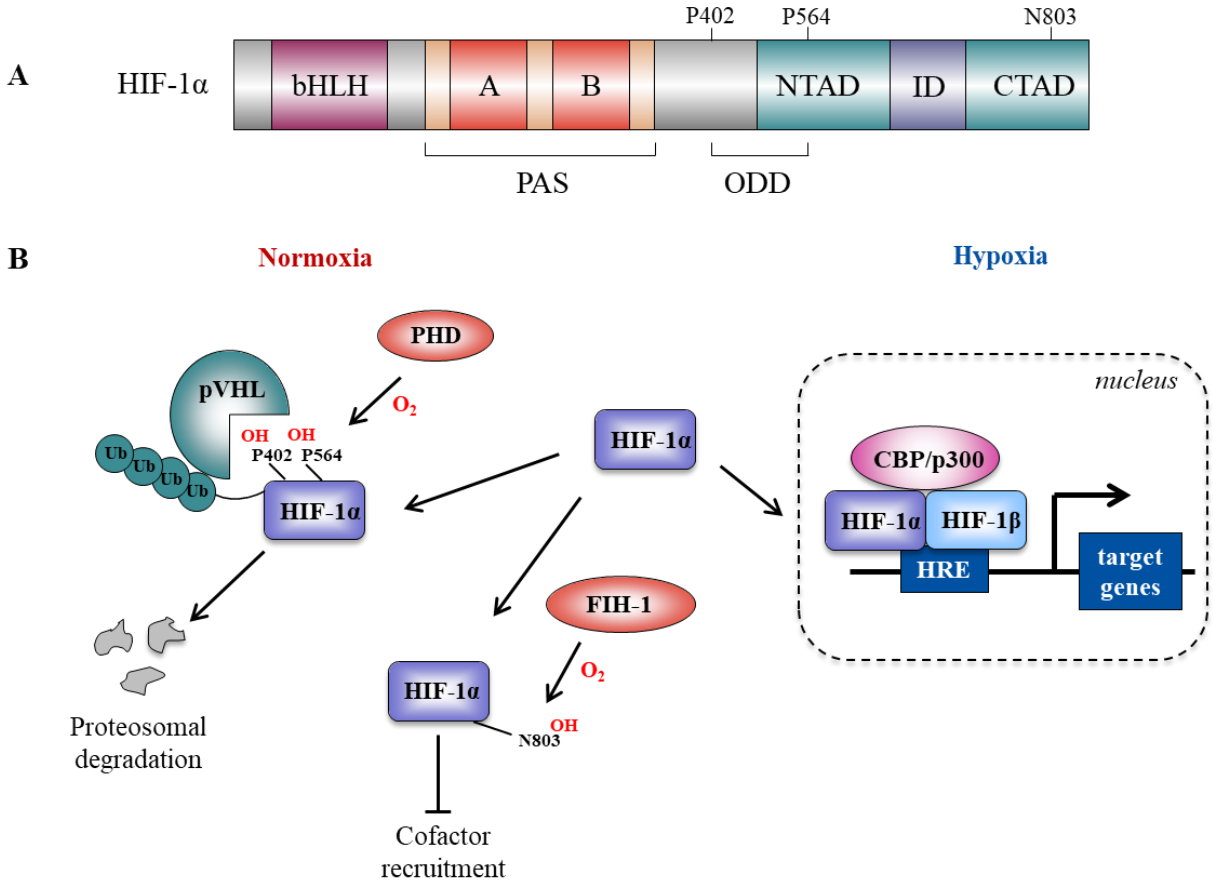

Figure 1: Oxygen-dependent regulation of HIF-1

A) Domain structure of HIF-1α. bHLH: basic-helix-loop-helix, PAS: PER-ARNT-SIM, ODD: oxygen-dependent degradation domain, NTAD: N-teminal transactivation domain, ID: inhibitory domain, CTAD: C-terminal transactivation domain

B) HIF-1α pathway. Under normoxic conditions prolyl hydroxylase domain protein (PHD) hydroxylates HIF-1α at the proline residues P402 and P564 and enables interaction with von Hippel-Lindau protein (pVHL), which is a part of the E3 ubiquitin ligase complex. Ubiquitinated (Ub) HIF-1α is then targeted for proteosomal degradation. Factor inhibiting HIF-1 (FIH-1) hydroxylates the asparaginyl residue N803 and therefore prevents recruitment of cAMP response element-binding (CREB)-binding protein (CBP) and 300 kDa coactivator protein (p300) under normoxia. In the absence of oxygen, HIF-1α is stabilized and interacts with cofactors such as HIF-1ß and CBP/p300 to maintain binding to the hypoxia-responsible element (HRE) which activates transcription of HIF-1α target genes.

Several other posttranslational modifications of HIF-1α are essential for regulation and activity. Some protein kinases were reported being involved in regulating HIF-1α either directly or indirectly, suggesting that phosphorylation of HIF-1α is involved in hypoxia-dependent induction of HIF-1α stability, nuclear localization, binding to the DNA and transcriptional activity (Dimova et al., 2009; Kietzmann et al., 2016; Wang and Semenza, 1993a). Human studies of patient biopsies indicate that in some tumor types, such as breast carcinoma and non-small-cell lung cancer, the interaction between phosphatidylinositol 3-kinase (PI3K)/protein kinase-B (Akt) pathway and HIF-1α signaling is important for cell survival in hypoxia. However, these findings were not confirmed in all tumor cell lines (Stegeman et al., 2016). Another kinase, a polo-like kinase 3 (Plk3), which acts as a regulator of cell cycle progression and stress responses, has been shown to destabilize HIF-1α *in vitro* (Xu et al., 2010). Furthermore, acetylation by the arrest-defective-1 (ARD1), SUMOylation by small ubiquitin-related modifier-1 (SUMO-1), deSUMOylation by SUMO-specific protease 1 (SENP1) and S-nitrosylation have been reported to impinge on HIF-1 activity or stability (Bae et al., 2004; Berta et al., 2007; Carbia-Nagashima et al., 2007; Cheng et al., 2007; Jeong et al., 2002; Li et al., 2007; Yasinska and Sumbayev, 2003).

The regulation of glucose and energy metabolism under hypoxia is HIF-1-dependent (Figure 2). Besides the glucose transporters GLUT1 and GLUT3, hexokinase 2 (HK2) and lactate dehydrogenase A (LDHA), both of which enhance the glycolytic switch from glucose to pyruvate, also are direct targets of HIFs (Gwak et al., 2005; Mathupala et al., 2001; Semenza et al., 1996). Additionally, activation of the glycolytic enzymes glucose phosphate isomerase (GPI), enolase 1 (ENO1), aldolase A (ALDOA), phosphoglycerate kinase 1 (PGK1), phosphoglycerate mutase 1 (PGAM1), 6-phosphofructo-2-kinase/fructose-2,6-bisphosphatase 4 (PFKFB4) and pyruvate kinase isozyme M2 (PKM2) have been shown to be regulated by HIF-1 (Hamaguchi et al., 2008; Xia et al., 2009).

HIF-1 suppresses oxidative metabolism by transactivation of the pyruvate dehydrogenase (PDH) kinase isozyme 1 (PDK1). PDK1 inactivates PDH by phosphorylation and thereby prevents the conversion of pyruvate into acetyl-CoA and its entry into the TCA cycle. Furthermore, HIF-1 has been reported to induce a subunit switch from cytochrome c oxidase (COX) subunit 4-1 (COX4-1) to COX4-2, which improves the efficiency of electron transfer to oxygen and prevents an increase of ROS levels (Fukuda et al., 2007).

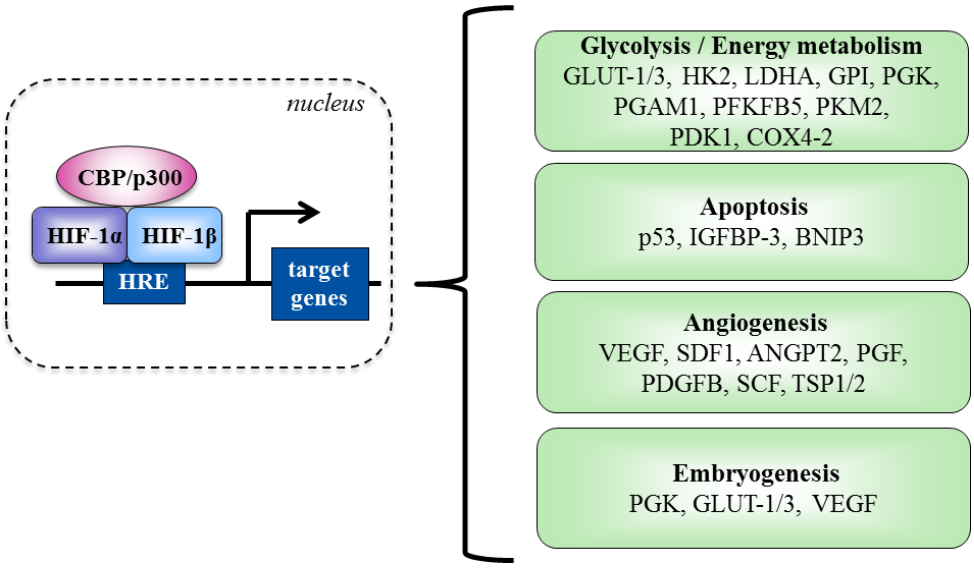

Figure 2: HIF-1α-induced activation of genes involved in different cellular processes

In normal tissue, HIF-1α induces transcription of target genes involved in processes such as glycolysis and energy metabolism, apoptosis, angiogenesis and embryogenesis. GLUT: glucose transporter, HK2: hexokinase 2, LDHA: lactate dehydrogenase A, GPI: glucose phosphate isomerase, ENO1: enolase 1, ALDOA: aldolase A, PGK1: phosphoglycerate kinase 1, PGAM1: phosphoglycerate mutase 1, PFKFB4: 6-phosphofructo-2-kinase/fructose-2,6-bisphosphatase 4, PKM2: pyruvate kinase isozyme M2, PDK1: pyruvate dehydrogenase kinase isozyme 1, COX4-2: cytochrome c oxidase subunit 4-2, IGFBP-3: insulin-like growth factor binding protein-3, BNIP3: Bcl2/adenovirus E1B 19 kDa-interacting protein 3, VEGF: vascular-endothelial growth factor, SDF1: stromal derived factor 1, ANGPT2: angiopoietin 2, PGF: placental growth factor, PDGFB: platelet-derived growth factor B, SCF: stem cell factor, TSP1/2: trombospondin 1/2

Vascular remodeling and angiogenesis are essential processes of adaptation to hypoxic conditions which are controlled by HIF-1α. VEGF is activated by HIF and is known to stimulate neovascularization during retinal disease and tumor growth (Forsythe et al., 1996). Moreover, HIF-1 induces expression of further angiogenic growth factors, such as stromal derived factor 1 (SDF1), angiopoietin 2 (ANGPT2), placental growth factor (PGF), platelet-derived growth factor B (PDGFB) and stem cell factor (SCF) (Ceradini et al., 2004; Kelly et al., 2003). The receptors of these angiogenic factors are expressed on the surface of vascular endothelial cells and vascular pericytes/smooth muscle cells. Additionally, activation of HIF-1 impairs expression of anti-angiogenic proteins such as thrombospondin-1 and -2 (TSP1 and TSP2) which interact with the microvascular endothelial cell receptor CD36 (de Fraipont et al., 2001).

Besides angiogenesis and glycolysis, which are essential for cell survival, hypoxia can also induce also apoptosis and growth arrest. HIF-1 was shown to be involved in activation of several pro-apoptotic genes. One of these is the important tumor suppressor p53 that interacts with HIF-1 to activate p53-dependent apoptosis. The transcriptional activity of p53 was found to be activated by a dephosphorylated form of HIF-1 and leads to the activation of pro-apoptotic proteins (An et al., 1998; Suzuki et al., 2001). One of these proteins, a B-cell lymphoma 2 (Bcl-2)-associated X protein (BAX), triggers the release of cytochrome c from mitochondria and eventually leads to apoptosis. However, it has been reported that p53 only accumulates in severe hypoxia and not only is HIF-dependent, but even correlates with replication arrest and requires an ataxia telangiectasia and Rad3-related (ATR)-signaling pathway (Hammond et al., 2002).

A HIF-1α-dependent expression of the pro-apoptotic member of the Bcl-2 family, the Bcl2/adenovirus E1B 19-kDa interacting protein 3 (BNIP3), mediates a mitochondrial dysfunction and induces rather necrosis-like cell death than apoptosis, as it does not involve cytochrome c release or caspases (Bruick, 2000; Sowter et al., 2001; Vande Velde et al., 2000). The typical phenotype of cellular necrosis is characterized by early plasma-membrane permeability, extensive cytoplasmic vacuolation and mitochondrial autophagy (Harris, 2002). Autophagy describes the mechanism of sequestration of cytoplasm or organelles in autophagic vacuoles or autophagosomes which are then degraded and potentially recycled (Levine and Klionsky, 2004). Cells exposed to prolonged hypoxia have been shown to use mitochondrial autophagy as an adaptive metabolic response to protect themselves from cell death (Zhang et al., 2008).

HIF-1α is essential for the mediation of cellular and developmental oxygen homeostasis (Iyer et al., 1998). HIF-1α knockout mouse embryos die at an early stage and demonstrate an abnormal vascular development such as a complete lack of cephalic vascularization, a reduction in the number of somites, abnormal neural fold formation and a greatly increased degree of hypoxia (Ryan et al., 1998). Furthermore, the expression of PGK is dramatically decreased in null embryos which imply indispensability of HIF-1α in the regulation of embryonic expression of PGK. High levels of aerobic glycolysis are characteristic for the early stages of embryogenesis. The expression levels of the high affinity glucose transporters GLUT-1 and GLUT-3 are normally enhanced during the early organogenesis period (Matsumoto et al., 1995).

All of the aspects mentioned above demonstrate the crucial involvement of HIF-1 in physiological processes, such as angiogenesis, metabolism, glycolysis and embryogenesis. However, HIF-1 has a serious drawback: it not only supports the maintenance of normal cells, but also cells with alterations such as tumor cells.

1.3 The role of HIF-1α in tumor biology

In 2000, Hanahan and Weinberg defined six hallmarks of cancer in their review (Hanahan and Weinberg, 2000). They suggest sustained angiogenesis, tissue invasion and metastasis, limitless replicative potential, resistance to apoptosis, self-sufficiency in growth signals and insensitivity to growth suppressors. A decade later, two additional hallmarks were added to this list – metabolic reprogramming of energy and evading immune destruction (Hanahan and Weinberg, 2011). Interestingly, it has been demonstrated that all these features can be affected by HIF-1α.

HIF-1α mediates maintenance of the glycolytic phenotype, activation of angiogenesis that induce cancer invasion, metastasis, cell proliferation and as a result promote tumor growth (Figure 3) (Gatenby and Gillies, 2004; Semenza, 2003). Characteristic for many solid tumors with poor patient prognosis is overexpression of HIF-1α (Talks et al., 2000). *In vivo* studies have demonstrated that HIF-1 influences angiogenesis and tumor growth (Carmeliet et al., 1998; Maxwell et al., 1997; Ryan et al., 2000). Due to changes in energy metabolism, deletion of HIF-1α results in a reduced rate of tumor growth, elimination of increased lactate production and decrease of ATP levels in response to hypoxia (Seagroves et al., 2001). Loss of HIF-1α reduces hypoxia-induced expression of VEGF and impairs vascularization, which leads to development of a hypoxic microenvironment within the tumor mass (Carmeliet et al., 1998). HIF-1α overexpression was shown to be caused by intratumoral hypoxia as well as by genetic alterations. One of these alterations is a loss-of-function in tumor suppressor genes, such as pVHL, phosphatase and tensin homolog (PTEN) and p53. The tumor suppressor p53 has also been reported to mediate mouse double minute 2 homolog (MDM2)-mediated ubiquitination and proteasomal degradation of HIF-1α (Ravi et al., 2000). Moreover, the upregulation of HIF-1α can be induced by gain-of-function in oncogenes, which are involved in activation of PI3K and mitogen-activated protein kinase (MAPK) pathways (Laughner et al., 2001; Richard et al., 1999). A number of oncogenes, as *fps*, *scr*, *ras*, are involved in

regulation of glucose transport and upregulation of GLUT1 in tumors (Flier et al., 1987; Racker et al., 1985).

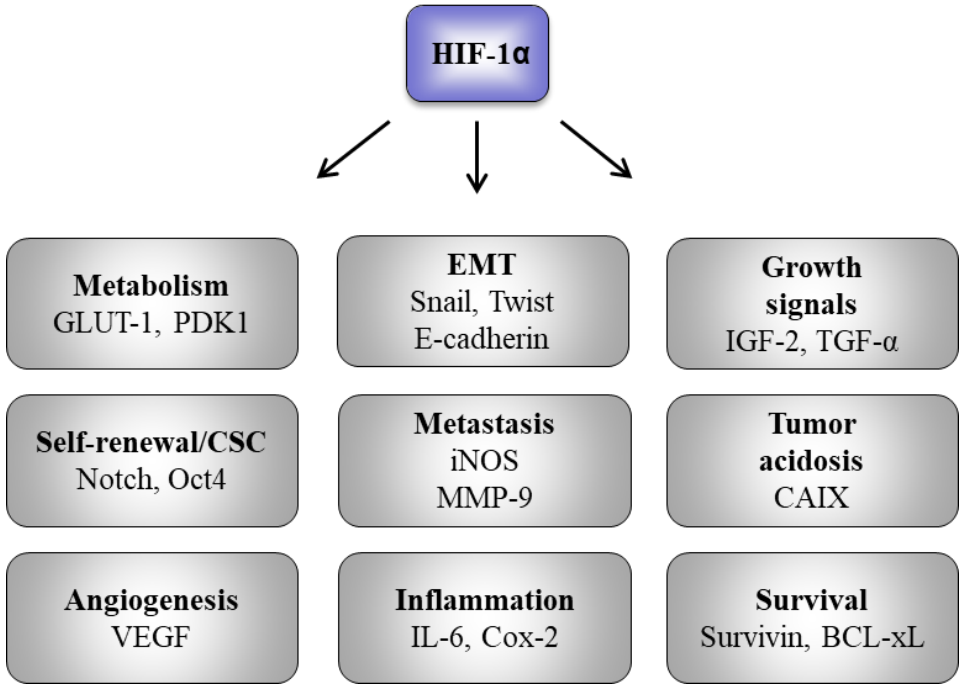

Figure 3: The role of HIF-1α in tumor progression.

Scheme is representing several pathways of cancer cells which are regulated by HIF-1α with examples of direct target genes. GLUT-1: glucose transporter 1, PDK1: pyruvate dehydrogenase kinase isozyme 1, Oct4: octamer-binding transcription factor 4, VEGF: vascular endothelial growth factor, iNOS: inducible nitric oxide synthase, MMP-9: matrix metalloprotease 9, IL-6: interleukin 6, Cox-2: cyclooxygenase 2, IGF-2: insulin-like growth factor 2, TGF-α: transforming growth factor alpha, CAIX: carbonic anhydrase 9, BCL-xL: B-cell lymphoma-extra large

In several tumors an overexpression of HIF-1α correlates with overexpression of tumor growth factors. In colon cancer and 25-40 % of all invasive breast cancer the demonstrated upregulation of HIF-1α was associated with upregulation of insulin growth factor-2 (IGF-2), which was found to facilitate activation of cell survival pathways (Mancini et al., 2014; Richardson et al., 2011). Transforming growth factor alpha (TGF-α), which is elevated in many tumor types and induces cell motility, was also demonstrated to interact with HIF-1α (Fanelli et al., 2012; Gunaratnam et al., 2003; Tarhini et al., 2014).

Besides the HIF-1α-dependent activation of metabolism proteins, such as GLUT-1/3 and PDK1, hypoxia-induced alteration of cell metabolism includes the regulation of glycogen and lipid metabolism. HIF-1α induces an activation of fatty acid binding protein 3 and 7 (FABP3, FABP7) and adipophilin (ADRP). FABP3, FABP7 and ADRP are essential for reduced

nicotinamide adenine dinucleotide phosphate (NADPH) production and survival under hypoxic conditions. *In vivo* studies have shown that loss of FABP3 and FABP7 impairs tumor growth (Bensaad et al., 2014). In some tumor cells, the overexpression of carbon anhydrase isoform IX (CAIX) was demonstrated to be regulated by HIF-1α. CAIX contributes to the acidification of the tumor microenvironment leading to a poor response to chemo- and radiotherapies (Hussain et al., 2007; Potter and Harris, 2004; Thiry et al., 2006). The cross-talk between apoptosis and HIF-1α is very controversially discussed in the literature. In several tumor cells, HIF-1α was demonstrated to be involved in the activation of some pro-apoptotic factors, such as BNIP3 (Farrall and Whitelaw, 2009). However, HIF-1α also has been demonstrated also to contribute to an activation of anti-apoptotic proteins, such as B-cell lymphoma extra-large (BCL-xL) and a member of the inhibitor of apoptosis protein Survivin (Chen et al., 2009; Sun et al., 2014)

Uncompromised function of the immune system normally prevents tumor development. The immune system can recognize tumor cells because of tumor-specific antigens and induce killing of the cancer cells. However, this process of immune surveillance can be defeated by cancer cells using the so-called immunoediting, resulting in the selection of tumor cells, which are able to avoid or suppress the immune response (Dunn et al., 2002; Swann and Smyth, 2007). Hypoxia has been shown to play a significant role in protecting tumors from the immune system by contributing to immune suppression in several ways.

Hypoxic areas in solid tumors often include necrotic cells, which release proinflammatory mediators that in turn recruit inflammatory cells to the tumors (Mantovani et al., 2008). Additionally, oncogenes such as Ras and Myc induce transcription of certain genes leading to increased recruitment of immune cells (Soucek et al., 2007; Sparmann and Bar-Sagi, 2004). In some cancer types the crosstalk between nuclear factor kappa B (NF-κB) and HIF-1α has been demonstrated to enhance an inflammatory response by inducing transcriptional activation of pro-inflammatory genes such as cyclooxygenase 2 (COX-2), interleukin 6 (IL-6), matrix metalloprotease 9 (MMP-9) and inducible nitric oxide synthase (iNOS) (Bruning et al., 2012; D'Ignazio et al., 2017). The resulting tumor-associated inflammatory response is involved in tumor growth, angiogenesis, metastasis, and remodeling of the tumor microenvironment (TME). The TME or tumor stroma contains cancer associated fibroblasts (CAFs), vascular cells including endothelial cells, and immune cells. The immune components of TME are composed of tumor infiltrating lymphoid cells (TILs) and myeloid

cells. Myeloid cells can be differentiated in tumor-associated macrophages (TAMs), myeloid-derived suppressor cells (MDSCs) and dendritic cells (DCs) (Kumar and Gabrilovich, 2014).

HIF-1α induces the expression of VEGF in tumors, which acts as a chemokine for myeloid cells, such as TAMs. Activation of TAMs is essential for maintenance of tumor-promoting chronic inflammation, immune suppression and metastasis (Condeelis and Pollard, 2006). In addition, regulation of function and differentiation of tumor MDSC has been demonstrated to depend on HIF-1α expression that leads to the suppression of antigen-nonspecific T cell activity and differentiation of tumor MDSC to TAMs (Corzo et al., 2010). HIF-1α has been shown to act as a negative regulator of T cells (Lukashev et al., 2006). The decrease of tumor cell susceptibility to cytotoxic T lymphocyte-mediated lysis is associated with the influence of HIF-1α (Noman et al., 2009). Furthermore, *in vivo* studies have demonstrated that the balance between pro-inflammatory T_H17 and anti-inflammatory regulatory T cell (T_{reg}) differentiation is regulated in a HIF-1α-dependent manner by enhancing T_H17 and attenuating T_{reg} development (Dang et al., 2011). The activation of DCs in tumor tissue correlates with the accumulation of HIF-1α and its glycolytic target genes (Jantsch et al., 2008).

HIF-1α also contributes to the development of a heterogeneous TME by supporting the activation of cancer stem cells (CSC), a subset of cancer cells with infinite self-renewal properties and unlimited proliferation (Lan et al., 2018; Liang et al., 2012). Accumulation of these pluripotent cells correlates with a post-treatment relapse and spreading of new tumors (Chen et al., 2012). HIF-1α regulates the activity of several transcriptional factors, which are essential for CSC formation, such as Notch and octamer-binding transcription factor 4 (Oct4), because they regulate CSC self-renewal and pluripotent properties (Keith and Simon, 2007; Mimeault and Batra, 2013). Moreover, HIF-1α has been shown to be unregulated in CAFs, which are a major component of the tumor stroma and promote tumor growth, metastasis, therapy resistance and poor prognosis (Martinez-Outschoorn et al., 2014; Petrova et al., 2018).

Tumor metastasis has been shown to be linked with hypoxia and HIF proteins (Rofstad et al., 2010; Voss et al., 2011). The process of metastasis includes an endothelial cell hypoxic response which is critical for the fate of the tumor. Endothelial cells play the role of a natural barrier to the tumor cells in their migration toward other organs, and alteration of their function favors metastatic dissemination. The endothelial response to hypoxia includes the regulation of nitric oxide (NO) induction (Branco-Price et al., 2012). The activation of iNOS increases the NO levels in the tissue. Expression of iNOS in the endothelium mediates a

vascular dysfunction (Gunnett et al., 2005). Endothelial cell-derived NO has been shown to mediate angiogenesis and recruitment of mural cells, such as pericytes and vascular smooth muscle cells, which are essential for vascular morphogenesis (Kashiwagi et al., 2005). Loss of HIF-1α in endothelial cells reduces NO synthesis and migration of tumor cells through the endothelial layer, and therefore decreases the metastatic rate. Interestingly, HIF-2α provides the opposite effect in tumor cells by induction of arginase 1 (ARG1) expression, which inhibits NO (Branco-Price et al., 2012).

Initiation of metastasis requires invasion, which is enabled by epithelial-mesenchymal transition (EMT), a process of differentiation of epithelial cells, which lose their polarity and junctions, into motile mesenchymal cells (Lamouille et al., 2014; Thiery et al., 2009). HIF-1 is involved in the induction of EMT by activating factors, such as Snail, Slug, Twist and zinc finger E-box binding homeobox 1 (ZEB1) (Yang et al., 2008; Zhang et al., 2013a; Zhu et al., 2013). Furthermore, HIF-1 represses the expression of E-cadherin, which is important for adherent junction formation (Krishnamachary et al., 2006). In some cancer types EMT was associated with activation of the PI3K/Akt pathway that mediated HIF-1α activation (Jiao and Nan, 2012).

TME has been shown to contribute to the radioresponsiveness of tumors. Hypoxia, as well as the response of stromal and endothelial cells are involved in the undesirable survival of tumor cells after irradiation (Joyce and Pollard, 2009; Karar and Maity, 2009). Enhanced radioresistance of tumor cells is one of the major reasons of therapeutic failure during the radiation treatment of cancer patients.

1.4 HIF-1α-mediated radioresistance of cancer cells

Radiation treatment is one of the major therapeutic approaches for cancer treatment. After the discovery of X-rays in 1895 by Wilhelm Conrad Röntgen a lot of research was done to achieve a sophisticated treatment with ionizing radiation (IR) for killing tumor cells and sparing normal tissue. X- and γ-rays produce fast recoil electrons that can directly ionize the target molecule or interact with water surrounding the DNA to produce free radicals which break chemical bonds in the DNA and lead to DNA damage (Hall and Giaccia, 2012). However, radiotherapy often fails to achieve a complete remission. Poor prognosis of cancer patients including tumor recurrence and metastasis is in part a result of radioresistance of tumor cells.

Radioresistance has been shown to be characteristic for hypoxic regions in solid tumors (Brizel et al., 1997). Radiation preferentially targets well-oxygenated tumor cells because sensitivity to radiation requires oxidation, and this is why oxygenated cells are 2.5- to 3-times more sensitive than hypoxic cells (Gray et al., 1953). This physiological principle is known as the oxygen enhancement effect. After the death of oxygenated radiosensitive cells oxygen diffuses to the surviving hypoxic regions, leading to the reoxygenation of hypoxic tumor cells (Moeller and Dewhirst, 2006). Reoxygenation induces oxidative stress and formation of ROS, which in turn may be involved in the stabilization of normoxic HIF-1α. Additionally, ROS may contribute to the stabilization of HIF-1α by generation of NO in TAMs and S-nitrosylation of HIF-1α (Li et al., 2007; Moeller et al., 2004). Accumulation of HIF-1α can be supported by the PI3K/Akt pathway in a glucose- and reoxygenation-dependent manner in irradiated tumors (Harada et al., 2009). Therefore, radiation treatment potentially leads to the upregulation of HIF-1α in tumors.

Moreover, radiation treatment has been shown to elevate translation of downstream HIF-1α signals, such as VEGF and CAIX (Moeller et al., 2004). VEGF expression induces angiogenesis, which improves oxygenation within tumors. However, the elevated expression of VEGF also supports endothelial cell (EC) resistance (Gorski et al., 1999). Tumor endothelial vasculature has been demonstrated to protect tumors from ionizing radiation (Garcia-Barros et al., 2003). Inhibition of HIF-1α results in an inhibition of tumor vascularization (Moeller et al., 2005). Furthermore, HIF-1α is involved in repopulation of radio-surviving tumor cells. Perinecrotic tumor cells from the hypoxic areas which survive radiation treatment have been suggested to translocate to the proximal regions of tumor blood vessels in a HIF-1α-dependent manner. As HIF-1α is involved in induction of cell migration, upregulation of HIF-1α after radiation treatment supports the EMT and translocation of cells (Harada et al., 2012). These radio-surviving cells are then responsible for tumor recurrence and metastasis after radiation treatment. In addition, IR-induced HIF-1α upregulation correlates with generation and radioresistance of CSCs. CSCs are involved in providing radioresistance through the activation of DNA repair pathways (Bao et al., 2006).

The radiosensitivity of cells depends on the distribution of cells going through the cycle. Cells are more radioresistant in late S phase when they rapidly proliferate and in early G_1 phase, if the cells are very slowly proliferating (Hall and Giaccia, 2012). Hypoxia induces the expression of cell cycle regulators (Box and Demetrick, 2004; Gardner et al., 2001). HIF-1α has been shown to be essential for cell cycle arrest, as hypoxia induces HIF-1α-dependent

enhancement of cyclin-dependent kinase (CDK) inhibitors p21 and p27 expression (Goda et al., 2003). Furthermore, HIF-1 has been suggested to promote cell cycle arrest by antagonizing Myc activity which leads to activation of p21 even in the absence of hypoxia (Koshiji et al., 2004).

The effect of HIF-1α upregulation on radiosensitivity is complex. On one hand, HIF-1α acts as an anti-apoptotic factor and increases radioresistance of tumor cells by vascular protection (Akakura et al., 2001; Xia et al., 2018). On the other hand, HIF-1α also demonstrates pro-apoptotic features and can favor radiosensitivity in tumor cells. HIF-1α induces phosphorylation of p53 in the irradiated cells, which promotes apoptosis (Moeller et al., 2005). Additionally, HIF-1α enhances metabolism and proliferation of cancer cells which leads to radiosensitization of the irradiated cells. Furthermore, it is known that chronic, but not acute hypoxia increases cellular radiosensitivity by inhibiting the expression of genes involved in DNA damage repair (Bristow and Hill, 2008; Chan et al., 2008). In general, it has been assumed that the effect of HIF-1α stabilization on promoting radioresistance outweighs enhanced radiosensitivity.

1.5 HIF-1α and DNA damage response

Cells have evolved distinct mechanisms for DNA repair depending on the extent of damage. Mismatches, insertion or deletion of DNA sequences are processed by the mismatch repair (MMR), while chemical alterations of DNA bases are corrected by base excision repair (BER) (David et al., 2007; Jiricny, 2006). Nucleotide excision repair (NER) is responsible for correction of more complex helix-distorting base lesions, such as pyrimidine dimers and intrastrand crosslinks (Batty and Wood, 2000). IR leads to the oxidation of DNA bases and induces single-strand and double-strand DNA breaks (DNA SSBs and DNA DSBs). Whereas SSBs are processed by single-strand break repair (SSBR), four mechanisms are involved in the DSBs repair: non-homologous end joining (NHEJ), alternative-NHEJ (alt-NHEJ), single-strand annealing (SSA) and homologous recombination (HR). Alt-NHEJ and SSA are thought to operate as a backup for HR and NHEJ, therefore it is anticipated that HR and NHEJ are the most important mechanisms for the repair of DSBs (Frankenberg-Schwager et al., 2009; Iliakis et al., 2015).

Formation of the DSBs causes the activation of PI3K-like kinases, including ataxia telangiectasia mutated (ATM), ATR and DNA-dependent protein kinase (DNA-PK), which in turn phosphorylate the histone protein H2AX among other DNA repair proteins (Figure 4) (Rogakou et al., 1998; Stiff et al., 2004; Stiff et al., 2006). The phosphorylated form of H2AX, γH2AX, acts as a marker of DNA damage at nascent DSB sites. It has been found, that γH2AX co-localizes with several proteins involved in the DSB repair, such as breast cancer protein 1 (BRCA1), Nijmegen breakage syndrome protein 1 (NBS1), p53 binding protein 1 (53BP1) and mediator of DNA damage checkpoint (MDC1) (Kobayashi, 2004), which are involved in initiation of DNA damage repair (DDR). The activation of BRCA1, 53BP1 and MDC1 by phosphorylation occurs in an ATM-dependent manner (McKinnon, 2004).

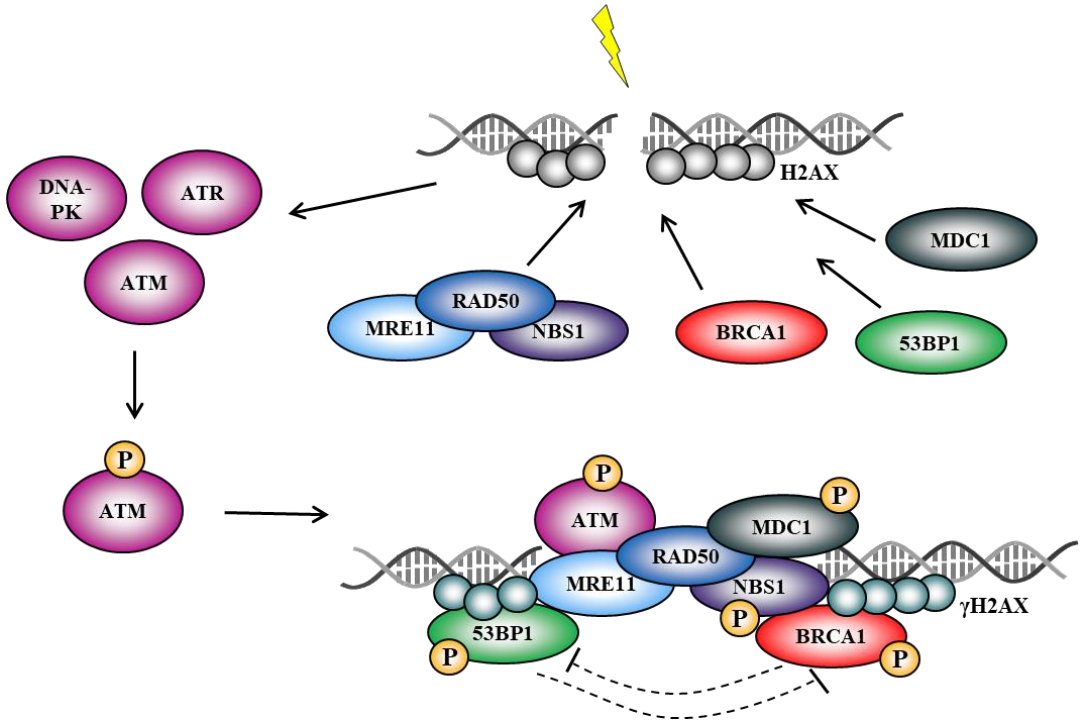

Figure 4: Initial response to ionizing radiation (IR)-induced DNA double-strand breaks (DSB)
In response to the DSB the kinases ATM, ATR and DNA-PK are activated. ATM undergoes autophosphorylation and phosphorylates the histone protein H2AX (γH2AX) which is essential for the tethering of other repair factors. Binding of the MRE11-RAD50-NBS1 complex recruits BRCA1, MDC1 and 53BP1 to the DSB site. These proteins co-localize with γH2AX and are phosphorylated in an ATM-dependent manner. DSB repair choice is regulated by the cell-cycle-dependent antagonistic process: 53BP1 mediates end protection and favors NHEJ, whereas BRCA1 mediates end resection and HR. ATM: ataxia telangiectasia mutated, ATR: ataxia telangiectasia and Rad3-related, DNA-PK: DNA-dependent protein kinase, DNA-dependent protein kinase, BRCA1: breast cancer 1, MDC1: mediator of damage checkpoint 1, 53BP1: p53-binding protein 1, P: phosphorylation, NHEJ: non-homologous end-joining, HR: homologous recombination.

NHEJ operates in all cell cycle phases and is very fast, but also error-prone (Rothkamm et al., 2003). The double-stranded DNA end-binding protein heterodimer Ku, containing Ku70 and Ku80, binds with a high affinity to the ends of DSBs, thereby protecting the DSB ends from end resection (Figure 5) (Walker et al., 2001). Ku recruits DNA-PKs to the DSB site and stimulates its activation (Singleton et al., 1999). After binding to DNA, DNA-PK autophosphorylates and activates ARTEMIS, which is critical for hairpin opening and overhang processing (Goodarzi et al., 2006; Ma et al., 2002). Members of the DNA polymerases, pol μ and pol λ, are recruited by the Ku to the DNA for gap-filling in non-compatible DSBs (Capp et al., 2006; Capp et al., 2007). The DNA-PK dissociates then from the blunt ends providing space for further processing factors. In addition, Ku has been shown to recruit XLF to the DSB site which in turn stimulates X-ray cross complementing 4/DNA Ligase 4 (XRCC4/LIG4)-mediated joining of DSBs (Wang et al., 2004; Yano et al., 2008). XRCC4 activates LIG4, thus initiating the ligation step (Grawunder et al., 1997).

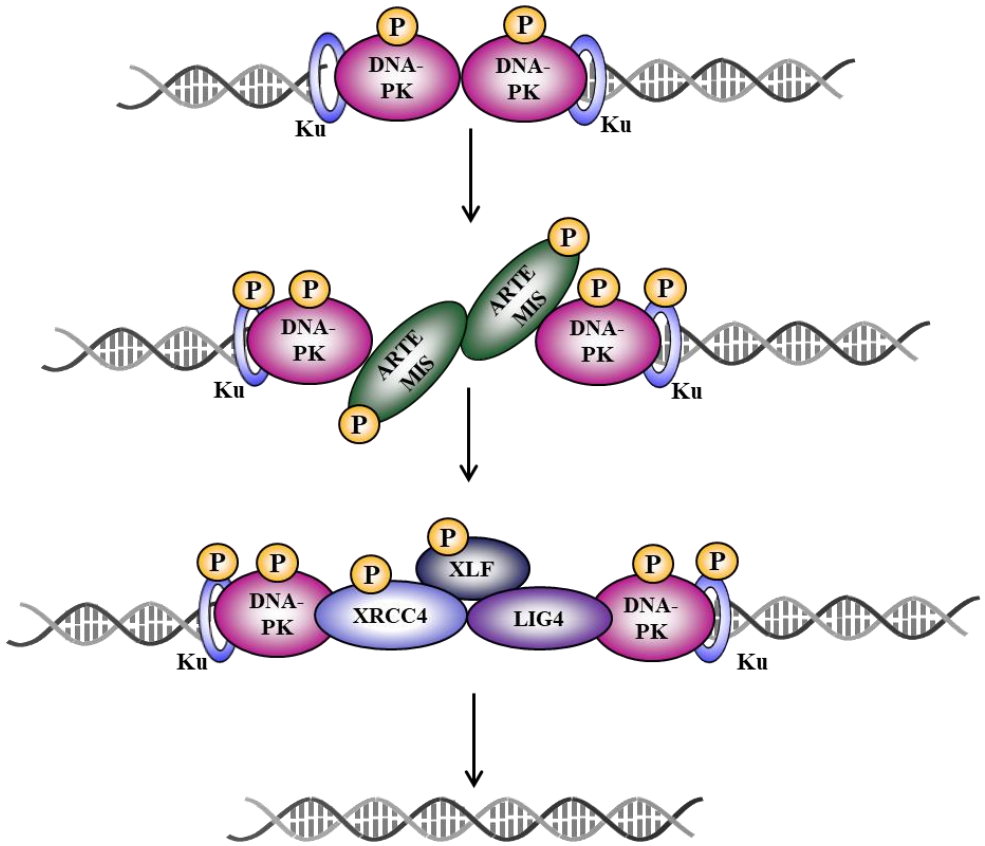

Figure 5: Non-homologous end-joining (NHEJ)

Rapid recruitment of Ku to the DSB protects ends from resection and is an initial step of NHEJ. The Ku/DNA complex activates DNA-PK. DNA-PK-dependent phosphorylation of ARTEMIS induces initial processing, followed by ligation of broken ends after recruitment of the XRCC4/LIG4/XLF complex. XRCC4: X-ray repair cross complementing 4, LIG4: DNA ligase 4, XLF: XRCC4-like factor

Another important DDR mechanism, HR, is most important in late S and G_2 phases of the cell cycle and has a high fidelity (Rothkamm et al., 2003). A complex Mre11-Rad50-NBS1 (MRN) recognizes a DSB and stabilizes it (Figure 6). Therefore, the Mre11 directly binds NBS1, DNA and Rad50. Rad50 contains an ATPase that interacts with Mre11 and thereby stimulates DNA binding and DNA end processing by Mre11 (Williams et al., 2007). NBS1 interacts with ATM and C-terminal binding protein-interacting protein (CtIP) which regulates the initiation of the end resection generating 3´single-stranded DNA (ssDNA) overhangs (Iijima et al., 2008). DSB resection stimulates the accumulation of replication protein A (RPA) which stabilizes ssDNA regions (Wold, 1997). In the next step BRCA2 is recruited to the DSB through BRCA1 and facilitates the loading of RAD51 monomers onto ssDNA replacing RPA (Prakash et al., 2015). The accumulation of RAD51 monomers leads to the formation of RAD51 nucleoprotein filaments which can be visualized as sub-nuclear RAD51 foci by immunofluorescence microscopy (Haaf et al., 1995). The RAD51 filaments invade into the homologous sequence of the sister chromatid and form a displacement loop structure, following restoration of DNA integrity by DNA synthesis (West, 2003). DNA end resection is induced in the S and G2 phases of the cell cycle, when sister chromatids are available as a template for HR, providing a predominantly error-free repair. HR undergoes cell-cycle regulation and can be positively regulated by CDK by phosphorylation of NBS1 and CtIP, however the CDK-mediated phosphorylation of BRCA2 negatively regulates HR repair (Esashi et al., 2005; Falck et al., 2012; Yu and Chen, 2004). ATM protein kinase activates CtIP via phosphorylation (Shibata et al., 2011).

Furthermore, the choice between NHEJ and HR depends on the interplay between 53BP1 and BRCA1 (Bakr et al., 2016). 53BP1 is a DNA-damage response protein and is essential for maintaining genomic stability promoted NHEJ by enhancing chromatin mobility (Dimitrova et al., 2008). BRCA1 interacts with RAD51 and promotes accurate DSB repair during HR (Boulton, 2006; Durant and Nickoloff, 2005). It has been demonstrated that ATM-dependent resection can be inhibited by 53BP1 in G_1 phase thereby favoring the repair by NHEJ, while BRCA1 can remove 53BP1 from replication-associated breaks (Bunting et al., 2010; Isono et al., 2017).

Hypoxia can trigger the ATR checkpoint and induce a G_1 and an intra-S phase arrest (Bristow and Hill, 2008). Activation of ATR also induces phosphorylation of p53 and γH2AX in response to hypoxia (Hammond et al., 2003). In addition, hypoxia induces a phosphorylation of CHK2 in an ATM-dependent manner that leads to the initiation of the signaling cascade

resulting in cell cycle arrest in G_2 phase (Freiberg et al., 2006). Moreover, hypoxia-induced activation of ATM was suggested to mediate the phosphorylation of HIF-1α at S696 and its stabilization (Cam et al., 2010). HIF-1α has been shown to be involved in mechanisms of DDR, such as NHEJ, by activation of DNA-PK and Ku70/80 (Wirthner et al., 2008). HIF-1α also downregulates the Myc-activated gene BRCA1, although an overexpression of HIF-1α has been demonstrated in BRCA1 related tumors (Koshiji et al., 2004; van der Groep et al., 2008). In general, HIF-1α-dependent mechanisms maintain genomic instability and are crucial for DDR, but there are still a lot of aspects of these interactions that remain unclear.

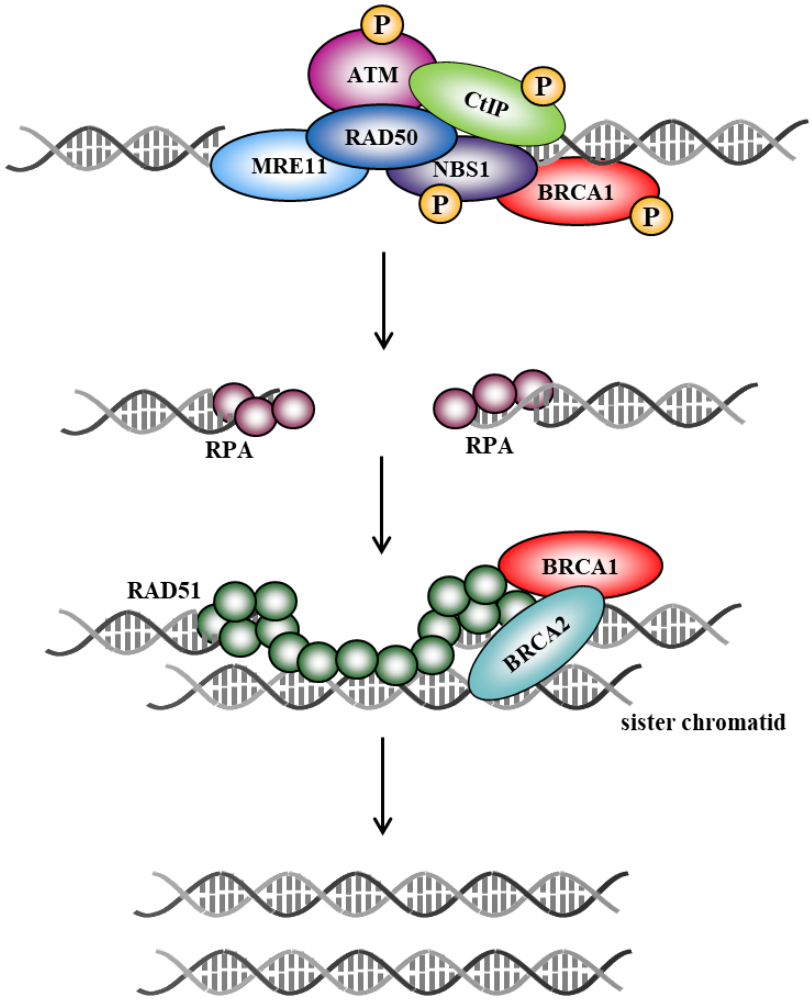

Figure 6: Homologous recombination (HR)

A MRN complex composed of Mre11, RAD50, and NBS1 binds to the DSB and together with CtIP and BRCA1 mediates the initiation of DSB end resection in an ATM-dependent manner. The resulting ssDNA open ends are coated by RPA. BRCA1 recruits BRCA2 to DSB site, which in turn mediates replacing of RPA through RAD51 monomers on ssDNA ends. RAD51 filaments induce a strand invasion into homologous DNA sequences and DNA synthesis. ATM: ataxia telangiectasia mutated, CtIP: C-terminal binding protein-interacting protein, RPA: replication protein A

2 Aim of the study

In the last decades the research concerning HIF-1α has demonstrated that HIF-1α is a crucial factor in the regulation of tumor progression via a broad range of mechanisms. HIF-1α is involved in the IR-induced increase of radioresistance that leads to cancer recurrence and poor prognosis for cancer patients. There are indications that HIF-1α activity is increased after radiation treatment and promotes low radiation sensitivity. Thus, HIF-1α is accepted as a promising target molecule for cancer therapy. Of date, the interaction of HIF-1α with other molecules involved in radioprotection of tumor cells is very often discussed, although the exact mechanism remains highly controversial and unclear. Recently, the contribution of TME to radioresponsiveness also came into focus. Therefore, one of the paramount tasks of HIF-1α research is the identification of further interactions with the DDR molecules and influence of the surrounding stromal cells on the HIF-1α signaling in tumors. It is essential to understand how the complex mechanisms including HIF-1α-mediated protection of stromal endothelial cells, HIF-1α signaling in irradiated tumor cells and interaction with TME converge to bring about a change in tumor radiosensitivity.

The first aim of this study was to clarify the effect of HIF-1α deficiency on radiosensitivity *in vitro*. Therefore, doxycycline-inducible HIF-1α knockdown cells were generated for the investigation of proliferation, long term survival and apoptosis after IR. In addition, it was particularly important to determine how HIF-1α signaling affects DNA repair. For this purpose, the recruitment of DDR proteins involved in the response to IR, NHEJ and HR, was investigated in HIF-1α-depleted cells.

The next aim was to investigate an effect of surrounding microenvironment on HIF-1α signaling in tumor cells and the effect of this interaction on the radiation sensitivity *in vivo*. Firstly, the effect of HIF-1α depletion in tumors on radiosensitivity was investigated in a allograft mouse model with wild-type C57BL/6 mice. Secondly, using a floxed HIF-1α allele in combination with a ubiquitously expressed tamoxifen-inducible recombinase Cre-ER(T2) HIF-1α conditional knockout mice were generated. A murine xenograft model with a HIF-1α knockout was used to investigate whether HIF-1α elimination in surrounding stroma cells simultaneously with tumor cells affects the radiosensitivity of tumors. Thus, we intended to determine an effect of interaction between stromal and tumor cells on the HIF-1α signaling pathway and radiation sensitivity.

3 Material and methods

3.1 Material

3.1.1 Reagents and kits

Table 1: Reagents and kits

Reagent/Kit	Company
BaseScope™ Assay Kit	ACDBio (Newark, USA)
BCA Protein Assay Kit	Thermo Fisher Scientific (Waltham, USA)
Direct PCR Kit	highQu (Kraichtal, Germany)
Dual-luciferase reporter assay system	Promega (Madison, USA)
MESA Green qPCR™ Mastermix Plus for SYBR Assay	Eurogentec (Liège, Belgium)
QuantiTect Reverse Transcription Kit	Qiagen (Hilden, Germany)
ReliaPrep™ RNA Tissue Miniprep System	Promega (Madison, USA)
SuperSignal West Femto Maximum Sensitivity Substrate	Thermo Fisher Scientific (Waltham, USA)
Trans-Blot® Turbo™ RTA Transfer Kit	Bio-Rad (Munich, Germany)

3.1.2 Technical devices

Table 2: Technical devices

Device	Company
Cellometer™ Auto T4	Nexcelom Bioscience (Lawrence, USA)
Dounce tissue grinder set	Sigma-Aldrich (Munich, Germany)
FACS Canto II	BD Biosciences (Franklin Lakes, USA)
Fusion-FX7 chemoluminescence documentation system	Peqlab (Erlangen, Germany)
Gelelectrophoresis chamber	Bio-Rad (Munich, Germany)
GloMax luminometer	Promega (Madison, USA)
Hypoxic chamber	Toepffer Lab System (Göppingen, Germany)
C1000 Touch Thermal Cycler CFX96 Real-Time System	Bio-Rad (Munich, Germany)
Light Microscope ScanScope	Leica biosystems (Wetzlar, Germany)
Microm HM 340E Microtome	Thermo Fisher Scientific (Waltham, USA)
Synergy HT Multi-Detection Microplate Reader	BioTek (Bad Friedrichshall, Germany)
Take3 Micro-Volume Plate	BioTek (Bad Friedrichshall, Germany)
Thermal cycler T100	Bio-Rad (Munich, Germany)
Trans-Blot Turbo Transfer System	Bio-Rad (Munich, Germany)
Typhoon 9400 fluorescence imager	GE Healthcare (Amersham, UK)
X-Ray research irradiator cabinet RS320	Xstrahl Ltd (Camberley, UK)
X-ray research irradiator cabinet X-RAD 320	Precision X-Ray (North Branford, USA)
Zeiss LSM 710 confocal microscope	Carl Zeiss (Oberkochen, Germany)

3.1.3 Buffers and media

Table 3: Buffers and media

Buffer/Medium	Concentration	Ingredients
PBS	138 mM	Tris (pH 7.4)
	8.1 mM	Na_2HPO_4
	2.7 mM	KCl
	1.5 mM	KH_2PO_4
TBS	20 mM	Tris (pH 7.4)
	137 mM	NaCl
TBS-T	1x	TBS
	0.05 % (v/v)	Tween 20
RIPA lysis buffer	50 mM	Tris HCl (pH 7.4)
	150 mM	NaCl
	1 % (v/v)	NP-40
	0.5 % (w/v)	sodiumdesoxycholate
Stacking gel buffer	5 % (w/v)	Acrylamide
(5 %)	125 mM	Tris (pH 6.8)
	0.1 % (w/v)	SDS
	0.05 % (w/v)	APS
	0.1 % (v/v)	TEMED
Separating gel buffer	5-12.5 % (w/v)	Acrylamide
	375 mM	Tris (pH 8.8)
	0.1 % (w/v)	SDS
	0.05 % (w/v)	APS
	0.05 % (v/v)	TEMED
Running buffer	25 mM	Tris (pH 7.4)
(for SDS-PAGE)	0.192 M	Glycine
	0.1 % (w/v)	SDS
SDS sample buffer	62,5 mM	Tris (pH 7.4)
	2 % (w/v)	SDS
	3 % (v/v)	ß-mercaptoethanol
	10 % (v/v)	Glycerol
	0.25 mg/ml	Bromophenol blue
	25 mM	DTT

TAE	40 mM	Tris (pH 7.4)
	20 mM	Acetic acid
	1 mM	EDTA
Hypotonic citrate buffer	0.1 % (w/v)	Sodium citrate
	0.1 % (v/v)	Triton-X100
	20 µg/ml	Propidium iodide
FACS buffer	0.5 % (w/v)	BSA
	20 µg/ml	Propidium iodide
		PBS
Coomassie Brilliant Blue solution	0.1 % (w/v)	Coomassie Brilliant Blue
	5 % (v/v)	Acetic acid
	45 % (v/v)	Methanol
ACK buffer	0.155 M	NH_4Cl
	10 mM	$KHCO_3$
	0.1 mM	EDTA
Agarose gel (3 %)	3 %	Agarose
	75 ml	TAE
Caspase lysis buffer pH 7.3	50 mM	Tris (pH 7.4)
	150 mM	NaCl
	1 % ‘(v/v)	NP-40
Caspase substrate buffer	20 mM	HEPES
	100 mM	NaCl
	10 % (w/v)	Saccharose
	0.1 % (w/v)	CHAPS
	10 mM	DTT
	66 µM	DEVD-AMC
4 % PFA pH 7.4	4 % (w/v)	PFA
	1x	PBS
	1 M	NaOH
PFGE lysis solution pH 7.6	10 mM	Tris
	100 mM	EDTA
	50 mM	NaCl
	2 % (w/v)	N-lauroylsarcosin
	0.2 mg/ml	Protease A
PFGE washing solution pH 7.6	10 mM	Tris
	100 mM	EDTA
	50 mM	NaCl

PFGE RNase solution	10 mM	Tris
pH 7.6	100 mM	EDTA
	50 mM	NaCl
	0.1 mg/ml	RNaseA
PFGE serum-free HEPES-buffered medium	5 mM	$NaHCO_3$
	20 mM	HEPES serum-free medium
PFGE 5x TBE	890 mM	Tris
	890 mM	Boric acid
	10 mM	EDTA
DEPC water	0.1 % (v/v)	DEPC
(1 h at 37 °C incubation)		A. dest
10x MOPS buffer	0.2 M	MOPS
	50 mM	Sodium acetate
	10 mM	EDTA
		DEPC water
RNase decontamination solution (15 min at 100 °C incubation)	0.1 M	NaOH
	1 mM	EDTA
		DEPC water
1 % RNA gel	1 % (w/v)	Agarose
		A. dest
	10 %	10x MOPS buffer
	2,5 % (v/v)	Formaldehyde
	0.003 % (v/v)	SYBR-Safe

3.1.4 Cell lines

Table 4: Cell lines used for this study

Strain	Origin	Medium	Characteristics	Reference
B16F10	murine metastatic melanoma	DMEM high glucose (Gibco, Life Technologies)	C57BL/6J mouse strain; adherent spindle-shaped and epithelial cells; dark brown medium by high level of confluence due to melanin production	ATCC #CRL-6475
HCT116	human colorectal carcinoma	McCoy´s 5A (PAN Biotech)	adherent epithelial cells; mutation in codon 13 of the *ras* proto-oncogene	ATCC #CCL-247
HEK293T	human embryonic kidney	DMEM high glucose	adherent, oval to fibroblastoid cells; highly transfectable, carrying a plasmid containing the mutant of SV-40 T-antigen	DSMZ #ACC-635
Lewis Lung Carcinoma (LLC1) cells	murine lung carcinoma	DMEM high glucose	C57BL mouse strain; adherent and suspension cells form multilayers; highly tumorigenic, but weakly metastatic (Bertram and Janik, 1980)	ATCC #CRL-1642

3.1.5 Plasmids, shRNA sequences, and PCR oligonucleotides

All short hairpin ribonucleic acid (shRNA) sequences and plasmids used in this study are listed in Table 5 and 6, respectively.

Table 5: shRNA sequences

shRNA	Characteristics	Reference
shHIF-1α	TGGATAGCGATATGGTCAATG corresponding to nucleotides 2030-2050 of mouse HIF-1α mRNA	(GenBank acc. no. NM_010431)
shscrambled	CCTAAGGTTAAGTCGCCCTCG non-coding scrambled shRNA	

Table 6: Plasmids

Plasmid	Characteristics	Reference
pLKO.1	constitutive pLKO.1 vector	#10879, Addgene
pLKO.1 Tet-On	lentiviral tetracycline (Tet)-inducible pLKO-shRNA vector	#21915, Addgene
pLKO.1 shscrambled	pLKO.1 control plasmid containing unspecific shRNA sequence	#1864, Addgene
pLKO.1 shscrambled Tet-On	lentiviral Tet-inducible pLKO.1 vector containing unspecific shRNA sequence	#21915, Addgene
pGLHIF1.3	firefly luciferase containing 3 copies of the HRE	(Kvietikova et al., 1995)
pGL4.74hR	renilla reporter as a control for transfection efficiency	E6921, Promega
CMV-sport6-mHIF2α	constitutive expression vector containing murine HIF-2α sequence	GenomeCube
pcDNA3	control plasmid	

All oligonucleotides used for polymerase chain reaction (PCR) and quantitative PCR (qPCR) are listed in Table 7 and Table 8 and were purchased from Sigma (USA).

Table 7: PCR primers used for mouse genotyping

Primer	Sequence 5´-3´	fragment length [bp]	T_{ann} [°C]
Rosa26-Cre-ER for **Rosa26-Cre-ER rev**	TGAGCTACACCAGAGACGGA TTGGCAGAACGAAAACGCTG	120 (knock-in)	65
mHIF-1α_E2seq for **mHIF-1α_E2seq rev**	CTAGTACTAGATAACCAGTG GGTAAACCAAAACAACTTAC	1405 (wt) 681 (E2 junction)	50
mHIF-1α_flox for **mHIF-1α_flox rev**	GGAGCTATCTCTCTAGACC GCAGTTAAGAGCACTAGTTG	200 (HIF-1α wt) 250 (HIF-1$\alpha^{fl/fl}$)	57

Table 8: Primer used for qPCR gene expression assay

Primer	Sequence 5´-3´	fragment length [bp]
RT_mHIF-1α for	GAAATGGCCCAGTGAGAAA	119
RT_mHIF-1α rev	CTTCCACGTTGCTGACTTGA	
RT_mGLUT-1 for	GGATCCCAGCAGCAAGAAGGT	81
RT_mGLUT-1 rev	TAGCCGAACTGCAGTGATCC	
RT_VEGF for	AATGCTTTCTCCGCTCTGAA	143
RT_VEGF rev	GATCATGCGGATCAAACCTC	
RT_mBNIP3 for	CCCAGACACCACAAGATACCA	81
RT_mBNIP3 rev	CTTCCTCAGACAGAGTGCTGTT	
RT_mB2M for	GGCTCACACTGAATTCACCC	102
RT_mB2M rev	ATGTCTCGATCCCAGTAGACG	

3.1.6 Antibodies

The primary and secondary antibodies used in this study are listed in Table 9 and Table 10 with the molecular weight (MW) of their target protein and dilution applied for Western blot (WB), immunofluorescence staining (IF) and immunohistochemistry (IHC).

Table 9: Primary antibodies

Antibody	MW [kDa]	Host	Catalog number, company	Dilution
53BP1	220	rabbit	NB100-304, Novus (USA)	1:10000 (IF)
HIF-2α	110	rabbit	NB100-122, Novus (USA)	1:1000 (WB)
mHIF-1α	110	mouse	10006421, Cayman Chemical Company (USA)	1:1000 (WB) 1:100 (IHC)
PARP-1	116 89 cleaved	rabbit	9542S Cell Signaling (USA)	1:1000 (WB)
RAD51	43	rabbit	ab-1, Calbiochem (Germany)	1:1000 (WB) 1:200 (IF)
ß-actin	24	mouse	ab6276, abcam (UK)	1:6000 (WB)
γH2AX	15	rabbit	#2577, Cell Signaling (USA)	1:1000 (WB) 1:800 (IF)

Table 10: Secondary antibodies

Antibody	Host	Specificity	Catalog number, company	Dilution
IgG/HRP	goat	anti-mouse	P0447, Dako (Denmark)	1:3000 (WB)
IgG/HRP	goat	anti-rabbit	P0448, Dako (Denmark)	1:3000 (WB)
IgG Alexa 488	goat	anti-rabbit	A11070, Invitrogen (Germany)	1:500 (IF)
IgG Alexa 488	goat	anti-mouse	A11017, Invitrogen (Germany)	1:500 (IF)
IgG Alexa 594	goat	anti-mouse	A11005, Invitrogen (Germany)	1:500 (IF)

3.2 Methods *in vitro*

3.2.1 Cell culture conditions

The cell lines listed in Table 4 were cultivated in a humidified atmosphere composed of 5 % CO_2 in air. All media were supplemented with 100 U/ml penicillin, 100 µg/ml streptomycin (Pen/Strep) and 10 % fetal bovine serum (FBS), all components were purchased from Thermo Fisher/Life Technologies (Darmstadt, Germany). After reaching 70-80 % confluence cells were passaged to maintain an adherent monolayer of cells. Cells were detached from the dishes by treatment with 0.25 % trypsin/EDTA solution, centrifuged at room temperature for 3 min at 280 times gravity (x *g*) and seeded at a ratio of 1:10 into new culture flasks.

3.2.2 Cryopreservation of cell lines

For long-term storage cells were cryopreserved. After trypsinization and centrifugation, the cells were resuspended in FBS with 10 % DMSO and transferred into cryotubes, which were then immediately placed in an isopropanol-filled freezing jar and stored at -80 °C and stored in liquid N_2 the following day.

3.2.3 Lentiviral particle production in HEK293T cells

For the production of lentiviral particles 7.5-8 x 10^5 of HEK293T cells were transferred into a 25 cm^2 flask. During overnight incubation the cells reached 50-70 % confluence. The transfection mixture contained 500 µl serum-free DMEM, 6 µg of pLKO.1 vector (expressing the shRNA) or 6 µg of pWPXL GFP (control vector), 4 µg psPAX2 (the packaging plasmid) and 2 µg pMD2.G (the envelope vector). GeneJuice (Novagen, Darmstadt, Germany) was used as a transfection reagent in a ratio of 3:1 (µl reagent per µg DNA). The transfection mixture was added dropwise to the cell culture medium. After further incubation for 48-60 h the supernatant was collected by filtering through a 0.45 µm filter. The virus containing supernatant was either used immediately for transduction of target cells or stored at -80 °C.

3.2.4 Lentiviral transduction of cells

The knockdown (KD) cell lines LLC shHIF-1α Tet-On, B16F10 shHIF-1α Tet-On and HCT116 shHIF-1α were generated by transduction with lentiviral particles expressing shHIF-1α or non-coding scrambled shRNA (shscr) cloned into a tetracycline (Tet)-inducible pLKO-shRNA vector or a constitutive pLKO.1 vector as a control. For transduction, 2 ml of the viral supernatant was added to 2 x 10^5 cells and seeded into a 25 cm^2 flask. Next, 8 µg/ml

polybrene (hexadimethrine bromide) were added to enhance the efficiency of the cell transduction. Then, the virus solution was replaced with full growth medium and transduced cells were selected with puromycin for at least 3 days. After selection, the cells were cultivated in full growth medium without selection pressure und used for further experiments. Gene knockdown was induced by addition of 250 ng/ml doxycycline (Dox) (Ratiopharm, Ulm, Germany) for 72 h. For *in vivo* experiments LLC cells were transduced with virus containing pLKO.1 vector with Emerald green fluorescent protein (EmGFP) fused to the blasticidin (bsd) resistance gene (EmGFP-Bsd) that generated shHIF-1α GFP and shscrambled (shscr) GFP cells. Stability of the knockdown was controlled by WB and luciferase assay.

3.2.5 Radiation exposure and hypoxic treatment of cell cultures

Cells were irradiated with an X-ray irradiating machine X-RAD 320 (Xstrahl Ltd) operated at 320 kV, 12.5 mA with a 1.65 mm aluminium filter at a distance of 50 cm. Hypoxic treatments were performed in an airtight chamber (Toepffer Lab System) filled with a humidified mixture of 1 % O_2, 5 % CO_2, and balance N_2. For irradiation of hypoxic cells the culture flasks and plates were tightly sealed with parafilm in the hypoxic chamber and transported to the irradiation machine. After irradiation, the cells were immediately placed back into the hypoxic chamber.

3.2.6 Transfection of cells

Transient transfection was conducted using the transfection reagent Viafect (Promega, Madison, USA) in a ratio of 3:1 (µl reagent per µg DNA) as recommended by the manufacturer. Overexpression of mHIF-2α was achieved by transient transfection with 500 ng of the plasmid CMV-sport6-mHIF2α, using 500 ng of the empty vector pcDNA3 as a transfection control.

3.2.7 Dual-Luciferase reporter assay

To test the efficiency of the HIF-1α knockdown *in vitro*, 6 x 10^4 cells were seeded in 24-well plates. After 24 h the cells were transfected with 500 ng of the hypoxia-responsive firefly luciferase reporter plasmid pGLHIF1.3 which contains 3 copies of a HRE and 100 ng of the pGL4.74hR renilla reporter as a control for transfection efficiency. The transfection reagent Viafect (Promega) was used. 4 h after transfection, the cells were placed in the hypoxic chamber and incubated for another 24 h. Whole cell extracts were prepared using a passive

lysis buffer from the Dual-Luciferase Reporter Assay System (Promega) as recommended by the manufacturer. Firefly and renilla luciferase activities were detected with a GloMax luminometer (Promega). The ratio between renilla and firefly luciferase allows comparison of the expression levels of HIF-1α between separately transfected samples.

3.2.8 Sodium dodecyl sulfate polyacrylamide gel electrophoresis (SDS-PAGE)

For the preparation of whole cell lysates the cells were seeded in 6-well plates. After reaching 70-80 % confluence the cells were scratched from the well and washed with ice-cold PBS. The cells were then lysed in radioimmunoprecipitation assay (RIPA) lysis buffer containing proteinase/phosphatase inhibitors for 30 min at 4 °C. After centrifugation for 3 min at 4 °C and 19064 x *g* the supernatant was collected and stored at -80 °C. The protein concentration of cell extracts was determined using a BCA Protein Assay Kit (Thermo Fisher Scientific) in 96-well plates as recommended by the manufacturer. Bovine serum albumin (BSA) was used as a standard. After incubation for 20 min at 37 °C the absorbance of the samples was measured spectrophotometrically at 562 nm. Equal amounts of protein (10-20 µg) were mixed with SDS sample buffer and 1 µl DTT and boiled for 5 min at 95 °C. Cell lysates were then separated by gel electrophoresis using reducing 5 – 12.5 % separating SDS gels with 5 % stacking gels. SDS-PAGE was run at 120 V for approximately 1 h.

3.2.9 Western blotting (WB)

Protein transfer was performed using a Trans-Blot Turbo Transfer System with Trans-Blot® Turbo™ ready-to-assemble (RTA) Transfer Kit (Bio-Rad) as recommended by the manufacturer. The PVDF membrane was blocked with 5 % BSA in TBS-T for 1 h at room temperature and incubated with a primary antibody overnight. The HRP-conjugated secondary antibody was detected with SuperSignal West Femto Maximum Sensitivity Substrate (Thermo Fisher Scientific) using a Fusion FX7 chemoluminescence documentation system (Peqlab).

3.2.10 Cell cycle distribution

Cell cycle distribution was measured by fluorescence-activated cell sorting (FACS) analysis using only the cell nuclei. Therefore, the cell lysis was performed by incubation of 2 x 10^5 cells in 200 µl hypotonic citrate buffer for 30 min at 4 °C. After centrifugation, the cells were resuspended in 350 µl FACS buffer. Samples were analysed by flow cytometry with a FACS Canto II (BD Biosciencies) counting 10000 nuclei per sample. Data analysis was performed

by discrimination gating of phycoerythrin (PE)-area versus PE-width in linear area with BD FACSDiva software.

3.2.11 Colony formation assay

The clonogenic assay was used to monitor cell survival after exposure of cells to increasing doses of radiation. Cells were seeded in T25 flasks, incubated for 48 h with Dox and then exposed to hypoxia for 24 h in the presence of Dox. After IR with 0-10 Gy, cells were incubated in Hx for another 24 h. After the incubation, the cells were trypsinized and seeded in 6-well plates at various densities (100-6400 cells per well). Following 7-10 days of incubation under normoxic conditions, the colonies were fixed with 0.25 % paraformaldehyde, permeabilized with 70 % ethanol and stained with Coomassie Brilliant Blue solution. Colonies of more than 50 cells were counted with ImageJ using a colony area plug-in. Survival fractions (SF) were quantified as number of colonies divided by the plating efficiency multiplied with the number of cells seeded.

3.2.12 Caspase assay

Caspase-3 activity was measured for quantification of apoptosis. The assay is based on the caspase-3 specific cleavage reaction of caspase-3 substrate N-acetyl-Asp-Glu-Val-Asp (DEVD) from N-acetyl-Asp-Glu-Val-Asp-7-amino-4-methylcoumarin (DEVD-AMC), which leads to the release of fluorescent 7-amino-4-methylcoumarin (AMC). Thus, the fluorescence intensity of AMC correlates with the activity of caspase-3 (Garcia-Calvo et al., 1999).

Cells were lysed in caspase lysis buffer containing protease and phosphatase inhibitors. After incubation on ice for 45 min and a subsequent centrifugation step for 3 min at 4 °C and 19064 x *g* the protein concentration of the supernatant was measured using a BCA Kit (Thermo Fisher Scientific). 10-20 µg of protein were incubated with 66 µM DEVD-AMC and 10 mM DTT in caspase substrate buffer at 37 °C. Release of fluorescent AMC was measured every 10 min at an excitation wavelength of 360 nm and emission of 460 nm for 2.5 hours. The results from the linear range of the reaction were used for analysis.

3.2.13 Immunofluorescent staining

To study the nuclear localization of DNA repair proteins, 5 x 10^3 LLC cells were seeded onto glass coverslips coated with rat collagen-I (Biozol, Eching, Germany). After Dox and Hx treatment and exposure to 5 Gy IR, the cells were fixed with 1 % paraformaldehyde for 10 min at the indicated time points. Cells were washed with PBS, incubated at room

temperature in 0.2 % Triton-X100 for 5 min, washed again, and incubated with PBS containing 2 % BSA for 1 h at room temperature or overnight at 4 °C. Cells were then incubated with a primary antibody diluted as indicated in Table 9 with the addition of 2 % BSA for 1.5 h, washed, and incubated in a 1:500 dilution of an appropriate secondary antibody labelled with a fluorescent dye. After washing, the cells were counterstained with 1.5 µM Hoechst 33342 (Sigma-Aldrich, Munich, Germany) suspended in PBS and mounted with coverslips using mounting medium (Dako, Santa Clara, USA). Images were taken using a Zeiss LSM 710 confocal microscope with a 63x/1.4 oil immersion lens (under the control of ZEN software). Automated image analysis was processed with the open source software Cell Profiler.

3.2.14 Pulsed field gel electrophoresis

Cells were irradiated with 20 Gy and trypsinized at the indicated time points. All steps were performed in a cold chamber at 4 °C. The cells were resuspended in PFGE serum-free HEPES-buffered DMEM medium. 6 x 10^6 cells were mixed with an equal volume of 1 % warm (50 °C) low melt agarose (Bio-Rad, Munich, Germany). The cell suspension was filled into 3 mm thin glass tubes, cooled down on ice, pulled out from the tubes and cut into plugs that had a length of 5 mm. The agarose cell plugs were incubated in PFGE lysis buffer with freshly added 0.2 mg/ml protease A for 1 h at 4 °C and then for 18 h at 50 °C. Next, the plugs were washed with PFGE washing buffer for 1 h at 37 °C and digested with washing buffer with freshly added 0.1 mg/ml RNAseA for 1 h at 37 °C. Subsequently, the plugs were prestained with 2 µg/ml ethidium bromide suspended in washing buffer for 2 h at 37 °C. The cell plugs were then placed into the slots of a 0.5 % agarose gel and covered with a 1 % standard agarose gel. PFGE was run in 0.5 x TBE at 8 °C for 40 h with a pulsed electric field at 50 V (1.25 V/cm) for 900 s in the forward direction and 200 V (5.00 V/cm) for 75 s in the reverse direction. The gel was then scanned using a fluorescence imager Typhoon 9400. The fraction of DNA release was analysed by ImageQuant 5.2.

3.3 Methods *in vivo*

3.3.1 Ethic statement

All animal experiments were carried out in accordance with the guidelines of the National Institutes of Health. Animal protocols were approved by the State Office of North Rhine-Westphalia for Nature, Environment and Consumer Protection (Landesamt für Natur, Umwelt und Verbraucherschutz, LANUV) with reference numbers Az. 87-51.04.2010.A343 and Az. 84-02.04.2015.A243.

3.3.2 Mouse keeping and breeding

All mice were kept under controlled conditions in the central animal facility (Zentrales Tier-Laboratorium, ZTL) of the University Hospital Essen. Food and water were provided *ad libitum*. Not more than 5 animals were kept together in an individually ventilated cage (IVC) (Sealsafe Blue Line) with a constant temperature of 20 °C and 12 h day-night rhythm.

C57BL/6 mice were obtained from Harlan (Horst, Netherlands). B6.129-*Hif1a*^{tmRsjo}/J or HIF-1α^{flox} mice were originally generated by the research team of Randall S. Johnson (University of San Diego, California, USA) and distributed by Jackson Laboratory (Bar Harbor, USA, JAX stock #007561), and are carrying a loxP-flanked exon 2 of HIF-1α (Ryan et al., 2000). Homozygous HIF-1α^{flox} mice (HIF-1α$^{fl/fl}$) are viable, fertile, normal in size and do not display any gross physical or behavioral abnormalities.

C57BL/6-*Gt(ROSA)26Sor*$^{tm9(Cre/ESR1)Arte}$ or ROSA26Cre-ER mice were used in co-operation with the team of E. Gulbins (University Hospital Essen). These mice were originally developed by Artemis Pharmaceuticals (now Taconic, Germany) by a targeted knock-in mutation of the high affinity CreER^{T2} into the Gt(ROSA)26 locus. CreER^{T2} was developed by fusion of the bacteriophage P1 (Cre) gene to the high affinity estrogen receptor gene ESR1 and is expressed ubiquitously under the control of the Gt(ROSA)26Sor reporter (Seibler et al., 2003).

ROSA26Cre-ER mice (homozygous for the knock-in gene, ki/ki) were crossed with HIF-1α^{flox} mice (homozygous for the transgene, fl/fl) to generate the heterozygous F1 progeny (HIF-1α$^{fl/wt}$Cre-ER$^{ki/wt}$), which were crossed again with homozygous HIF-1α$^{fl/fl}$ mice. The F2 progeny with a HIF-1α$^{fl/fl}$Cre-ER$^{ki/wt}$ genotype were selected and used for cross-breeding with homozygous HIF-1α$^{fl/fl}$ mice. The F3 progeny contained approximately 50 % of

HIF-1α$^{fl/fl}$Cre-ER$^{ki/wt}$ (heterozygous for the Cre-ER knock-in) and 50 % of HIF-1α$^{fl/fl}$Cre-ER$^{wt/wt}$ (negative for the Cre-ER knock-in) (Figure 7).

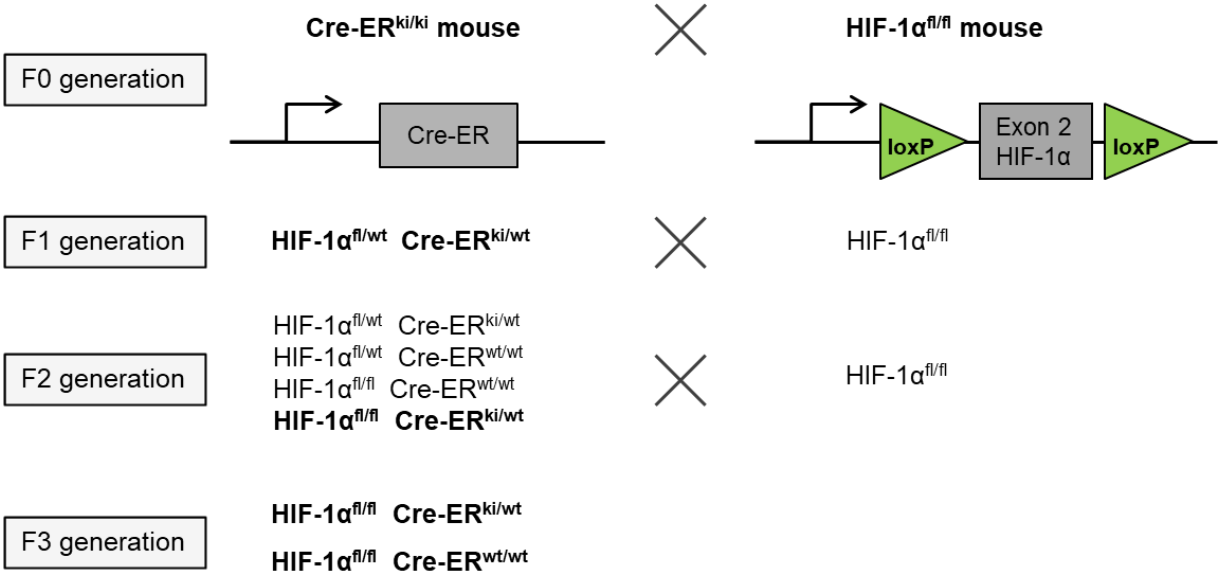

Figure 7: Scheme for mouse breeding.

Homozygous ROSA26Cre-ER mice were crossed to homozygous HIF-1α$^{fl/fl}$ mice to generate the heterozygous F1 progeny (HIF-1α$^{fl/wt}$Cre-ER$^{ki/wt}$). The Exon 2 of HIF-1α$^{fl/fl}$ mice is flanked with loxP sites, ROSA26Cre-ER mice have a mutated estrogen receptor which can be activated by treatment with the synthetic estrogen receptor antagonist tamoxifen. HIF-1α$^{fl/wt}$Cre-ER$^{ki/wt}$ mice from F1 generation, as well as HIF-1α$^{fl/fl}$Cre-ER$^{ki/wt}$ mice from the F2 generation were cross-bred with homozygous HIF-1α$^{fl/fl}$ mice to obtain the HIF-1α$^{fl/fl}$Cre-ER$^{ki/wt}$ and HIF-1α$^{fl/fl}$Cre-ER$^{wt/wt}$ mice in the F3 generation.

3.3.3 Genotyping of animals

3.3.3.1 DNA extraction from ear biopsy

Genotyping of mice was performed using ear biopsies which were a product of ear punching for mouse identification. DNA extraction from ear biopsies were performed with Direct PCR Kit (highQu) by addition of 20 µl lysis buffer, 10 µl protease buffer and 70 µl nuclease-free water to the sample as recommended by the manufacturer. For lysis, the samples were incubated for 5 min at 75 °C on a shaker. After the incubation, the protease was inactivated by heating the samples to 95 °C for 10 min. The samples with genomic DNA were then diluted 1:10 in nuclease-free water and stored at -20 °C until further examination.

3.3.3.2 End-point PCR for genotyping

The amplification of DNA fragments for mouse genotyping was performed using the Direct PCR Kit. A mixture of oligonucleotides (forward and reverse, 1 µM each), 2x Red Tag Mastermix, nuclease-free water and 1 µl of extracted genomic DNA solution were placed in the PCR cycler. The settings for the PCR were: 1x (initial denaturation: 2 min, 95 °C), 40 cycles of: denaturation (15 sec at 95 °C), annealing (15 sec at 55-65 °C (depending on the length of the amplicon)) and extension (90 sec at 72 °C).

For the analysis of Cre-ER knock-in genotype, ROSA26-Cre-ER oligonucleotides were used. Determination of heterozygous or homozygous status of HIF-1α^{flox} mice was performed using mHIF-1α_flox primer (see Table 7). Analysis of tamoxifen-induced excision of exon 2 of HIF-1α was performed by end-point PCR with mHIF-1α_E2seq primers (see Table 7). The PCR product was additionally analysed by sequencing (LGC Genomics, Berlin, Germany).

3.3.3.3 Agarose gel electrophoresis

The length of PCR products was analyzed by DNA fragment separation using agarose gel electrophoresis. An agarose gel was prepared by dissolving 3 % agarose powder in TAE buffer. SYBR Green nucleic acid stain was added to the gel for DNA staining. Gel electrophoresis was run in TAE at room temperature for 45 min at 75 V. The DNA fragments were then visualized using a Fusion-FX7 system (Peqlab).

3.3.4 Administration of tamoxifen

Tamoxifen (Tam) was dissolved in corn oil and 10 % of ethanol with a final concentration of 80 mg/ml and incubated overnight on a shaker at 37 °C. The aliquots were stored at -20 °C for up to 4 weeks. For oral administration the solution was thawed at 37 °C and 4 mg or 50 µl were administered to the mice by a feeding needle for 5 consecutive days. Analysis of the efficiency of tamoxifen-induced recombination was performed 2 weeks after treatment.

3.3.5 Tumor injection

Before injection, excess fur was shaved from the left flanks of recipient mice. The mice were then given a subcutaneous injection of 150 µl matrigel (BD Biosciences, Franklin Lakes, USA) containing 5x 10^5 LLC shHIF-1α GFP or LLC shscr GFP cells in the left flank.

3.3.6 Irradiation of animals

Mice were irradiated with the X-ray research irradiator cabinet RS320 operated at 300 kV, 10 mA at a distance of 50 cm and 1.733 Gy/min. During the irradiation mice were anesthetized with a mixture of 100 mg/kg$_{mouse}$ ketamine and 5 mg/kg$_{mouse}$ xylazine in NaCl and placed in irradiation protection containers made of brass (Figure 8). These protection containers were designed to shield the whole mouse body from radiation, except for the flank tumors which protrude from the special aperture of the container. Additionally, the 6 mm thick upper cover made of lead was placed on the containers to assure best possible protection of the mice from X-rays.

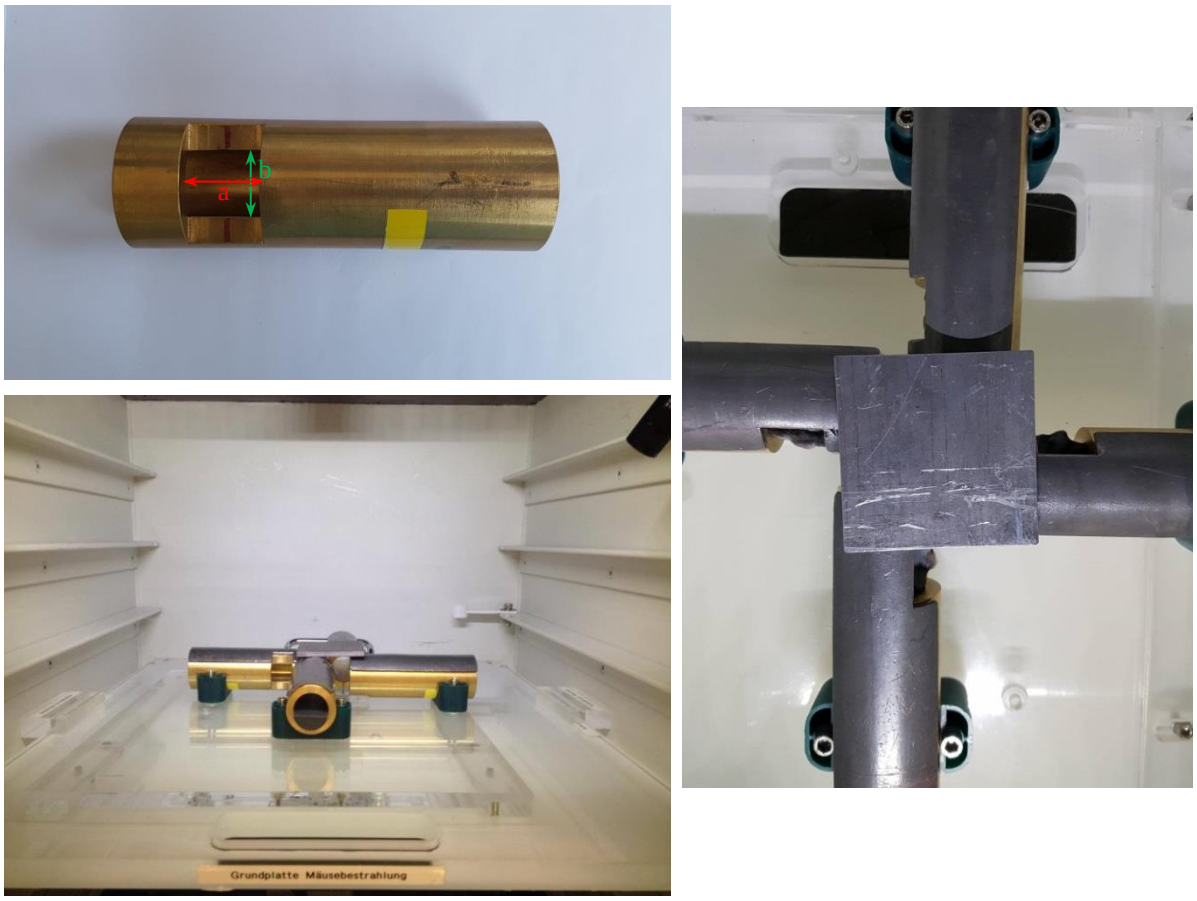

Figure 8: *In vivo* setup for irradiation of animals.
The radiation containers were optimized for the appropriate size of the aperture (a=22 mm, b=21 mm). Four containers were fixed on the radiation plate and covered with a lead plate. Anaesthetized mice were placed in the containers so that only the tumors which were protruding through the aperture were irradiated.

3.3.7 Monitoring of tumor growth and tumor removal

Tumor growth was monitored every 2 days by exact measurement of the length, width and depth of tumor using a digital caliper. The tumor volume was calculated as $\frac{\text{length}\times\text{width}\times\text{depth}}{2}$. After an ulceration of a tumor or after reaching 20 days post tumor injection the mice were sacrificed by cervical dislocation. Approximately 1 h before euthanizing, mice were given an i.p. injection of pimonidazole (60 µg/kg_{mouse}). Pimonidazole is a 2-nitroimidazole that is reductively activated specifically in hypoxic cells and forms stable adducts with thiol groups in proteins and amino acids (Varia et al., 1998). Therefore, pimonidazole is a hypoxia marker as it is directly correlated to the extent of hypoxic regions in the tumor. After tumor excision, one third of the tumor was immediately placed into liquid nitrogen and stored at -80 °C for further analysis by qPCR or WB. The remaining part of the dissected tumor was fixed with 4 % PFA overnight at 4 °C for paraffin embedding.

3.3.8 Isolation of murine splenocytes

Mice were sacrificed and spleens were removed and washed in chilled PBS. The spleen was sliced into fragments with scissors and placed in a 70 µl strainer attached to a 50 ml conical tube. Using the plunger end of a syringe, the spleen was pressed through the strainer. The cell solutions were centrifuged at 280 x *g* for 4 min. For the lysis of erythrocytes, cell pellets were resuspended in 1 ml of ACK buffer and incubated on ice for 5 min. The reaction was then stopped by addition of 9 ml PBS, followed by centrifugation and resuspension in 10 ml RPMI medium supplemented with 10 % FBS and 100 µg/ml Pen/Strep.

3.3.9 Immunohistochemistry (IHC)

After fixation with 4 % PFA overnight at 4 °C the tumors were dehydrated through graded alcohols (two changes of 70 % ethanol, 2 changes of 96 % ethanol, 2 changes of isopropanol, for 1 h each) and cleared with xylene (2 changes, first overnight, second for 1 h). Subsequently, the tissue samples were incubated in paraffin (two changes for 1 h each) and embedded in a paraffin block. The paraffin tissue block can either be stored at room temperature for years or directly used for IHC to visualize expression of specific proteins in the context of tissue morphology. Paraffin-embedded tumors were cut into 4-5 µm sections with a microtome. Antibody staining requires the removal of paraffin and rehydration of the samples. For deparaffination the slides were placed in 2 containers of xylene for 5 min each. The tissue was rehydrated through graded alcohols (100 %, 100 %, 70 %, 50 % ethanol) for

3 min each. PFA fixation of tissue leads to the development of protein cross-links, which can mask the epitopes. Therefore, a heat-induced antigen retrieval was performed with citrate buffer for 20 min at 95 °C to recover antigen reactivity and to improve protein detection (Yamashita, 2007). To avoid high background staining, endogenous peroxidases were quenched by incubation in 3 % H_2O_2 for 20 min and washed with TBS. Using a hydrophobic pen a circle around the sample was drawn to decrease the volume of antibody solution. To prevent non-specific binding of the antibody, the slides were blocked in antibody diluent solution with 2 % BSA for 1 h at room temperature in a humidified chamber. Then, the slides were stained with primary antibody for 2 h at room temperature or overnight at 4 °C in a humidified chamber. After a washing step with TBS, the slides were stained with the secondary HRP-linked antibody for 2 h at room temperature in a humidified chamber. Subsequently, the slides were stained with diaminobenzidine (DAB) chromogen for 10-60 s and counterstained with hematoxylin for 20 s. After dehydration through graded alcohols (50 %, 70 %, 100 %, 100 % ethanol) for 3 min each and incubation in xylene twice for 5 min each, the coverslips were mounted onto the slides using Entellan (Merck), carefully avoiding any introduction of bubbles. Slides were analyzed using a ScanScope light microscope (Leica Biosystems).

3.3.10 RNA isolation

The most crucial requirement for RNA isolation is a ribonuclease-free (RNase-free) environment. RNAses are difficult to inactivate and may obscure the results. To prevent RNase contamination, sterile techniques, reagents and disposable plasticware were used and gloves were worn at all time. All surfaces were cleaned with RNase decontamination solution and diethyl pyrocarbonate (DEPC) water was used for dilution steps.

The isolation of RNA from tumor tissue was performed as recommended by the manufacturer of ReliaPrep RNA Tissue Miniprep System (Promega). Briefly, LBA buffer with 1-thioglycerol (LBA-TG) was added to the frozen tissue which was then extensively homogenized with a dounce tissue grinder set. After a centrifugation step at 14 000 x *g* for 3 min, the eluate was transferred to a new tube. Following an incubation with 100 % isopropanol for 5 s, the lysate was transferred into a minicolumn which was placed in a collection tube and centrifuged at 14 000 x *g* for 1 min. The RNA wash solution was added to the minicolumn and centrifuged twice for 15 s and 30 s. Then the minicolumn was transferred to a new collection tube and washed again. Finally, the total RNA was eluted from the column by addition of nuclease-free water and centrifugation at 14 000 x *g* for 1 min. The RNA

samples were stored at -80 °C. The concentration of RNA was determined using the Take3 Micro-Volume Plate and the Synergy HT Multi-Detection Microplate Reader (Biotek). The purity of the RNA after isolation was analysed using RNA gel electrophoresis. 2 µg of RNA with 2x RNA loading buffer were placed into the slots of a 1 % RNA gel. Gel electrophoresis was run in 1x MOPS buffer at room temperature for 1 h at 100 V. The RNA was then visualized using a Fusion-FX7 system (Peqlab).

3.3.11 Reverse transcription of RNA

Reverse transcription (RT), a process of generating complementary DNA (cDNA) from an RNA template, is required prior to the quantitative PCR (qPCR) gene expression assay. In order to obtain accurate results by qPCR genomic DNA (gDNA) must be eliminated. RT of RNA samples was performed as recommended by the manufacturer of QuantiTect Reverse Transcription Kit (Qiagen). Briefly, for gDNA elimination 2 µg of RNA, 4 µl gDNA Wipeout Buffer and DEPC water with a total volume of 28 µl were incubated for 2 min at 42 °C. Subsequently, 28 µl of template RNA was mixed with 2 µl RT Mastermix, 2 µl RT buffer and 2 µl RT primers for cDNA synthesis. RT was performed by incubation at 42 °C for 20 min, followed by heat-treatment at 95 °C for 3 min to inactivate the RT enzyme. The cDNA samples were stored at -20 °C or used for qPCR.

3.3.12 qPCR gene expression assay

The essential difference of qPCR compared to standard PCR is the measurement of a fluorescent reporter dye which increases in line with the sample amount. This reaction was also named ‘real-time’ because of the live monitoring of the reaction progress. Quantitative PCR gene expression assay was performed as recommended by the manufacturer of MESA Green qPCR^{TM} Mastermix Plus for SYBR Assay (Eurogentec). Briefly, 5 µl (50 ng) of cDNA was mixed with 10 µl 2x reaction buffer, oligonucleotides (see Table 8, forward and reverse, 0.6 µl each) and DEPC water with a total volume of 20 µl. The 96-well plate was placed into a C1000 Touch Thermal Cycle CFX96 Real-Time System with the following settings: 5 min at 95 °C, 45 cycles with 95 °C for 15 sec and 60 °C for 1 min, 30 cycles melting curve from 65 °C for 5 sec +1°C/cycle. RT_mB2M (ß2-microglobuline) was used as a housekeeping gene for qPCR, as it has a most stable expression level among frequently used reference genes (Matsuzaki et al., 2015). The oligonucleotides for genes of interest (GOFs) were used as listed in Table 8. The threshold cycle (ct) is defined as a cycle at which the fluorescence level reaches a certain amount. The ct values of control RNA samples were analyzed by qPCR

simultaneously with the target gene. The expression value of the target gene was normalized to the ct value for B2M using the ΔΔct method. The log base 2 of this value ($2^{-\Delta\Delta ct}$) was used to determine the expression fold change (Livak and Schmittgen, 2001).

$$2^{-\Delta\Delta ct} = 2^{-(\Delta ct(GOF_{sample} - B2M_{sample}) - \Delta ct(GOF_{control} - B2M_{control}))}$$

The specificity of PCR products was controlled by analysis of the melting curves of the products.

3.3.13 Statistical analysis

All statistical analyses were performed using Graphpad Prism 6 and one-way or two-way analysis of variance ANOVA with post-hoc Bonferroni test. Data are presented as mean ± standard deviation (SD), significance is presented as * $p<0.05$, ** $p<0.01$, *** $p<0.001$.

4 Results

4.1 In vitro

4.1.1 Generation of a doxycycline-inducible HIF-1α KD

Previous studies have indicated the involvement of HIF-1α in adaptation and survival of cells under hypoxic conditions and its interaction of proteins which are involved in DNA damage repair (Rohwer et al., 2013). In this study, the effect of HIF-1α on radiation sensitivity and cell survival was first analyzed *in vitro*. For this reason, a doxycycline-inducible (Dox) HIF-1α knockdown (KD) was generated in LLC cells using a lentiviral approach (LLC shHIF-1α Tet-On). The advantage of the Dox-inducible system is that it can be induced with a high temporal precision avoiding the adaptation of cells. The efficacy of the HIF-1α KD was analyzed by WB with a HIF-1α antibody, which demonstrated a significant decrease of HIF-1α protein amount in the cells 72 h after treatment with Dox and 12 h Hx (Figure. 9 A). An additional KD test was performed using a luciferase assay where a firefly luciferase was under control of three HREs. The data demonstrated reduction to approximately 20 % of HIF-1α activity after Dox treatment under hypoxic conditions (Figure 9 B). Both results showed a significant reduction in HIF-1α after KD.

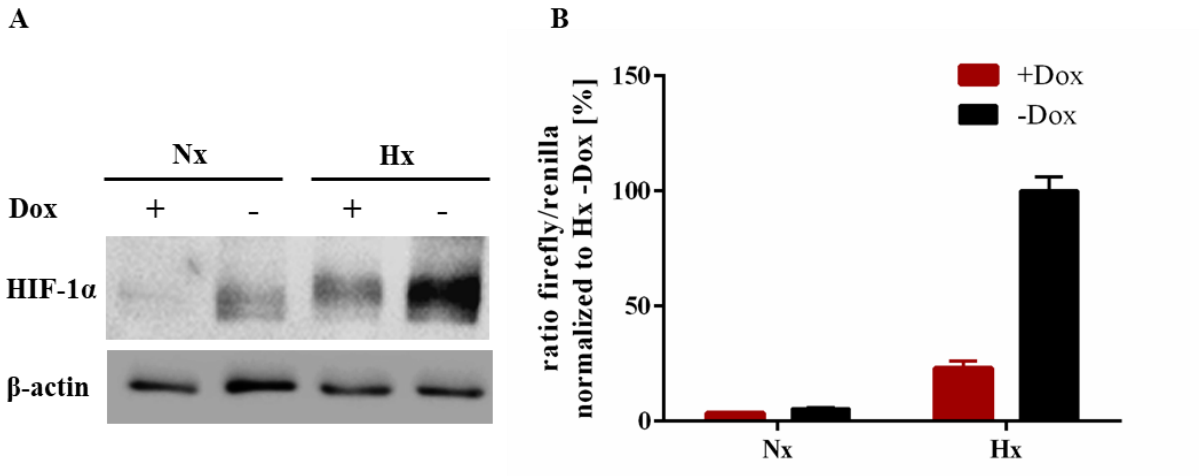

Figure 9: Generation of doxycycline-inducible HIF-1α knockdown (KD) in Lewis Lung Carcinoma (LLC) cells

A) HIF-1α WB displayed a reduction of the protein amount 72 h after Dox-treatment and 12 h Hx incubation. **B)** Luciferase assays demonstrated HIF-1α activity normalized to hypoxic cells without Dox treatment.

For further experiments, it was essential to prove the suitability of the KD tool and to investigate whether Dox treatment has an impact on cell cycle distribution. We used LLC cells tranduced with lentiviral particles which led to production of shRNA that targeted HIF-1α (shHIF-1α) for KD and LLCs transduced with non-target shscrambled RNA (shscr) with a Dox-inducible (Tet-On) promoter or a constitutively active shRNA expressing system to examine unspecific effects of Dox treatment. The possible alterations in the cell phenotype were analyzed by FACS after staining the cells with PI. The cell cycle distribution of cells treated with Dox did not show any differences compared to untreated cells, demonstrating that treatment with Dox alone did not affect the cells (Figure 10). Therefore, this HIF-1α KD tool was used for further *in vitro* experiments.

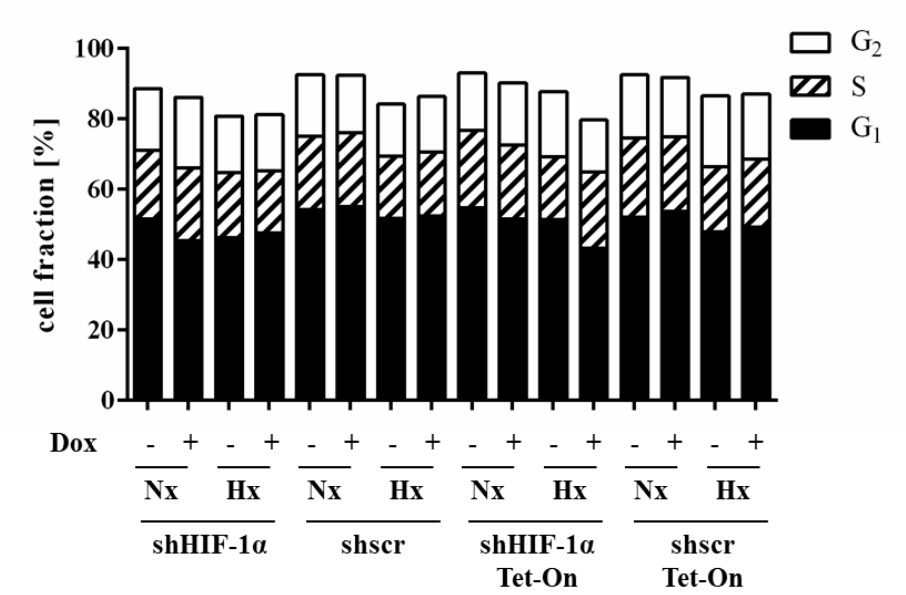

Figure 10: Analysis of unspecific effects of Dox treatment on cell cycle distribution of LLC cells
LLC cells with HIF-1α KD (shHIF-1α) and a non-target shRNA (shscr) with a constitutive or a Dox-inducible (Tet-On) system were treated for 72 h with Dox. FACS data with PI stained cells were analyzed based on distribution of the cells in the G_2, S and G_1 phase. The data demonstrated that Dox treatment did not affect the cell cycle in an unspecific way.

In addition, LLC cells were chosen for further experiments because of another special feature: previous results of our group demonstrated that HIF-2α is not expressed in LLC cells, neither on the protein nor on the mRNA level (data not shown), which makes these cells most suitable for our investigation of the specific role of HIF-1α in response to radiation treatment.

4.1.2 Effect of HIF-1α knockdown on apoptosis after IR

In previous studies HIF-1α was described as a mediator of radioresistance in cancer cells. Thus, in this study the effect of HIF-1α on radiosensitivity was first investigated by analysis of apoptosis after irradiation of the cells. LLC cells have been reported to be highly radiosensitive, hence the radiation dose of 5 Gy was chosen for IR treatment.

To investigate the effect of HIF-1α KD on apoptosis, WB was performed using a poly [ADP-ribose] polymerase 1 (PARP-1) antibody which detects endogenous levels of full length PARP-1, as well as the large PARP cleavage fragment. PARP-1 is involved in the process of apoptosis and acts as a substrate for caspase-3 and caspase-7. Thus, PARP-1 cleavage fragments serve as a signature of apoptotic cell-death inducing proteases (Chaitanya et al., 2010). Apoptosis was investigated in LLC HIF-1α KD cells after 48 h Hx and 5 Gy IR. The data demonstrated an increased PARP cleavage in HIF-1α-depleted cells within the first 8 h after IR (Figure 11 A). Interestingly, the HIF-1α KD cells showed a moderate induction of PARP cleavage without radiation treatment.

To confirm these results, the analysis of pro-apoptotic caspase-3 activity was performed by caspase-3 assays. The samples were treated with Dox for 72 h, incubated for 48 h under Hx and then collected during the 24 h after IR with 5 Gy. The analysis of caspase-3 activity demonstrated an increase of apoptosis in HIF-1α KD cells after IR (Figure 11 B). Caspase-3 activity was already increased after HIF-1α KD without radiation treatment; a stronger effect was detected 8 h after IR.

To better understand the mechanism behind the demonstrated increase of apoptosis in HIF-1α depleted cells, cell cycle distribution was also analysed after radiation treatment in HIF-1α KD (Figure 11 C). PI staining and subsequent FACS analysis demonstrated a detectable increase (approximately 10 %) in the G_2 population 6 h after irradiation with 5 Gy in cells incubated for 24 h in Hx. Furthermore, there was an increase of the G_1 population 24 h after IR. Importantly, the cell cycle distribution between HIF-1α-depleted and Dox-untreated cells remained unchanged.

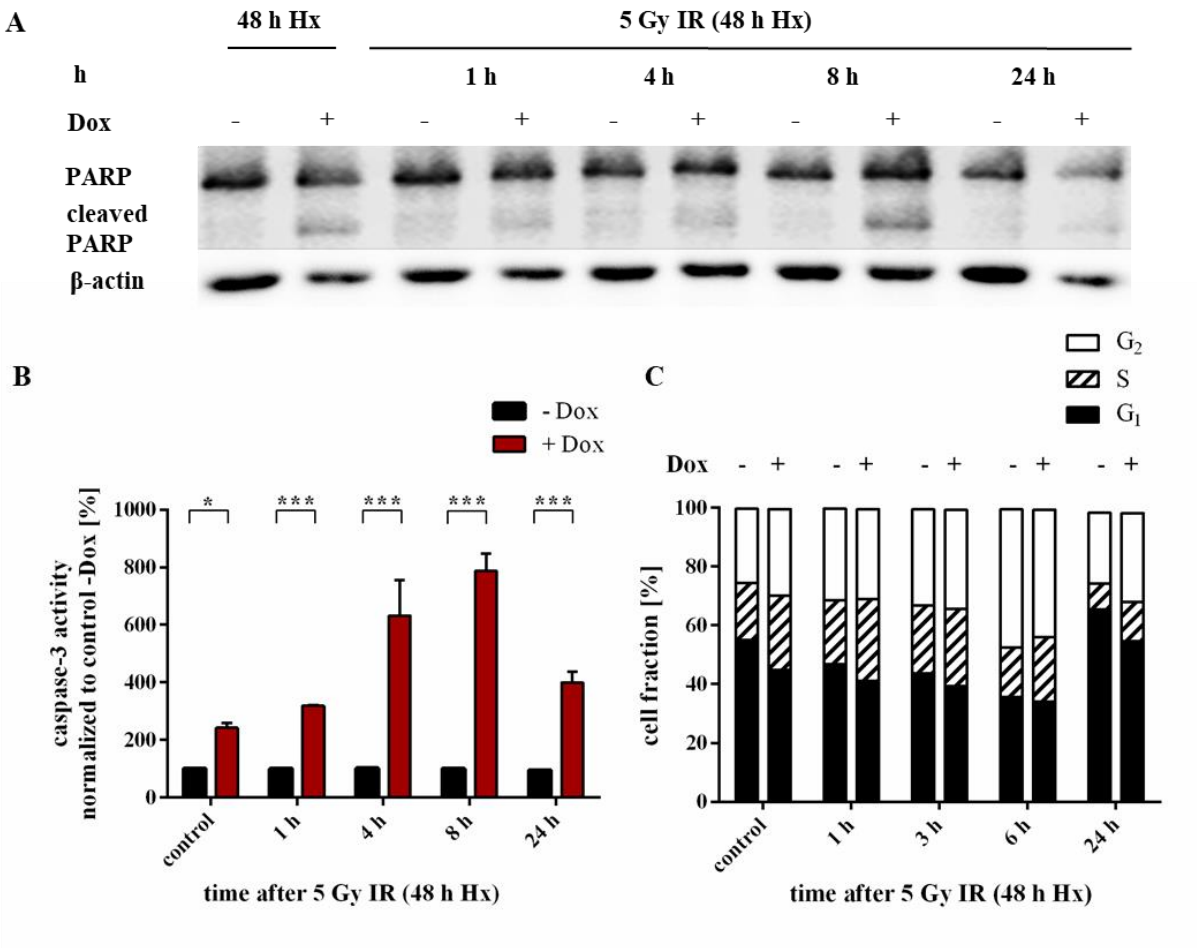

Figure 11: Apoptosis and cell cycle distribution after IR in LLC HIF-1α KD cells

A) PARP-1 WB was performed to investigate the apoptosis. Cells were incubated 48 h in Hx and irradiated with 5 Gy. The data displayed an increased PARP-1 cleavage, a marker for cell death, in the HIF-1α-depleted cells. **B)** Activity of apoptotic caspase-3 was measured in the HIF-1α KD cells during first 24 h after 48 h incubation under Hx and 5 Gy IR. The data demonstrated an increase of caspase-3 activity in HIF-1α KD cells. **C)** FACS analysis of the PI staining demonstrated an unchanged cell cycle distribution between HIF-KD and Dox-untreated cells.

To examine whether the demonstrated increase of apoptosis in HIF-1α KD cells is cell-line specific, the caspase-3 assay was also performed with murine B16F10 cells with Dox-inducible HIF-1α KD (B16F10 shHIF Tet-On) and human HCT116 with a constitutive HIF-1α KD (HCT116 shHIF-1α). These cells were treated in the same way as the LLC cells, except for the radiation dose. Melanoma cells B16F10 are highly radioresistant and were irradiated with 20 Gy; irradiation of these cells with 5 Gy did not induce any response. HCT116 were usually irradiated with 10 Gy, which consistently induced a substantial response. Interestingly, the analysis of caspase-3 activity did not demonstrate a significant

difference in HCT116 HIF-1α deficient cells after Hx for 36 h and IR, while B16F10 cells with HIF-1α KD displayed an increase 24 h after IR (Figure 12).

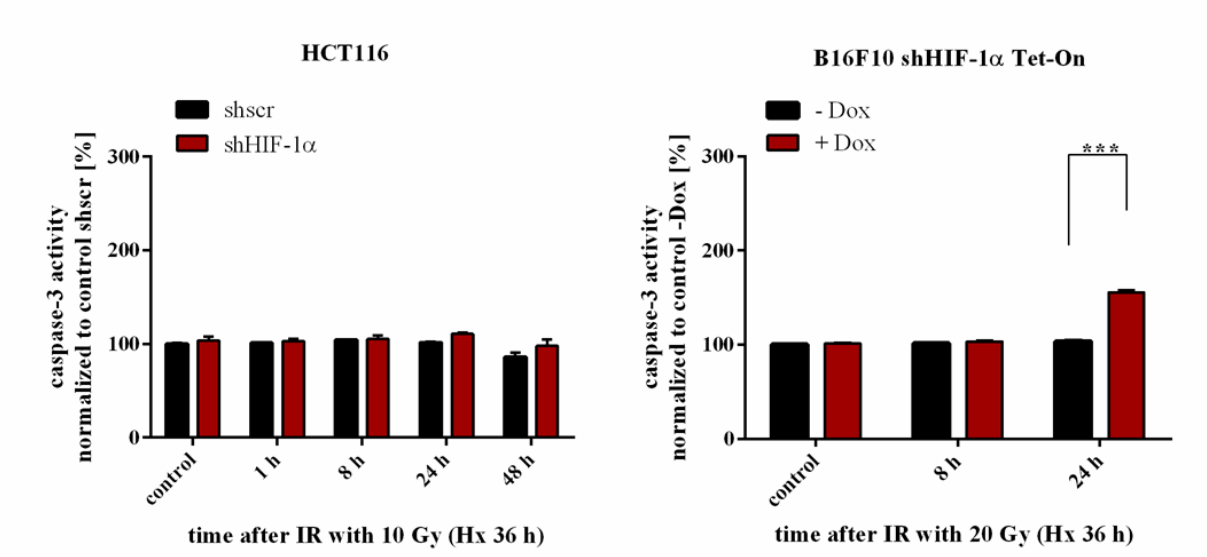

Figure 12: Effect of HIF-1α KD on apoptosis in HCT116 and B16F10 cells

Analysis of caspase-3 activity in **A)** human HCT116 cell with a constitutive HIF-1α KD (shHIF-1α and shscr as a control) and in **B)** murine B16F10 cells with Dox-inducible HIF-1α KD (shHIF-1α Tet-On) was performed after incubation under Hx for 36 h and irradiation with 10 Gy for HCT116 and 20 Gy for B16F10 cells. The data did not demonstrate a significant difference in caspase-3 activity in HIF-1α depleted cells.

These results implie that HIF-1α KD effect on apoptosis was specific for HIF-2α deficient LLC cells. To prove this hypothesis, the LLC cells with HIF-1α KD and induced overexpression of HIF-2α were investigated. The LLC HIF-1α KD cells were transfected with the pCMV-sport6-mHIF-2α plasmid or the empty vector pcDNA3 as a transfection control. The efficacy of the transfection and HIF-2α overexpression was analyzed by HIF-2α WB that demonstrated an increased amount of HIF-2α in the cells transfected with an overexpression plasmid (Figure 13 B). In addition the untreated control cells displayed the absence of HIF-2α in LLC cells, confirming the previous findings of our group. Afterwards, the effect of HIF-1α KD and HIF-2α overexpression in LLC cells were analyzed with respect to apoptosis. Therefore, the caspase-3 assay was performed after Hx for 48 h and irradiation with 5 Gy. Cells were analyzed 8 h after IR, because previous data (Fig. X) demonstrated the highest rate of caspase-3 activity for LLC cells at this time point. The data from Figure 13 A displayed a significant increase of caspase-3 activity in the irradiated cells with HIF-1α KD compared to

the non-irradiated group, confirming the previous results. However, the overexpression of HIF-2α did not affect the caspase-3 activity in the cells.

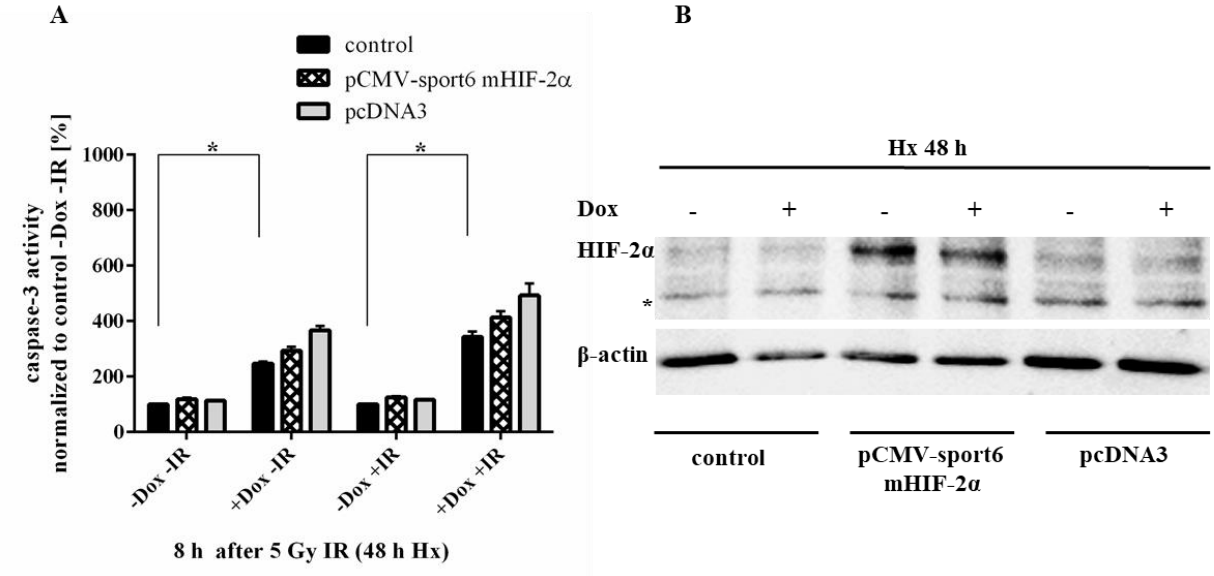

Figure 13: Effect of HIF-2α overexpression on the apoptosis in LLC cells

A) LLC HIF-1α KD cells were transfected with pCMV-sport6-mHIF2a plasmid. After Hx for 48 h and irradiation with 5 Gy cells were analyzed by caspase-3 assay at a time point of 8 h after IR. The caspase-3 activity in the cells with HIF-2α overexpression did not differ from the control cells. **B)** HIF-2α WB was performed to examine the efficacy of cell transfection with CMV-sport6-mHIF-2α plasmid. The specific HIF-2α band was detected at 118 kDa in lysates from cells with HIF-2α overexpression, * unspecific band

4.1.3 Effect of HIF-1α KD on the long term cell survival

To analyze the effect of HIF-1α depletion on cell survival beyond 24 h, the clonogenic survival assay with delayed plating was performed (Figure 14). This assay measures the ability of the single cell to repair the induced DNA damage and proliferate to a cell colony. LLC HIF-1α KD cells were incubated for 12 h in Hx, irradiated with 0-10 Gy, afterwards incubated again in Hx for 24 h and then seeded at various densities. HIF-1α KD cells demonstrated a decrease in the mean survival fraction after irradiation with 6 Gy or higher doses, with a significant difference ($p < 0.05$) at 6 Gy.

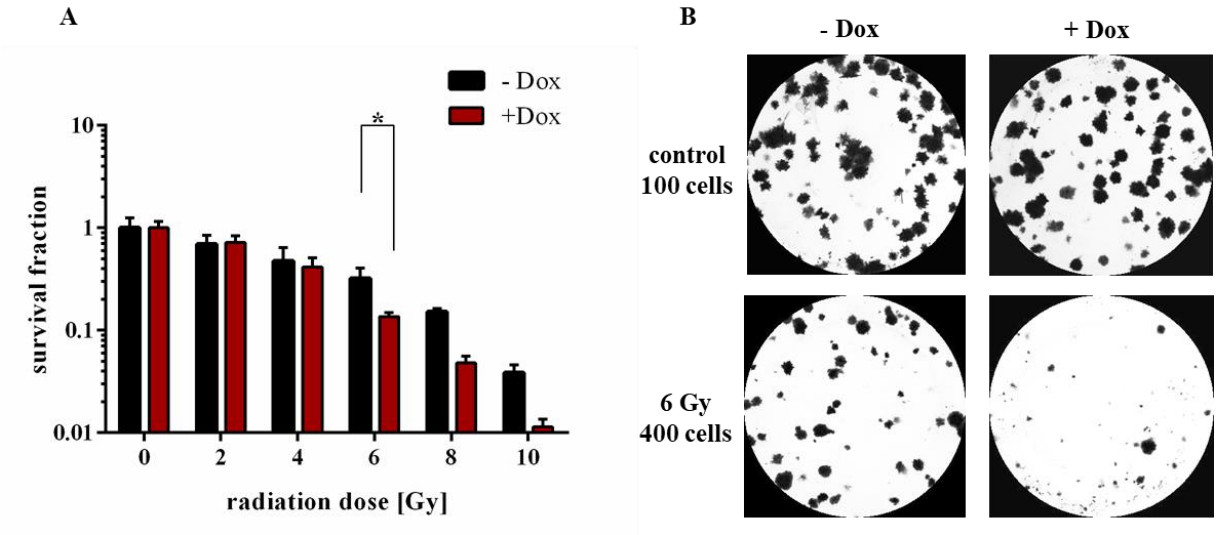

Figure 14: Impact of HIF-1α depletion on long term survival in LLC cells

A) Colony formation assay was performed with HIF-1α KD cells after incubation for 12 h in Hx, IR with 0-10 Gy, 24 h Hx and then seeding the cells at the indicated cell densities. Graph demonstrated a decreased survival of HIF-1α depleted cells with a significant difference after irradiation with 6 Gy 10 days after seeding. **B)** The representative picture showed the cell colonies of performed assay after IR with 6 Gy.

The data showed a decrease in cell survival and indicated that HIF-1α KD affects the DDR mechanisms by preventing a successful repair and/or ongoing proliferation of the irradiated cells. The next task of this study was to investigate the effect of HIF-1α on the repair of IR-induced DSBs.

4.1.4 Alterations in DNA repair mechanism in HIF-1α KD cells

There is evidence that hypoxia mediates an alteration of the DDR and repair abilities of cells causing genomic instability followed by an increase of cell radioresistance by radiation treatment (Bristow and Hill, 2008). Furthermore, some studies indicate the interaction of HIF-1α with factors which are involved in DDR and checkpoint control (Rohwer et al., 2013). To prove this hypothesis, we first investigated an effect of HIF-1α KD on IR-induced DNA damage itself by investigating the formation of DSBs using γH2AX, which is activated and phosphorylated on the DSB site in response to IR. Therefore, the kinetics of γH2AX activation was monitored by WB and immunofluorescence staining. WB demonstrated an elevated protein level of phosphorylated H2AX during the first 6 h after IR with 5 Gy in the HIF-1α KD cells that were previously incubated under Hx for 24 h (Figure 15 A). This effect was even stronger after incubation of cells under Hx for 48 h (Figure 15 B). In addition, the

quantification of immunofluorescence staining of γH2AX ionizing radiation-induced foci (IRIF), which is a more precise method, demonstrated a significant increase of γH2AX foci per cell in HIF-1α KD cells in the first hour after IR with 5 Gy (Figure 15 C-D).

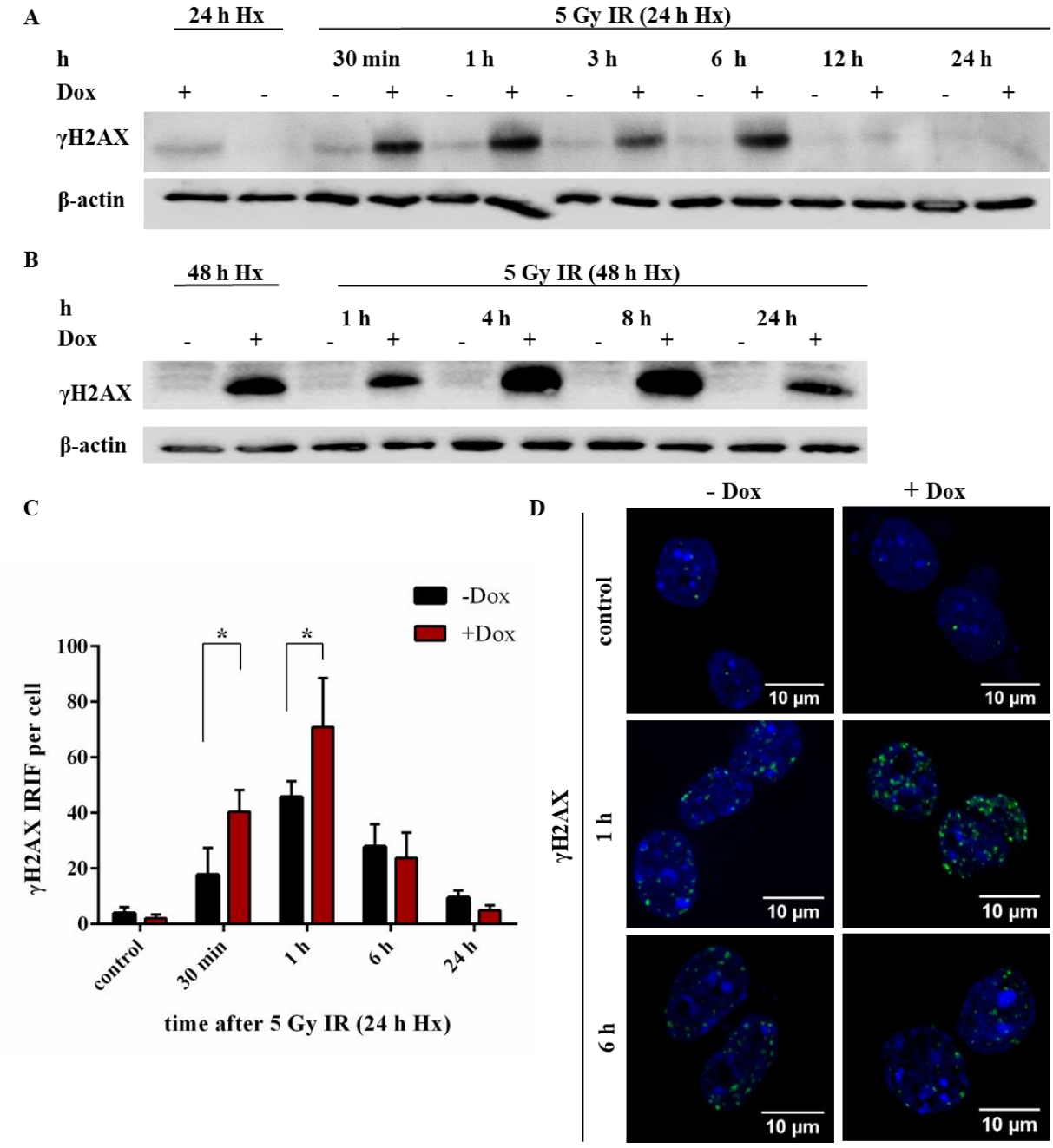

Figure 15: Activation of the DNA damage marker γH2AX in LLC HIF-1α KD cells

A-B) γH2AX WB demonstrated an increased amount of γH2AX protein in HIF-1α KD cells during the first 6 h after IR with 5 Gy. **C)** Immunofluorescence staining of γH2AX ionizing radiation-induced foci (IRIF) kinetic was performed after 24 h Hx and IR with 5 Gy. Quantification of γH2AX IRIF per cells and **D)** corresponding images displayed an enhanced activation of γH2AX by HIF-1α KD cells in the first hour after IR.

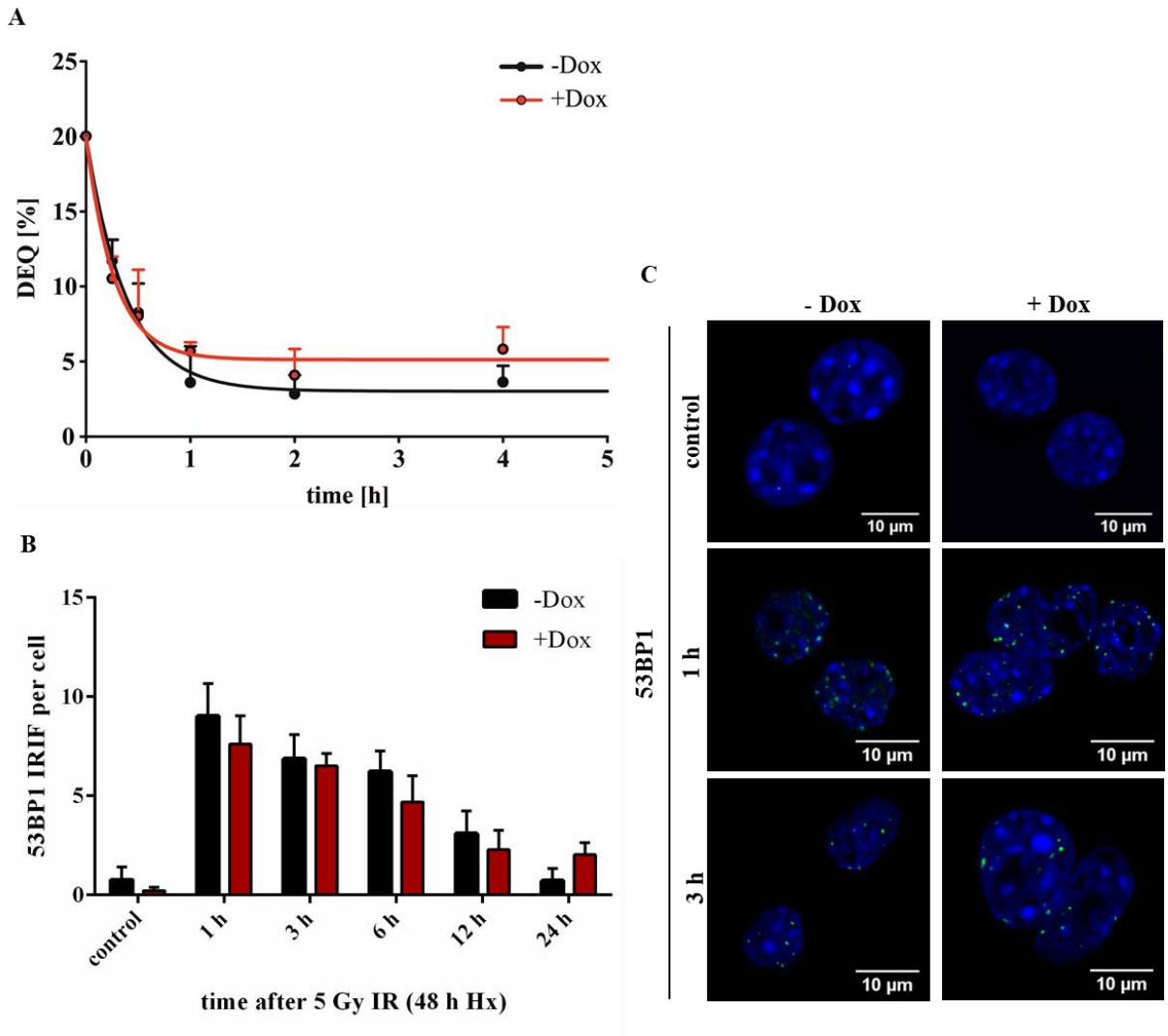

Figure 16: Effect of HIF-1α KD on non-homologous end-joining (NHEJ) in LLC cells

A) DNA repair kinetics were measured by PFGE in the first hours after IR. The remaining DNA damage is presented as dose equivalent (DEQ) expressed in Gy as a function of time. HIF-1α depleted cells demonstrated unchanged repair kinetics compared to the control cells. **B-C)** Immunofluorescence staining of 53BP1 IRIF analysis was performed after 48 h Hx and IR with 5 Gy. Quantification of 53BP1 IRIF per cell and the corresponding images showed an unchanged recruitment of 53BP1 after HIF-1α KD.

These results pointed out that the depletion of HIF-1α affects DNA damage repair after IR by increasing the number of DSBs. Next, it was important to clarify which mechanism of DDR is mostly impaired by HIF-1α KD. Two mechanisms are essential for DSB repair: NHEJ and HR. NHEJ is a fast mechanism occurring in the first hours after IR. Therefore, fast DNA repair kinetics of the first 4 h was analyzed using PFGE. The fraction of DNA release after IR was plotted in a graph, presenting dose equivalent (DEQ), which describes the remaining DNA damage expressed in Gy as a function of time (Figure 16 A). The regression curves of

HIF-1α KD and uninduced LLC cells did not demonstrate significant differences. Thus, the repair kinetics of the cells remained unchanged after HIF-1α depletion.

For further investigation, kinetics of 53BP1 recruitment, a crucial marker for NHEJ, were analyzed by counting 53BP1 IRIF after 48 h of Hx and IR with 5 Gy (Figure 16 B-C). The results of 53BP1 IF staining correlated well with the PFGE data showing an unchanged amount of 53BP1 IRIF after HIF-1α KD.

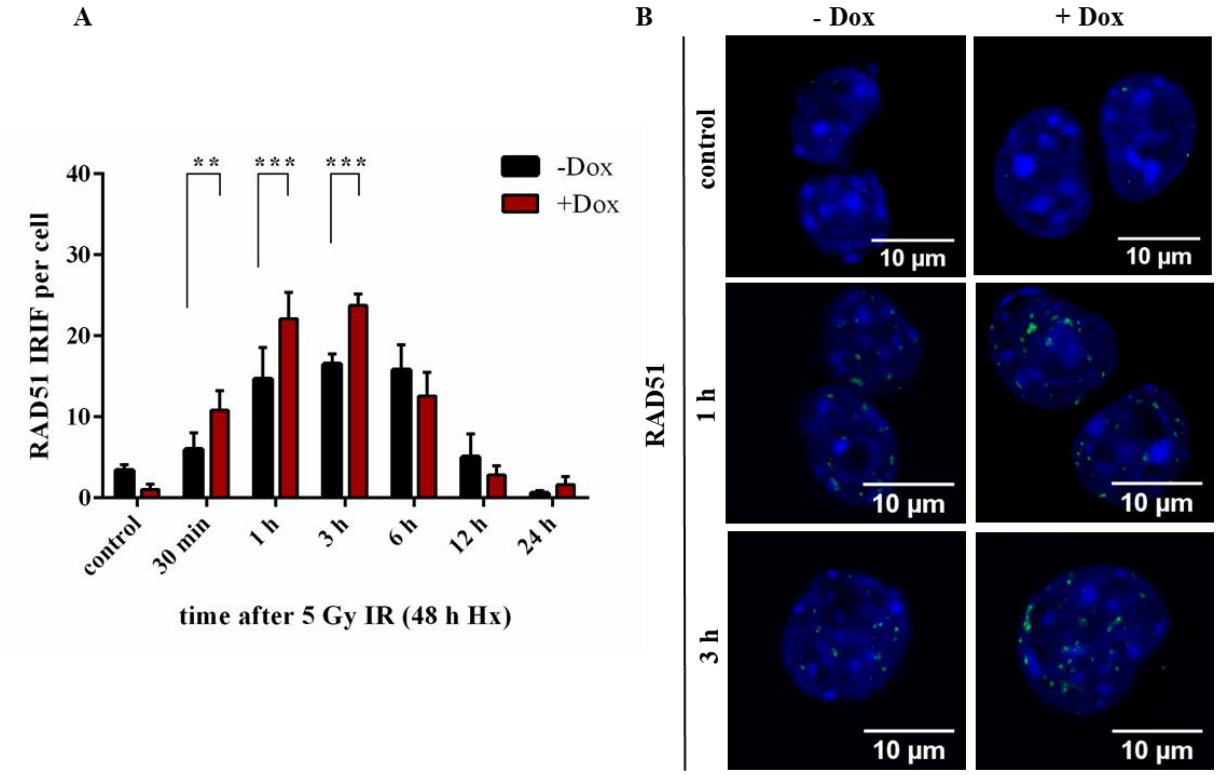

Figure 17: Effect of HIF-1α KD on homologous recombination (HR) in LLC cells

A) The kinetic of the HR protein RAD51 was measured by quantification of RAD51 IRIF after 48 h Hx and IR with 5 Gy. RAD51 IRIF per cell and **B)** Cell nuclei displayed an increased amount of RAD51 recruitment during the first 3 h after IR in HIF-1α depleted cells.

Another DSB repair mechanism termed homologous recombination (HR) was investigated by quantification of RAD51 IRIF kinetics after 48 Hx and IR with 5 Gy (Figure 17 A-B). The number of RAD51 foci per cell and images of cell nuclei demonstrated an elevated amount of RAD51 IRIF in the HIF-1α KD cells. Thus, the recruitment of RAD51, one of the essential proteins of HR, was significantly enhanced in the HIF-1α depleted cells in the first 3 h after IR.

These experiments were performed to understand the mechanism of HIF-1α-mediated radioresistance *in vitro*. In the next step, this mechanism was investigated in a substantially more complex, but physiologically more relevant model: *in vivo* experiments with mice.

4.2 *In vivo*

4.2.1 *Effect of HIF-1α KD on radiosensitivity of tumors in an allograft model with wild-type C57BL/6 mice*

To investigate HIF-1α KD effect on radiosensitivity of tumors *in vivo*, the allograft model with wild-type (wt) C57BL/6 mice was used. The experimental setup consisted of LLC cells with a lentiviral HIF-1α KD, which were injected into the flank of the mice. After reaching a certain size at day 10, the tumors were irradiated and afterwards the tumor size was monitored until the end of the experiment.

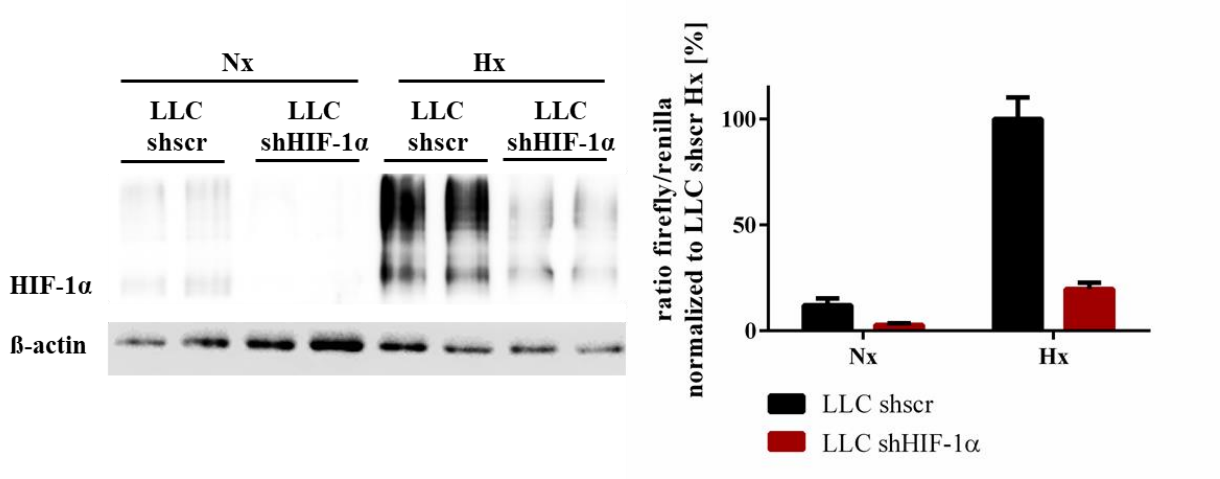

Figure 18: Analysis of HIF-1α KD efficacy in LLC shHIF-1α cells

A) HIF-1α WB showed a decrease of protein amount by shHIF-1α cells compared to shscr after 12 h incubation under Hx (1 % O_2). **B)** HIF-1α activity was assessed by luciferase assay. Values were normalized to hypoxic LLC shscr cells. The data demonstrated an approximately fivefold decrease of HIF-1α activity after incubation under Hx.

The first step was the generation of the LLC cells with a HIF-1α KD. Previous results of our group demonstrated that the Dox-inducible system has several disadvantages in mouse models, such as low control of Dox consumption in drinking water, effect on macrophages and hemorrhagic phenotype of tumors (Mersch, 2015). For this purpose, LLC cells with a constitutive HIF-1α KD were generated. Analysis of HIF-1α KD efficacy was performed by HIF-1α WB and luciferase assays that demonstrated a decrease of HIF-1α protein amount in the cells after 12 h Hx and impaired HIF-1α activity. After incubation under Hx luciferase activity was reduced to 20 % of the control level, respectively (Figure 18).

Next, it was necessary to determine the number of tumor cells most appropriate for tumor cell injections. Previous results of our group demonstrated that tumors which developed after

injection of 10^7 cells showed rapid growth and ulcerated very often. Therefore, the amount of injected cells was optimized by injection of $5x10^5$, 10^6, $5x10^6$ and 10^7 LLC shscr cells per animal into the flank of wt mice (Figure 19). The monitoring of tumor growth demonstrated that by of injection $5x10^5$ cells per mouse the tumors grew more slowly with less ulcerations and thus could be analyzed for a longer period compared to the other cell numbers. The increase of tumor growth in mice injected with $5x10^5$ cells began at day 10, which made this time point the most appropriate for irradiation in further experiments.

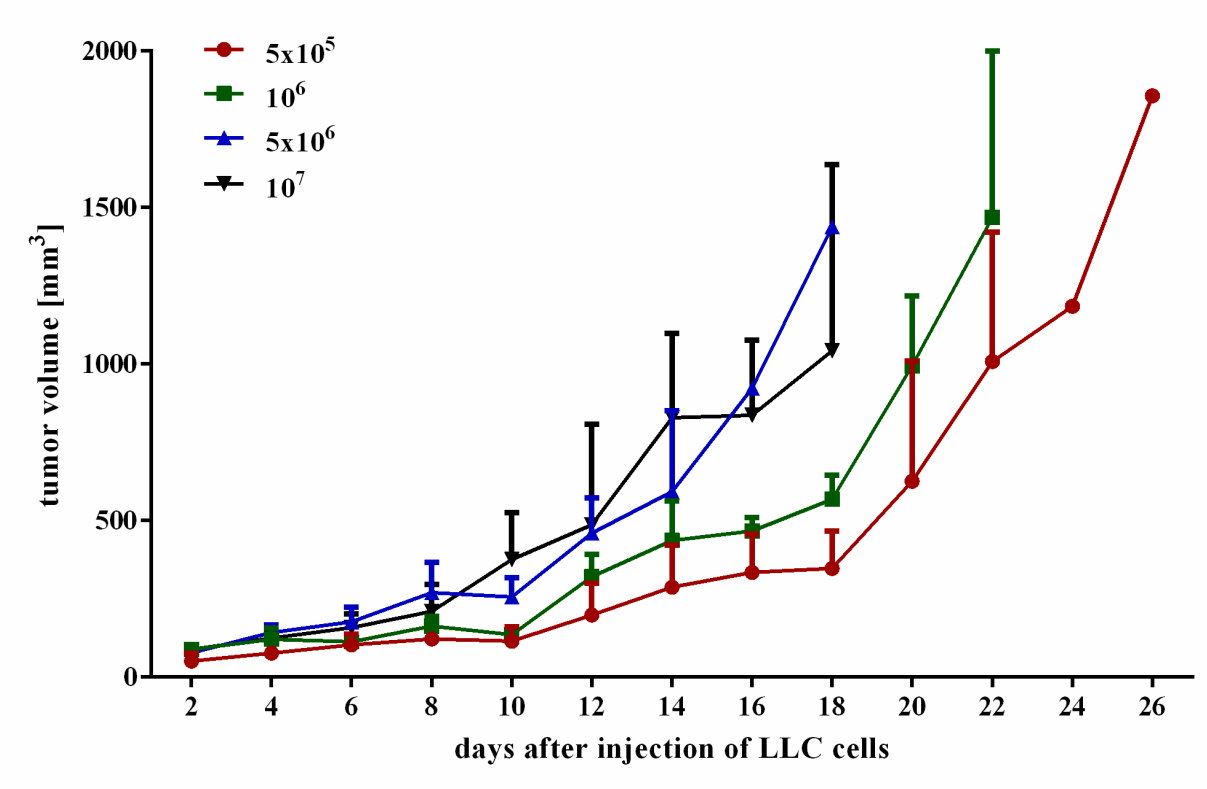

Figure 19: Optimization of tumor cell mass for tumor injection

Control cells (LLC shscr) were injected into the flank of wt mice. The concentrations of $5x10^5$, 10^6, $5x10^6$ and 10^7 cells per 150 µl injection were tested with n=5 animals per group. The tumor growth was measured every second day. The group with the initial cell amount of $5x10^5$ allowed the longest observation period.

For the investigation of the HIF-1α KD effect on radiosensitivity and tumor growth, the mice were injected with LLC shHIF-1α or LLC shscr as a control and 10 days later irradiated (+IR) with 15 Gy (Figure 20 A). Furthermore, two non-irradiated groups (-IR) with injected LLC shHIF-1α or shscr were used as a control of the effect of HIF-1α KD alone in tumors.

Tumor volumes were compared at day 22 and demonstrated that there were significant differences between well-growing –IR and slow-growing +IR tumor groups (Figure 20 B).

However, there was no difference in tumor growth between tumors with shHIF-1α and shscr cells within -IR and +IR groups. Figure 20 C presents the approximate size of the non-irradiated tumors without ulceration at the last day of the experiment. At the end of the experiment, mice were sacrificed and tumors excised for further analyses, such as quantification of RNA levels of HIF-1α and its targets in tumors by real-time qPCR and protein expression by IHC.

To ensure the quality of purified RNA for further quantification of mRNA levels, the RNA isolation from tissue was optimized. As RNAs are very sensitive to degradation, it was essential to find an appropriate isolation protocol for RNA isolation of mouse tumors. Figure 21 A showed a denaturing agarose gel with clear 18S and 28S ribosomal RNA (rRNA) bands without degradation smear in the RNA samples isolated with a commercial ReliaPrep^{TM} RNA Tissue Miniprep System (Promega) from mouse tumors. The gel indicated a high RNA integrity. The optimization of RNA isolation and high RNA purity allowed the performance of qPCR for mRNA level quantification. Using qPCR primer pairs for HIF-1α and its target GLUT-1, the tumor samples were analyzed (Figure 21 B). The results indicated that the relative mRNA levels of HIF-1α and GLUT-1 were not changed after HIF-1α KD or after IR. However, due to tumor ulcerations and a small size of irradiated tumors only a small number of samples was available for this experiment which resulted in a high standard deviation of the relative mRNA levels.

Next, the immunohistochemical analysis of HIF-1α protein expression was performed with mouse tumors. Paraformaldehyde-fixed, paraffin-embedded tumors were cut into 4-5 µm thick sections, which were stained with a HIF-1α antibody and counterstained with haematoxylin (Figure 22). The results of HIF-1α IHC demonstrated a wide distribution of HIF-1α in all sections. Tumors with initial injection of HIF-1α KD cells did not display the expected decrease of HIF-1α expression, as well as irradiated tumors did not show an enhanced HIF-1α expression, which has been reported in the literature.

Our next hypothesis was that during tumor growth the tumor stroma, including immune and endothelial cells from surrounding tissue, could infiltrate the tumor and compensate the lack of HIF-1α function of the injected tumor cells. Therefore, for the next experiments a new setup which allowed HIF-1α deficiency not only in tumors but also in the whole mouse body was essential. For this purpose, a mouse with a ubiquitous inducible HIF-1α knockout was generated.

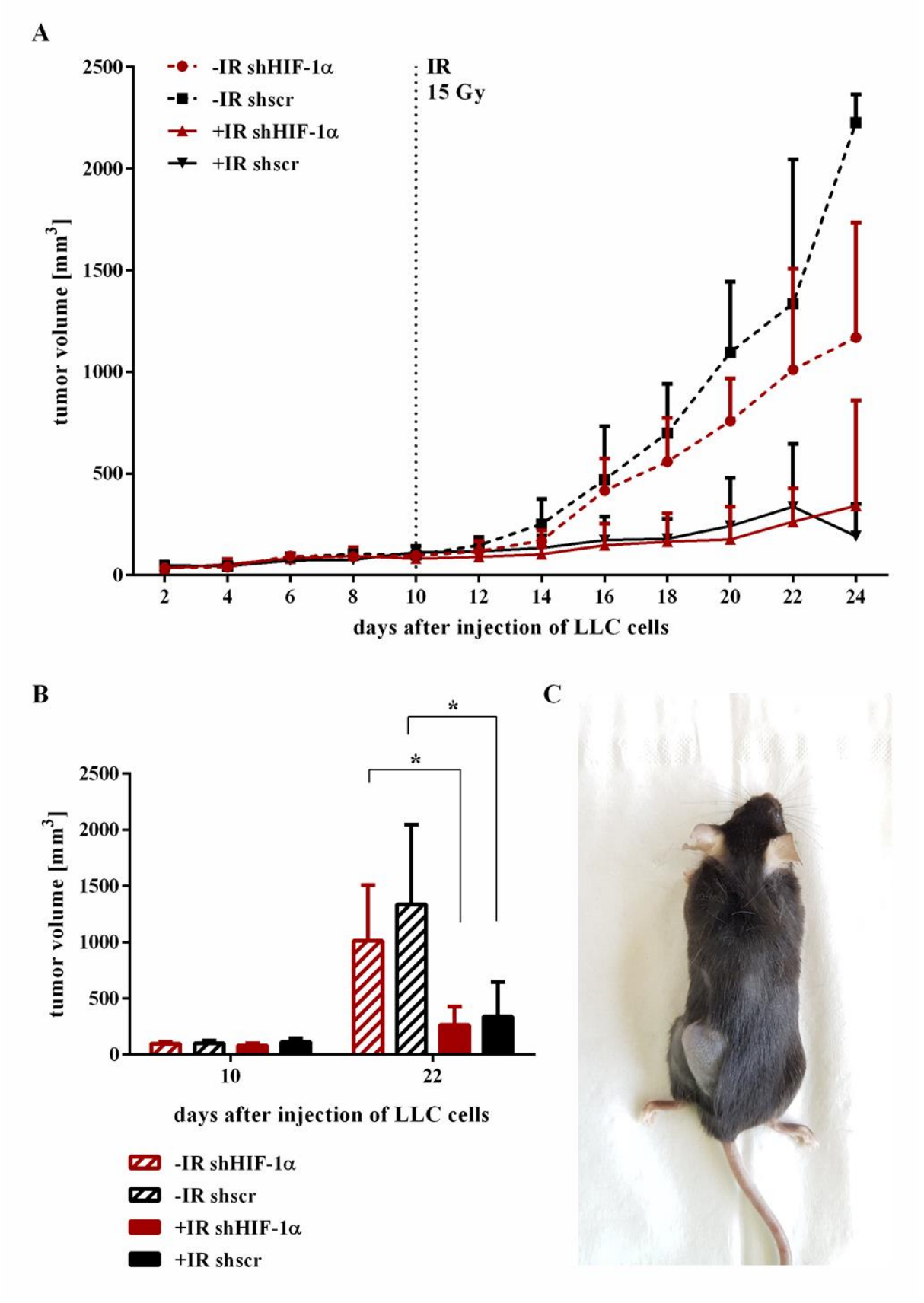

Figure 20: Tumor growth in an allograft model with C57BL/6 wt mice after 15 Gy IR

A) Mice were injected with $5x10^5$ cells, the tumors were irradiated with 15 Gy at day 10. The experiment consisted of four groups: irradiated tumors with shHIF-1α or shscr and, as a control, two

non-irradiated groups with shHIF1-1α or shscr (n=5 animals per group). The tumor growth was measured every second day. B) Analysis of tumor growth at day 22 demonstrated that non-irradiated (-IR) groups have a significant increase of tumor growth compared to the irradiated groups (+IR). The tumors with shHIF-1α did not differ from shscr cells in –IR and +IR groups. C) Representative picture of a mouse with subcutaneous tumor at the end of the experiment.

-IR shHIF-1α: non-irradiated tumor with shHIF-1α LLC cells, **-IR shscr:** non-irradiated tumor with LLC shscr cells, **+IR shHIF-1α:** irradiated tumor with LLC shHIF-1α cells, **+IR shscr:** irradiated tumor with LLC shscr cells.

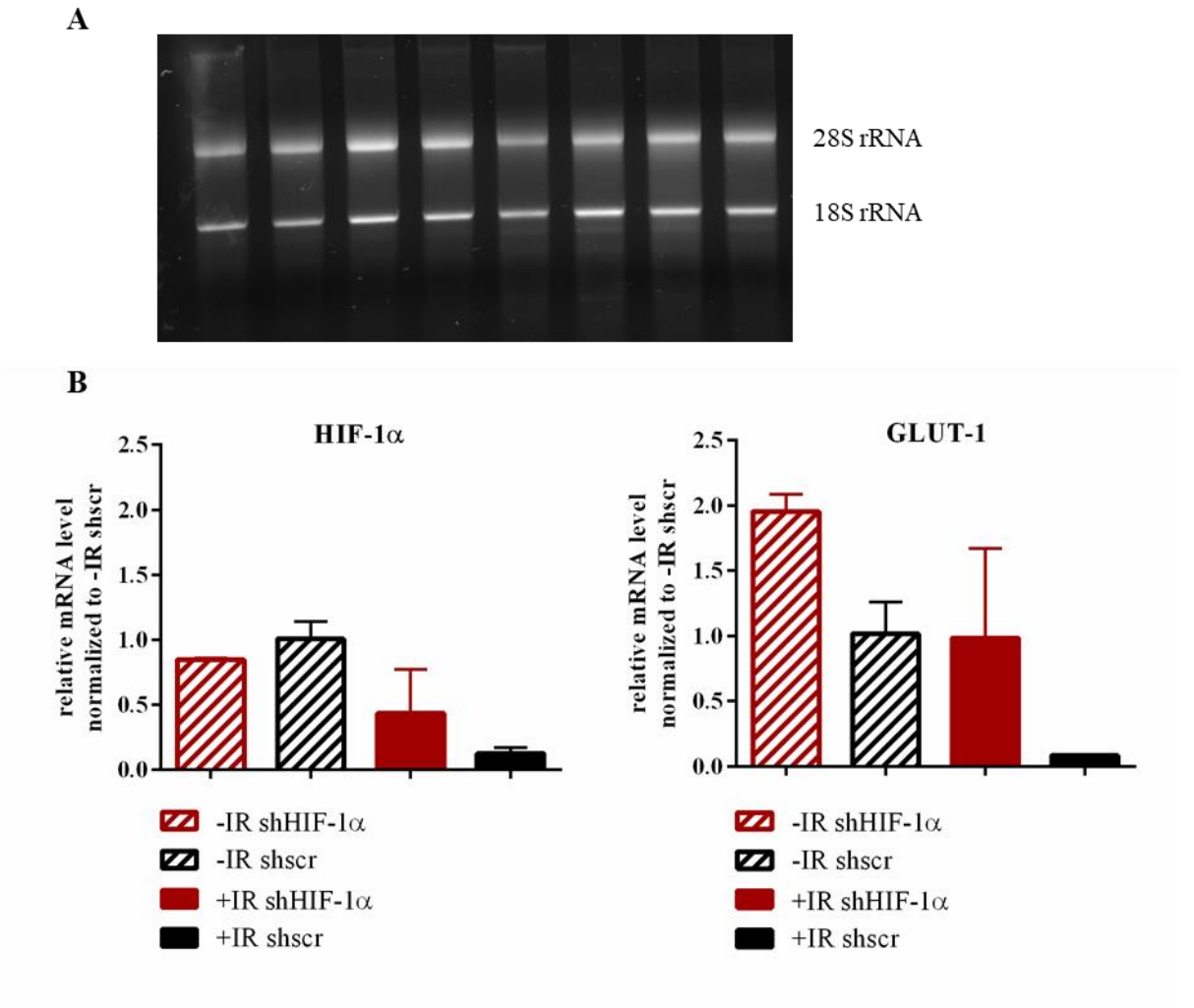

Figure 21: Analysis of HIF-1α and GLUT-1 mRNA expression in mouse tissue

A) Agarose gel with RNA samples demonstrated clear bands of 28S and 18S ribosomal RNA (rRNA) without signs of degradation. B) Quantification of qPCR performed with the RNA from mouse tumors demonstrated unchanged relative mRNA levels of HIF-1α and its target GLUT-1 in tumors with HIF-1α KD or IR compared to the untreated samples. –**IR shHIF-1α:** non-irradiated tumor with shHIF-1α LLC cells (n=2), **-IR shscr:** non-irradiated tumor with LLC shscr cells (n=2), **+IR shHIF-1α:** irradiated tumor with LLC shHIF-1α cells (n=2), **+IR shscr:** irradiated tumor with LLC shscr cells (n=3).

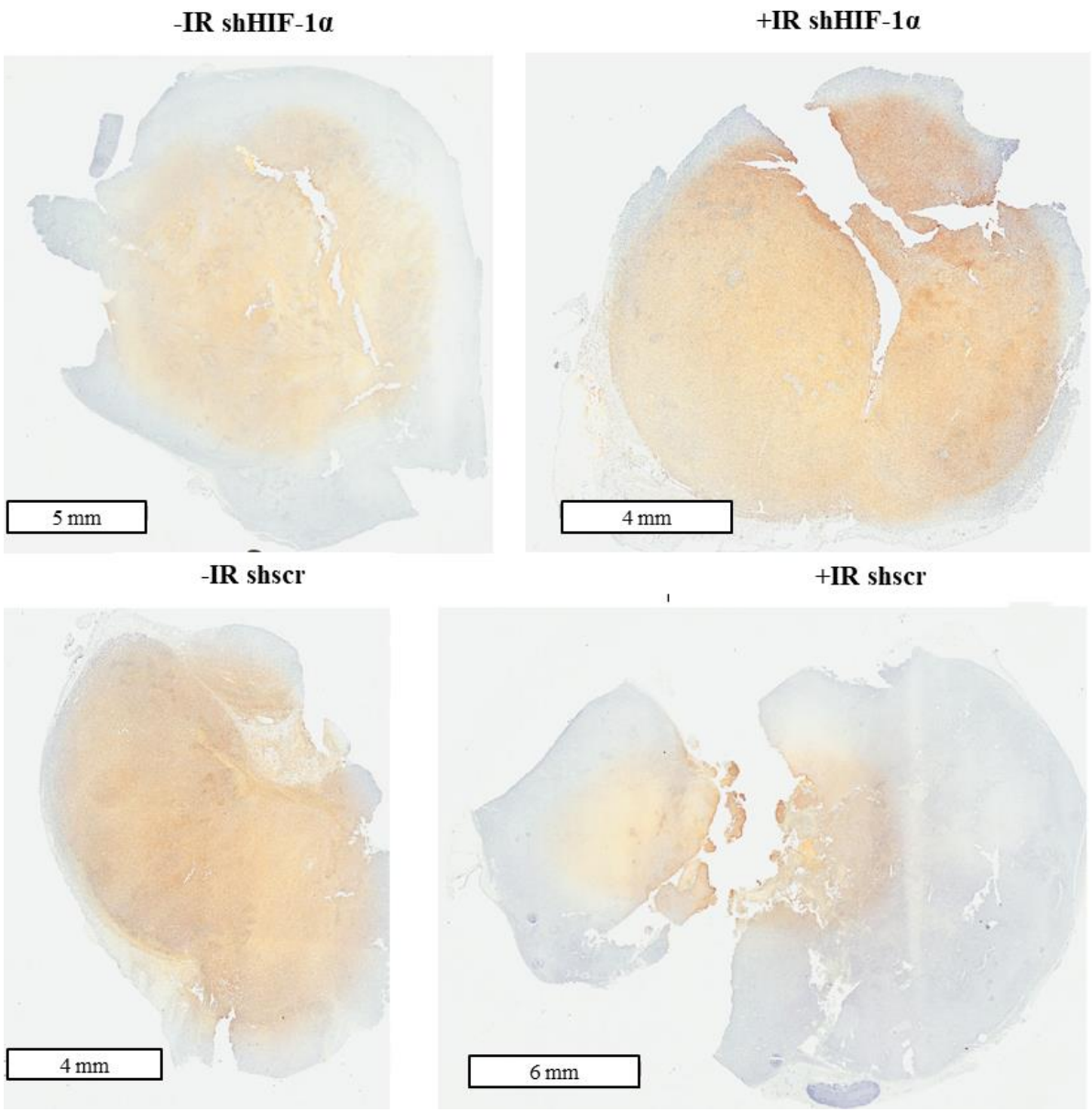

Figure 22: Representative images of immunochistochemical analysis of HIF-1α expression
Paraffin-embedded mouse tumors were cut into 4-5 µm sections. The tissue was stained with a HIF-1α antibody (brown) and counterstained with hematoxylin (blue). Immunochistochemical analysis of HIF-1α demonstrated widespread HIF-1α protein expression regardless of HIF-1α KD of initially injected cells or radiation treatment. **–IR shHIF-1α:** non-irradiated tumor with shHIF-1α LLC cells, **-IR shscr**: non-irradiated tumor with LLC shscr cells, **+IR shHIF-1α:** irradiated tumor with LLC shHIF-1α cells, +**IR shscr:** irradiated tumor with LLC shscr cells.

4.2.2 Generation of a mouse model with tamoxifen-inducible HIF-1α knockout

As global HIF-1α knockout with homozygous deletion results in embryonic death (Iyer et al., 1998; Ryan et al., 1998), mice with a conditional knockout (KO) of HIF-1α were used for this study. For this reason, two mouse strains were cross bred: Cre-ER$^{ki/ki}$ and HIF-1α$^{fl/fl}$. In HIF-1α$^{fl/fl}$ mice the second exon (E2) of HIF-1α is flanked by loxP sites. E2 encodes the helix-loop-helix/PAS motif and is essential for HIF-1α DNA binding and dimerization with ARNT following transcriptional activation (Jiang et al., 1997). Cre-ER$^{ki/ki}$ mice carry the knock-in (ki) mutation of the Cre recombinase fused to the mutated estrogen receptor, which can be activated by the estrogen receptor ligand tamoxifen (Tam). Thus, after administration of Tam the cross-bred HIF-1α$^{fl/fl}$Cre-ER$^{ki/wt}$ mice lack E2, therefore functional activity of HIF-1α is prevented (see Material and Methods 3.3.2).

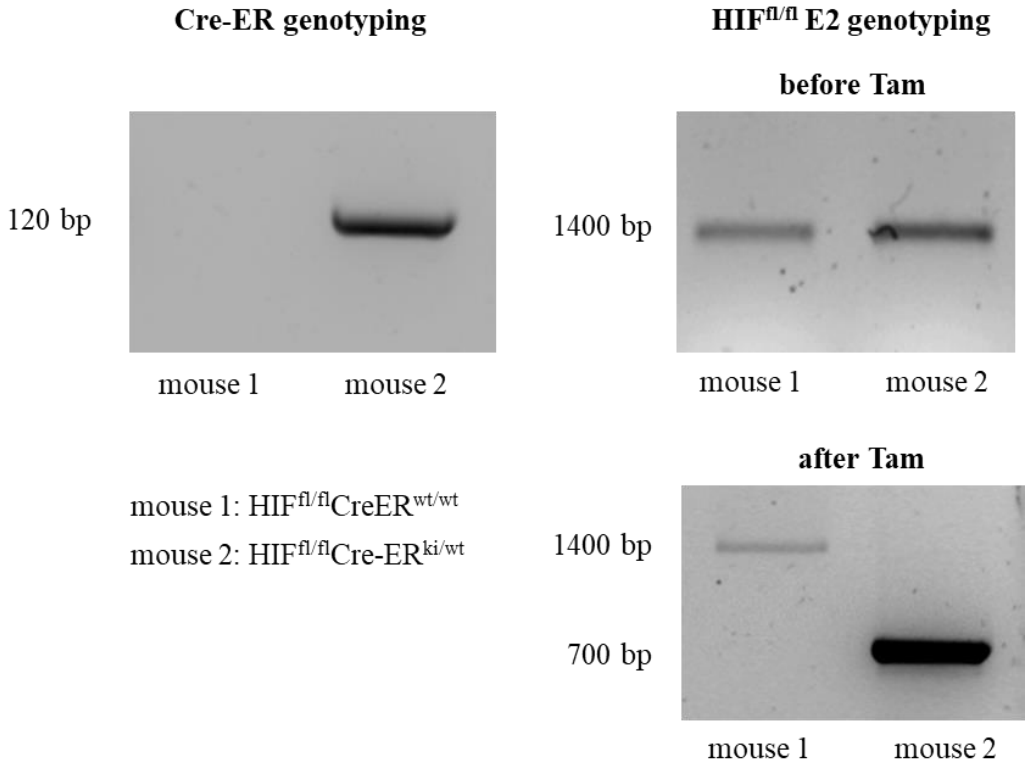

Figure 23: Representative example of mouse genotyping

The mice were genotyped for Cre-ER knock-in (ki) using Rose26-Cre-ER primer. The wt allele did not give rise to any PCR products; the ki allele led to production of a PCR fragment with a size of 120 bp. The genotyping for exon 2 (E2) demonstrated a shortened fragment in the HIF-1α$^{fl/fl}$Cre-ER$^{ki/wt}$ (Cre(ki)) mice after Tam treatment compared to the HIF-1α$^{fl/fl}$Cre-ER$^{wt/wt}$ (Cre(-)) mice, indicating an excision of E2.

To delineate whether the Tam treatment was successful, the mice were genotyped by end-point PCR. Figure 23 displayed a representative example of the genotyping procedure. The primer pair ROSA26-Cre-ER was used for Cre-ER genotyping and generated a 120 bp fragment in case of Cre-ER$^{ki/wt}$ (Cre(ki), mouse 2) and no fragments for Cre-ER$^{wt/wt}$ (Cre(-), mouse 1). Next, the HIF-1α$^{fl/fl}$ E2 genotyping with the mHIF-1α_E2seq primer pair was performed to prove that E2 is excised after Tam administration. The mHIF-1α_E2seq forward primer binds the sequence in the intron 1 and mHIF-1α_E2seq reverse primer binds in intron 2 of HIF-1α. The PCR results from the samples which were taken before Tam administration gave rise to an amplicon of approximately 1400 bp in both animals. After treatment with Tam, samples from animals were collected and genotyped again. The PCR product size of mouse 1 remained at the same length of 1400 bp, while the fragment of mouse 2 was approximately 700 bp shorter which is caused by deletion of exon 2. Therefore, these data demonstrated that Tam application induced E2 excision in the HIF-1α$^{fl/fl}$Cre-ER$^{ki/wt}$ mice and that this mouse model can be used for further studies.

In addition, it was important to clarify the effect of E2 excision on protein structure of HIF-1α. *In silico* analysis of the mRNA sequence of HIF-1α from (GenBank AH006789.2) showed that E2 contains 191 nucleotides (Figure 24). As a result, deletion of exon 2 is expected to lead to a frame shift and termination of translation due to a stop codon at the beginning of exon 3.

To prove this assumption, sequencing of the PCR products was performed. Therefore, RNA was isolated from the spleen, bone-marrow derived macrophages (BMDM), brain and kidney from Cre(ki) and Cre(-) mice. These RNA samples were transcribed to cDNA that, in turn was used for end-point PCR with the mHIF-1α_E2seq primer pair. The PCR products were then sequenced by the sequencing service LGC Genomics. The DNA sequences were translated to amino acid sequences. Translated amino acid sequences are presented in Table 11, sequences from BMDM samples are displayed as a representative result. The start codon (Met) initiates translation of the protein (marked in red). While the sequences of the Cre(-), theoretical and BMDM sample, demonstrated translation of the full length HIF-1α protein, sequences of the Cre(ki) show a stop codon after 16 amino acids.

Sequence of HIF-1α from exon 1 to exon 3

exon 1:

```
  1 cgcgaggact gtcctcgccg ccgtcgcggg cagtgtctag ccaggccttg acaagctagc
 61 cggaggagcg cctaggaacc cgagccggag ctcagcgagc gcagcctgca cgcccgcctc
121 gcgtcccggg ggggtcccgc ctcccacccc gcctctggac ttgtctcttt ccccgcgcgc
181 gcggacagag ccggcgttta ggcccgagcg agcccggggg ccgccggccg ggaagacaac
241 gcgggcaccg attcgccatg gagggcgccg gcggcgagaa cgagaagaaa aa
```

exon 2:

```
  1 gatgagttct gaacgtcgaa aagaaaagtc tagagatgca gcaagatctc ggcgaagcaa
 61 agagtctgaa gtttttatg agcttgctca tcagttgcca cttccccaca atgtgagctc
121 acatcttgat aaagcttctg ttatgaggct caccatcagt tatttacgtg tgagaaaact
181 tctggatgcc g
```

exon 3:

```
  1 gtggtctaga cagtgaagat gagatgaagg cacagatgga ctgtttttat ctgaaagccc
 61 tagatggctt tgtgatggtg ctaacagatg acggcgacat ggtttacatt tctgataacg
121 tgaacaaata catggggtta actcag
```

Sequence of HIF-1α from exon 1 to exon 3 after E2 excision

exon 1:

```
  1 cgcgaggact gtcctcgccg ccgtcgcggg cagtgtctag ccaggccttg acaagctagc
 61 cggaggagcg cctaggaacc cgagccggag ctcagcgagc gcagcctgca cgcccgcctc
121 gcgtcccggg ggggtcccgc ctcccacccc gcctctggac ttgtctcttt ccccgcgcgc
181 gcggacagag ccggcgttta ggcccgagcg agcccggggg ccgccggccg ggaagacaac
241 gcgggcaccg attcgccatg gagggcgccg gcggcgagaa cgagaagaaa aa
```

exon 3:

```
  1 gtggtctaga cagtgaagat gagatgaagg cacagatgga ctgtttttat ctgaaagccc
 61 tagatggctt tgtgatggtg ctaacagatg acggcgacat ggtttacatt tctgataacg
121 tgaacaaata catggggtta actcag
```

Figure 24: Theoretical HIF-1α mRNA sequence from exon 1 to exon 3.

The mRNA HIF-1α sequence from GenBank (AH006789.2) demonstrated, that exon 2 (E2) shares its first and last base triplets with exon 1 and exon 3 (overlapping triplet in green), respectively. After excision of E2 the sequence of triplets is disordered indicating a frame shift with premature termination of translation.

These data confirmed that HIF-1α KO is induced by administration of Tam in the generated mouse model making this model suitable for further experiments. Still, a few animals demonstrated abnormality by PCR genotyping (Figure 25). While samples from Cre(ki) and Cre(-) mice displayed fragments with 700 bp (E2 excision) and 1400 bp (E2 not excised) length, respectively, approximately 10 % of the animals with the Cre(-) genotype demonstrated E2 excision. These animals were not used for further experiments.

Table 11: HIF-1α amino acid sequence

The cDNA from HIF-1α$^{fl/fl}$Cre-ER$^{ki/wt}$ (Cre(ki)) and HIF-1α$^{fl/fl}$Cre-ER$^{wt/wt}$ (Cre(-)) mouse organs were sequenced and translated in amino acid sequences. Amino acid sequences of bone-marrow derived macrophages (BMDM) samples were shown. Theoretical and mouse sample sequences of the HIF-1α$^{fl/fl}$Cre-ER$^{ki/wt}$ genotype demonstrated a stop codon after 16 amino acids.

HIF-1α sequence from Cre(-) mice, E2 not excised	**HIF-1α sequence from Cre(ki) mice after E2 excision**
Theoretical:	
R G L S S P P S R A V S S Q A L T S Stop P E E R L G T R A G A Q R A Q P A R P P R V P G G S R L P P R L W T C L F P R A R G Q S R R L G P S E P G G R R P G R Q R G H R F A **Met** E G A G G E N E K K K **Met** S S E R R K E K S R D A A R S R R S K E S E V F Y E L A H Q L P L P H N V S S H L D K A S V **Met** R L T I S Y L R V R K L L D A G G L D S E D E **Met** K A Q Met D C F Y L K A L D G F V **Met** V L T D D G D Met V Y I S D N V N K Y **Met** G L T Q	R G L S S P P S R A V S S Q A L T S **Stop** P E E R L G T R A G A Q R A Q P A R P P R V P G G S R L P P R L W T C L F P R A R G Q S R R L G P S E P G G R R P G R Q R G H R F A **Met** E G A G G E N E K K K W S R Q **Stop** R **Stop** D E G T D G L F L S E S P R W L C D G A N R **Stop** R R H G L H F **Stop Stop** R E Q I H G V N S
Analysis of mouse samples:	
R G H R F A **Met** E G A G G E N E K K K **Met** S S E R R K E K S R D A A R S R R S K E S E V F Y E L A H Q L P L P H N V S S H L D K A S V **Met** R L T I S Y L R V R K L L D A G G L D S E D E **Met** K A Q **Met** D C F Y L K A L D G F V **Met** V L T D	R G H R F A **Met** E G A G G E N E K K K W S R Q **Stop** R **Stop** D E G T D G L F L S E S P R W L C D G A N R **Stop** R R H G

In addition, the swelling of the scrotum in male animals was observed during the monitoring of animals after Tam treatment (Figure 26). However, this side effect of Tam did not cause any pain for the animals and, therefore, did not compromise the experiments.

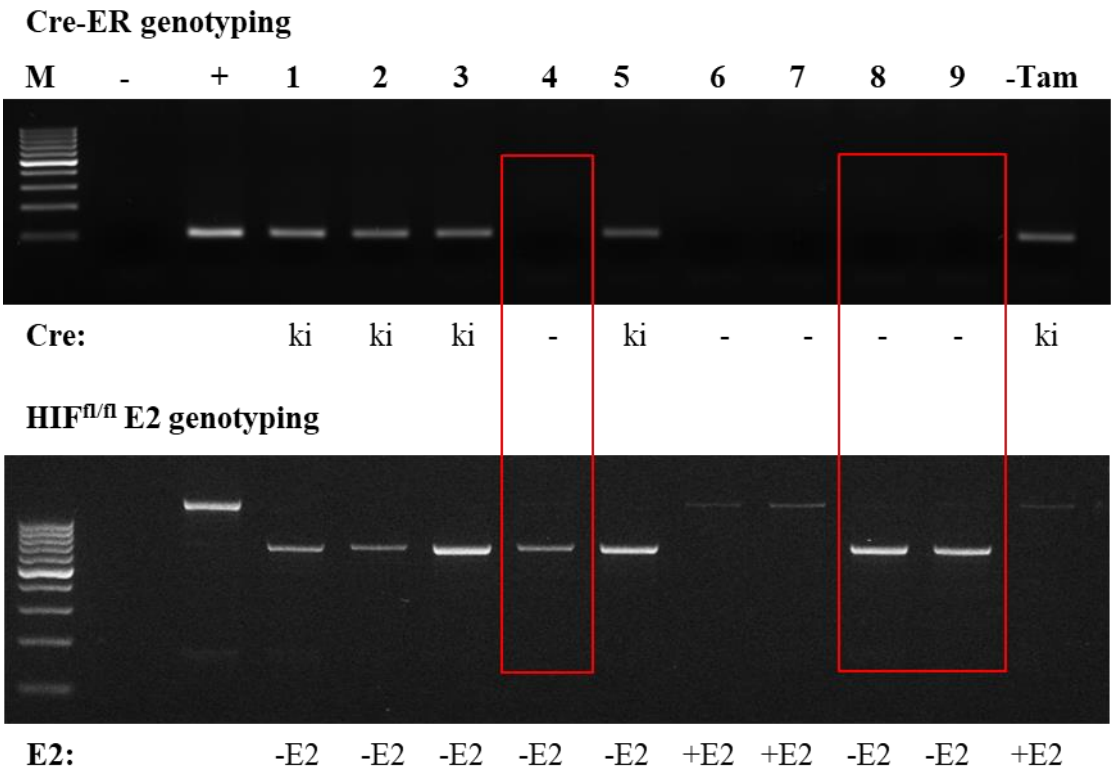

Figure 25: Genotyping phenomenon

Animals with Cre-ER$^{ki/wt}$ (Cre(ki)) genotype had the shortened fragment of HIF-1α PCR after treatment with Tam. Cre-ER$^{wt/wt}$ mice (Cre(-)) demonstrated an unchanged long fragment of HIF-1α without E2 excision (+E2). However, a few animals with wt genotype also demonstrated an excision of E2 (-E2).

Figure 26: Side effect of Tam in male animals

Treatment with Tam caused a scrotum swelling in male mice but no obvious phenotypic changes in females.

4.2.3 Effect of HIF-1α depletion on radiosensitivity of tumors in an allograft model with Tam-inducible HIF-1α KO mice

To distinguish between injected LLC cells and stroma cells in tumors, the LLC shHIF-1α GFP cells were generated and analyzed for HIF-1α KD efficacy. The data from the luciferase assay demonstrated an 80 % decrease of HIF-1α activity in shHIF-1α GFP cells after incubation in Hx (Figure 27).

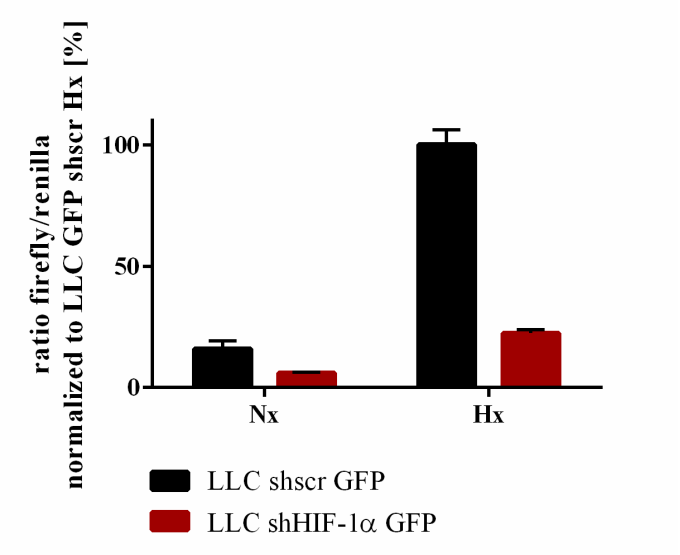

Figure 27: Analysis of HIF-1α KD efficacy in LLC shHIF-1α GFP cells

Luciferase assays demonstrated reduced HIF-1α activity when the values were normalized to hypoxic LLC shscr GFP cells. The data demonstrated that HIF-1α activity in shHIF-1α GFP cells was reduced to 20 % after incubation under Hx.

For investigation of the effect of HIF-1α depletion in tumor and stroma cells on radiosensitivity and tumor growth, the Tam-inducible allograft model with HIF-1α KO was used. For induction of the HIF-1α KO in the mice, animals were treated with Tam. Two weeks later, the mice were injected with LLC shHIF-1α GFP and shscr GFP as a control. The tumors were irradiated 10 days later with 15 Gy and their size was measured every second day. For better visualization, the data with the tumor volume at day 10 and day 20 is shown (Figure 28). Analysis of tumor volume at day 20 demonstrated a significant difference between non-irradiated and irradiated tumor groups. Furthermore, the non-irradiated groups demonstrated an interesting effect: tumors with HIF-1α KD cells in HIF-1α KO mice (-IR Cre(ki) shHIF-1α) and tumors with control shscr cells in HIF-1α KO mice (-IR Cre (ki) shscr) showed a significantly decreased volume compared to the tumors with HIF-1α KD cells in a wt mice (–IR Cre(-) shHIF-1α). At the end of the experiment, mice were sacrificed and tumors excised for the further quantification analysis of mRNA levels.

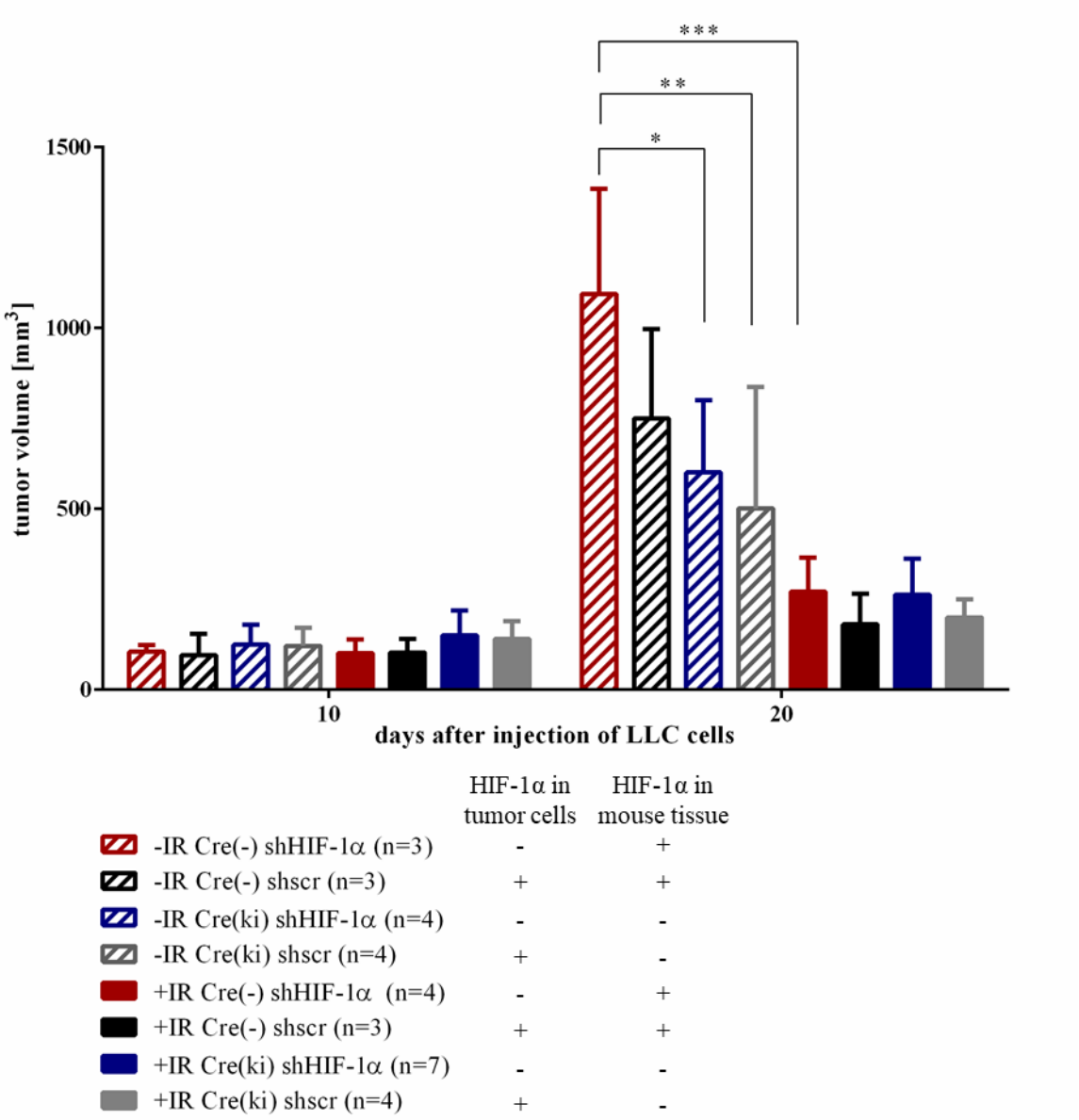

Figure 28: Analysis of tumor growth after irradiation with 15 Gy

HIF-1α$^{fl/fl}$Cre-ER$^{wt/wt}$ (Cre(-)) and HIF-1α$^{fl/fl}$Cre-ER$^{ki/wt}$ (Cre(ki)) mice were treated with Tam and 2 weeks later injected with 5x10^5 LLC shHIF-1α GFP or shscr GFP cells. The tumors were irradiated with 15 Gy at day 10 after tumor cell injection. The data demonstrate tumor volume at day 10 shortly before IR and at day 20. **–IR Cre(-) shHIF-1α**: non-irradiated tumor with LLC shHIF-1α cells in HIF-1α$^{fl/fl}$Cre-ER$^{wt/wt}$ mice (Cre(-)), **-IR Cre(-) shscr**: non-irradiated tumor with LLC shscr cells in Cre(-) mice, **–IR Cre(ki) shHIF-1α:** non-irradiated tumor with LLC shHIF-1α cells in HIF-1α$^{fl/fl}$Cre-ER$^{ki/wt}$ (Cre(ki)), **-IR Cre(ki) shscr:** non-irradiated tumor with LLC shscr cells in Cre(ki) mice, **+IR Cre(-) shHIF-1α:** irradiated tumor with LLC shHIF-1α cells in Cre(-), **+IR Cre(-) shscr:** irradiated tumor with LLC shscr cells in Cre(-) mice, **+IR Cre(ki) shHIF-1α:** irradiated tumor with LLC shHIF-1α cells in Cre(ki) mice, **+IR Cre(ki) shscr:** irradiated tumor with LLC shscr cells in Cre(ki) mice

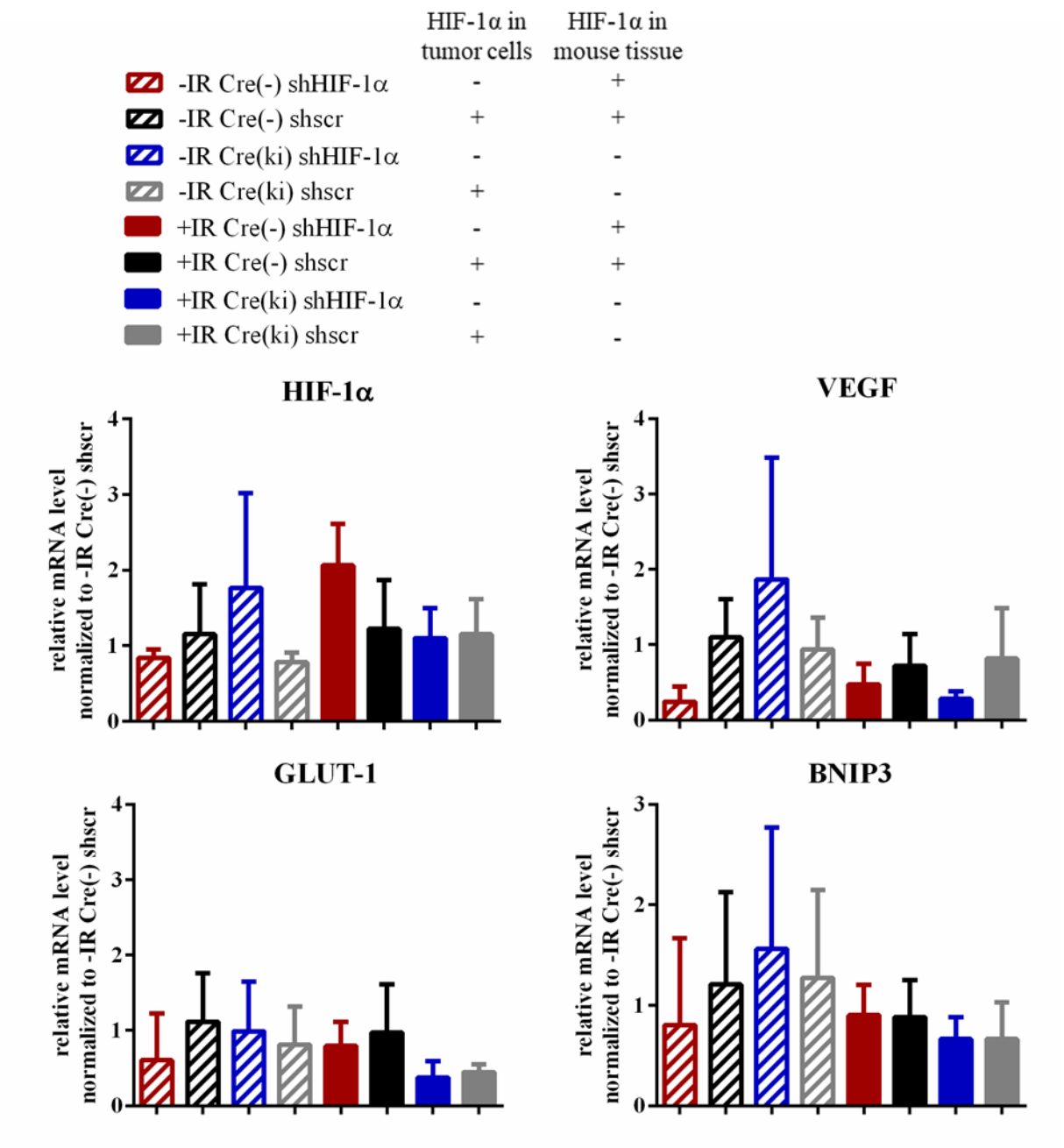

Figure 29: Analysis of mRNA levels of HIF-1α and its targets in mouse tissue

Quantification cDNA generated from mouse tumors demonstrated unchanged relative mRNA levels of HIF-1α and its targets GLUT-1, VEGF and BNIP3 in tumors with HIF-1α KD or IR compared to the untreated samples as analyzed by qPCR. **–IR Cre(-) shHIF-1α**: non-irradiated tumor with LLC shHIF-1α cells in HIF-1α$^{fl/fl}$Cre-ER$^{wt/wt}$ mice (Cre(-)) (n=3), **-IR Cre(-) shscr**: non-irradiated tumor with LLC shscr cells in Cre(-) mice (n=3), **–IR Cre(ki) shHIF-1α:** non-irradiated tumor with LLC shHIF-1α cells in HIF-1α$^{fl/fl}$Cre-ER$^{ki/wt}$ (Cre(ki)) (n=6), **-IR Cre(ki) shscr:** non-irradiated tumor with LLC shscr cells in Cre(ki) mice (n=3), **+IR Cre(-) shHIF-1α:** irradiated tumor with LLC shHIF-1α cells in Cre(-) (n=5), **+IR Cre(-) shscr:** irradiated tumor with LLC shscr cells in Cre(-) mice (n=4), **+IR Cre(ki) shHIF-1α:** irradiated tumor with LLC shHIF-1α cells in Cre(ki) (n=5), **+IR Cre(ki) shscr:** irradiated tumor with LLC shscr cells in Cre (ki) mice (n=6)

The mRNA levels of HIF-1α and its targets VEGF, GLUT-1 and BNIP3 were quantified by qPCR (Figure 29). The data demonstrated that the relative mRNA levels of all four target genes were not changed regardless of HIF-1α KD in tumors, irradiation or HIF-1α KO in mice. The results also showed a high standard deviation due to a small number of samples per group, notably in the non-irradiated groups.

The results from previous *in vivo* experiments demonstrated that after 15 Gy IR all tumors stopped growing, making further analysis of the HIF-1α depletion effect in irradiated groups impossible. For this reason, the next mouse experiment was performed with 7.5 Gy IR (Figure 30). After treatment with Tam and tumor injection, mice were irradiated at day 10 with 7.5 Gy and monitored for the next ten days. In contrast to the previous experiment, the tumor growth data did not demonstrate a significant difference between irradiated and non-irradiated groups. Moreover, the non-irradiated control group -IR Cre(-) shscr showed a significant decrease of tumor volume compared to the group with HIF-1α KD tumors in HIF-1α KO mice (–IR Cre(ki) shHIF-1α) group. These data are in contrast to the results of the previous experiment.

Despite some variations, both mouse allograft models with the HIF-1α KO mice indicated significant changes in the non-irradiated tumor groups. However, the non-irradiated well-growing tumors led to ulceration rapidly and frequently which made it necessary to sacrifice these mice for ethical reasons. Although 6 to 7 animals per group were used at the beginning for each experiment, the amount of animals was decreasing until the end of the experiment due to skin lesions and ulcerations. Therefore, the data from both experiments were summarized to analyze the tumor growth in non-irradiated tumors with a higher amount of animals per group (Figure 31). The tumor volume of the tumor with LLC shscr cells in Cre(ki) mice demonstrated a significant decrease compared to tumors with LLC shHIF-1α cells in Cre(-) mice. These data indicates the importance of global HIF-1α KO on the tumor growth in the murine allograft model.

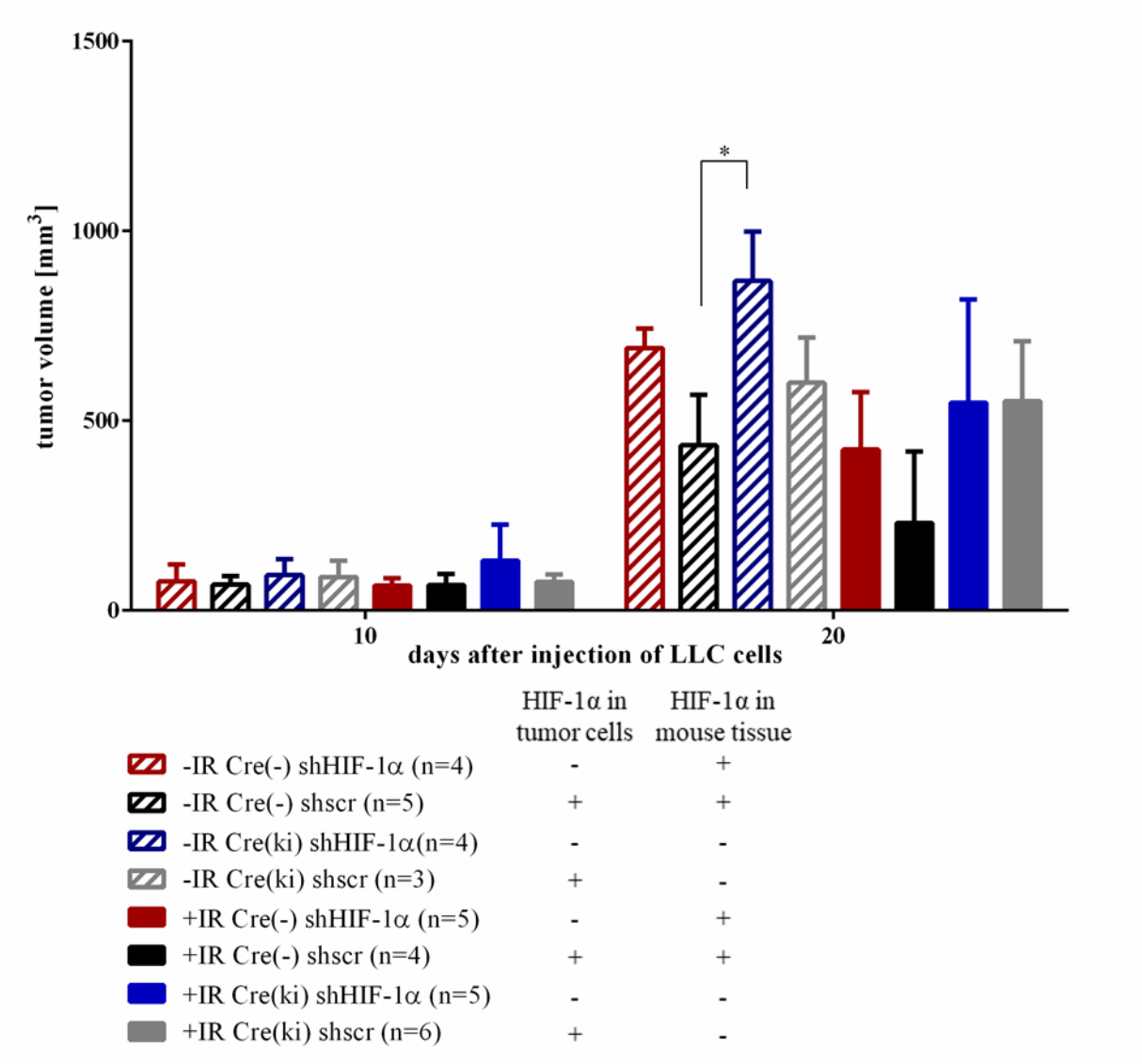

Figure 30: Analysis of tumor growth after 7.5 Gy IR

HIF-1α$^{fl/fl}$Cre-ER$^{wt/wt}$ (Cre(-)) and HIF-1α$^{fl/fl}$Cre-ER$^{ki/wt}$ (Cre(ki)) mice were treated with Tam and 2 weeks later injected with 5x10^5 LLC shHIF-1α GFP or shscr GFP cells. The tumors were irradiated with 7.5 Gy at day 10 after tumor injection. The data demonstrated the tumor volume at day 10 shortly before IR and at day 20. **–IR Cre(-) shHIF-1α**: non-irradiated tumor with LLC shHIF-1α cells in HIF-1α$^{fl/fl}$Cre-ER$^{wt/wt}$ mice (Cre(-)), **-IR Cre(-) shscr**: non-irradiated tumor with LLC shscr cells in Cre(-) mice, **–IR Cre(ki) shHIF-1α:** non-irradiated tumor with LLC shHIF-1α cells in HIF-1α$^{fl/fl}$Cre-ER$^{ki/wt}$ (Cre(ki)), **-IR Cre(ki) shscr:** non-irradiated tumor with LLC shscr cells in Cre(ki) mice, **+IR Cre(-) shHIF-1α:** irradiated tumor with LLC shHIF-1α cells in Cre(-), **+IR Cre(-) shscr:** irradiated tumor with LLC shscr cells in Cre(-) mice, **+IR Cre(ki) shHIF-1α:** irradiated tumor with LLC shHIF-1α cells in Cre(ki), **+IR Cre(ki) shscr:** irradiated tumor with LLC shscr cells in Cre(ki) mice

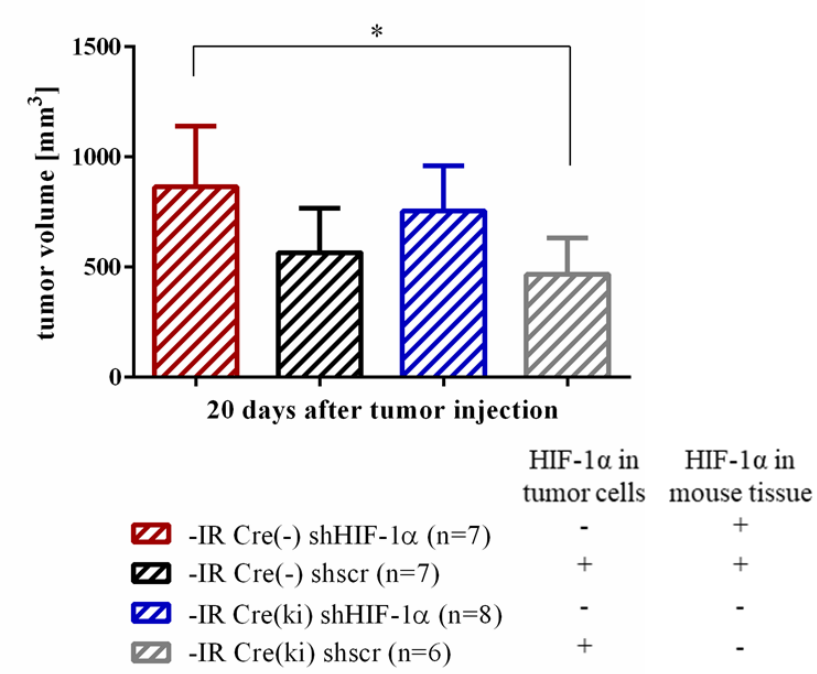

Figure 31: Analysis of tumor growth in non-irradiated tumors

The data of tumor volume of non-irradiated tumors at day 20 were summarized from both experiments. Tumor volume of -IR Cre(ki) shscr group demonstrated a significant decrease compared to –IR Cre(-) shHIF-1α group. **–IR Cre(-) shHIF-1α**: non-irradiated tumor with LLC shHIF-1α cells in HIF-1α$^{fl/fl}$Cre-ER$^{wt/wt}$ mice (Cre(-)), **-IR Cre(-) shscr**: non-irradiated tumor with LLC shscr cells in Cre(-) mice, **–IR Cre(ki) shHIF-1α:** non-irradiated tumor with LLC shHIF-1α cells in HIF-1α$^{fl/fl}$Cre-ER$^{ki/wt}$ (ki), **-IR Cre(ki) shscr:** non-irradiated tumor with LLC shscr cells in Cre(ki) mice

5 Discussion

Evidence for the involvement of HIF-1α in the induction of radioresistance of cancer cells accumulated over the last years. Upregulated expression of HIF-1α in tumors is often associated with an unfavorable prognosis for cancer patients. Several groups have reported that HIF-1α supports tumor growth by adaptation of cell metabolism and stimulation of tumor angiogenesis. Therefore, HIF-1α came into focus as an attractive target for radiation oncology. In order to precisely and efficiently treat cancer patients, a better understanding of mechanisms involved in radioresistance is needed.

The present study was focused on the translational aspects of HIF-1α expression level during radiation treatment. Based on findings which indicated that HIF-1α is involved in induction of radioresistance in tumors (Moeller and Dewhirst, 2006), the paramount task was to identify further interaction of HIF-1α with the DDR molecules. Furthermore, some studies reported the importance of TME in tumor development and induction of radioresistance (Harada, 2016). Therefore, the investigation whether and how surrounding stromal cells may influence HIF-1α signaling was also one of the tasks of this study. For this purpose, the effect of possible HIF-1α-mediated induction of radioresistance was investigated *in vitro* and *in vivo* by depletion of HIF-1α in tumor cells and a mouse model.

5.1 HIF-1α deficiency increased apoptosis in LLC cells

The impact of HIF-1α on apoptosis is controversially discussed in the literature as pro- and anti-apoptotic features of HIF-1α in cancer development have been described. The results of this study demonstrated elevated apoptosis levels after HIF-1α depletion and irradiation in LLC cells. Caspase-3, which is activated in apoptotic cells, showed an increased activity in HIF-1α KD LLC cells. In contrast, HIF-1α positive cells did not display an increase of apoptosis after irradiation. In line with this result, the increase of PARP-1 cleavage, which is a result of cell-death inducing protease activity, was also demonstrated in HIF-1α depleted cells. Notably, the induction of HIF-1α KD led to an increase of apoptosis even in non-irradiated cells.

Thus, these data underline the importance of HIF-1α in cell survival under hypoxic conditions, as already described in the literature (Kumar and Choi, 2015). Remarkably, LLC cells are HIF-2α negative, which allows specific investigation of HIF-1α effects independent

of possible effects of HIF-2α. This study demonstrated that in contrast to the results with LLC cells, the HIF-2α positive B16F10 cells with HIF-1α KD displayed an increase of IR-induced apoptosis only after 24 h, whereas HIF-2α positive HCT116 cells with HIF-1α deficiency did not demonstrate any changes in the apoptosis rate after IR at all. This observation implies that the demonstrated anti-apoptotic effect of HIF-1α, which is inhibited by HIF-1α depletion in LLC cells, is limited to specific cell lines. In addition, different cell lines may respond differently to graded hypoxia: mild hypoxia (1 % O_2) as used in our study, severe hypoxia (0.01-0.1 % O_2) and anoxia (0 % O_2). As expertly reviewed recently, apoptotic dynamics vary under different hypoxic conditions and some cell lines demonstrate an increase of caspase-3 activity under severe hypoxia or anoxia only (Zhou et al., 2015). It is important to mention that LLC cells are too sensitive for severe hypoxia, so that after incubation with 0.1 % O_2 and HIF-1α depletion the cells cannot survive IR at all, thus making further analysis impossible. Thus, it remains to be elucidated whether the HIF-1α KD in B16F10 and HCT116 cells will have an effect on radiation-induced apoptosis after incubation under severe hypoxic conditions instead of mild hypoxia that was applied in our study.

On the other hand, hypoxia was also described to play an anti-apoptotic role by regulating expression of anti- and pro-apoptotic proteins independently of HIF-1 in certain cell lines (Erler et al., 2004; Piret et al., 2006). For example, in a human liver cancer HepG2 cells HIF-1α is not involved in the hypoxia-induced anti-apoptotic pathway (Piret et al., 2006). These may be another explanation for the variable effect of HIF-1α depletion on apoptosis in HCT116 and B16F10 cells, respectively.

The effect of HIF-1α depletion on long term survival was also investigated in the cells up to 10 days by CFA. To imitate the physiological process of reoxygenation after IR, the hypoxic cells were placed in a normoxic environment for 10 days after hypoxic incubation and IR. Due to reduced ability of colony formation, LLC cells with HIF-1α KD demonstrated an impaired long term survival, in particular after 6 Gy IR. As the LLC cells are very radiosensitive, the amount of colonies irradiated with 8 and 10 Gy was very low even in the HIF-1α positive cells making a comparison impossible. The outcome revealed that HIF-1α depletion resulted in impaired clonogenic potential of hypoxic LLC cells.

Taken together, these *in vitro* data provided strong evidence that depletion of HIF-1α increased radiation-induced apoptosis and impairment of the clonogenic potential of LLC cells and thus increased radiosensititvity of the cells. However, the mechanism behind this effect requires further investigation. Several previous studies focused on the mechanisms of

HIF-1α-regulated gene expression for cell survival and apoptosis. Takasaki et al. demonstrated in their study on resected lung cancers that HIF-1α expression was significantly induced with the expression levels of anti-apoptotic proteins, such as Survivin (Takasaki et al., 2016). Moreover, a gastric cancer study led to the conclusion that the HIF-1α KD impaired the expression of Survivin, elevated expression of pro-apoptotic proteins such as Bax and caspase-3, and also increased radiotherapy-induced apoptosis of tumor cells (Zhao et al., 2016). The investigation of expression levels in our model may contribute to a better understanding of this mechanism.

5.2 Elimination of HIF-1α increases IR-induced DSB formation and alters DNA repair in LLC cells

The present study demonstrated that the protein amount of the phosphorylated H2AX form γH2AX, which is a marker for DSBs, is elevated in HIF-1α depleted cells. This effect was even stronger after longer incubation in Hx. In line with this result, an increase of the γH2AX IRIF formation in the first hours after IR was detectable. As the γH2AX recruitment to the IR-induced DSBs represents a first response that activates the DDR, these results indicated that HIF-1α depletion in LLC cells leads to an increase of DNA damage after IR. The amount of IR-induced DNA damage decreases after the first 6 hours, indicating that surviving cells completed DNA repair. However, the significant increase of DNA damage and the previously discussed increase of apoptosis in the first hours after IR pointed to a possible alteration of DNA repair after HIF-1α depletion.

The investigation of DNA damage repair in the first hours after IR demonstrated an unchanged DNA repair kinetic in the first 4 hours post-IR. The DNA repair in the first hours after IR is mainly affected by a fast repair mechanism termed NHEJ. Furthermore, the formation of 53BP1 IRIF also remained unchanged after depletion of HIF-1α in hypoxic LLC cells. 53BP1 is responsible for inhibition of end resection, thereby favoring the DSB repair by NHEJ. Another important DDR mechanism, HR, plays an important role in determining hypoxic cell radiosensitivity. The results of this study showed that the recruitment of the HR protein RAD51 is increased in the HIF-1α-deficient cells during the first hours after IR.

Although a number of findings of the last years indicated that DNA repair proteins are compromised under hypoxia, the results are still controversial. Thus, the expression of NHEJ

proteins in hypoxic cells is under debate in the literature. Some reports corroborated our investigation. In several tumor cell lines NHEJ proteins, such as DNA-PK, remain unaffected under hypoxia (Bindra et al., 2005; Sprong et al., 2006). Gene expression studies showed downregulation of mRNA encoding NHEJ proteins but without significant change in protein content (Meng et al., 2005). A study with murine fibroblasts reported that HIF-1α KO leads to an increase of γH2AX, which correlates with our results, although 53BP1 foci formation was shown to be increased and ATM activation reduced in response to DNA damage (Wirthner et al., 2008). Other studies proposed an increased NHEJ under Hx: an upregulation of Ku70 and DNA-PK expression was demonstrated under acute hypoxia as a result of direct interaction with HIF-1α (Kang et al., 2008; Ren et al., 2013; Um et al., 2004). Furthermore, the level of HIF-1α accumulation under Hx was decreased in DNA-PK deficient cells (Bouquet et al., 2011).

The reported findings about HR in hypoxic cells are not less controversial. However some studies report hypoxia-induced downregulation of HR in tumor cells. Chronic severe hypoxia has been demonstrated to decrease the expression of HR proteins (Chan et al., 2008). In a study with prostate cancer cells the hypoxia-induced impairment of DSB repair gene expression was reported (Meng et al., 2005). One study in which several squamous cell carcinoma cell lines were used described cell-line dependent effects of hypoxia whereby RAD51 was downregulated and DNA-PK phosphorylation was enhanced or delayed in different cell lines (Hauth et al., 2017).

In contrast to our results, in several studies hypoxia-induced HR repression including decrease of RAD51 and BRCA1 level was demonstrated to be independent of HIF-1α (Bindra et al., 2005; Bindra et al., 2004). Furthermore, HIF-1α was reported to contribute to the increase of radioresistance by promoting the upregulation of DNA repair proteins in mouse mesenchymal stromal cells, while depletion of HIF-1α led to a decrease of RAD51 foci (Sugrue et al., 2014).

However, another model proposes that HIF-1α inhibits BRCA1 and NBS1 transcription by counteracting Myc activity which maintains gene expression (Hayashi et al., 2011; Yoo et al., 2011). The study with human colon cancer cells reported that HIF-1α induces cell cycle arrest and inhibits BRCA1 activity indirectly by counteracting c-Myc (Koshiji et al., 2004). Furthermore, HIF-1α was reported to be critical for NBS1 downregulation by hypoxia (To et al., 2006). These results are in line with the finding from this study: if HIF-1α inhibits the HR proteins BRCA1 and NBS1, it is also expected to inhibit the recruitment of RAD51 to the

DSB sites at least indirectly. Depletion of HIF-1α may eliminate this inhibitory effect causing an increase of the RAD51 levels. The next question that arises is which effect an increased RAD51 level has on HR and genomic instability. Most of the reports agreed that increased level of DNA repair proteins correlates with increased DDR and, therefore, a better survival of the cells. However, it has also been postulated that hyperactivity of HR could also contribute to genetic instability by causing inappropriate recombination (Henning and Stürzbecher, 2003). Overexpression of RAD51 was observed in many tumors causing elevated rates of HR. Disruption of HR pathways can create genetic instability, one of the hallmarks of cancer, changing the balance between the high-fidelity HR pathway and error-prone NHEJ pathway of DNA repair.

The formation of RAD51 helical filaments, which are essential for searching for homology in duplex DNA and pairing the recombining DNA molecules, is ATP-dependent (Chi et al., 2006; Schay et al., 2016). The hypoxia-induced downregulation of RAD51 may contribute to the reduction of energy consumption, which is important for cell survival under hypoxic conditions. Overexpression of RAD51 caused by HIF-1α deficiency may increase ATP uptake into the cells, so that the cells consume too much energy for HR with compromised fidelity. In addition, as HIF-1α has been shown to be involved in cellular metabolism and glycolysis to provide ATP for hypoxic cells, absence of HIF-1α may result in a decrease of ATP. Cells which lack energy cannot survive and undergo apoptosis. This hypothesis can explain the increase of apoptosis and overexpression of RAD51 in HIF-1α deficient cells after IR as demonstrated in the present study. Thus, further investigation is needed to unravel the effect of HIF-1α depletion on HR. It would be interesting to analyze ATP consumption and also recruitment of other proteins involved in HR and NHEJ, such as BRCA1, BRCA2, RPA, NBS1 and DNA-PK to confirm this hypothesis. In addition, HR analysis by sister chromatid exchange assay may contribute to the understanding whether HIF-1α depletion affects genomic instability.

Although several studies showed that the activation of DNA repair pathways in some tumors contributes to radioresistance, data from our study demonstrated that activation of RAD51 in HIF-1α depleted LLC cells correlates with impaired survival and increased radiosensitivity. These results revealed that hypoxia induces several HIF-1α-dependent processes involved in providing radioresistance.

5.3 Characterization of allograft mouse models with wild-type and tamoxifen-inducible Cre-loxP mice

Mouse models are an important tool for understanding the complex interaction involved in tumor development that cannot be completely replicated *in vitro*. The current models include xenograft and allograft mouse models. Although the xenograft models allow transplantation of human cell lines, the limitation of all xenograft models is that they require immunocompromised or immunodeficient mice thus preventing investigation of the interaction of the immune system with the tumor (Gómez-Cuadrado et al., 2017). Therefore, in this study the allograft model was used which is based on transplantation of mouse-derived tumor cells into immunocompetent mice therefore allowing the investigation of the immune system in tumor growth.

Thus, LLC cells derived from the C57BL/6 mouse strain were injected subcutaneously into the flank of mice with a C57BL/6 background. The tumors were growing rapidly without metastases. The general problem of this model was a high rate of skin ulcerations approximately 10 to 15 days after tumor cell injection. As LLC cells are robustly proliferating cells, the tumors were growing faster than the skin could adapt, resulting in skin lesions and subsequent ulceration. Furthermore, some of the animals were observed to gnaw on the tumors, probably because of discomfort and the skin itching due to the growing tumor. Although most of the ulcerated tumors were non-irradiated, there were still some ulcerations of the irradiated slowly growing tumors. It has been reported before that radiation can cause acute skin reactions, such as irritation, itching and ulceration (Bray et al., 2016).

For the investigation of an effect of surrounding microenvironment of HIF-1α signaling in tumor cells, mice with a HIF-1α KO were essential. Because the global HIF-1α KO was reported to lead to embryonic lethality (Iyer et al., 1998), mice with tamoxifen-inducible conditional HIF-1α KO were generated. Within this model exon 2 of the HIF-1α gene is flanked by LoxP sequences which are recognized by Cre recombinase. Expression of Cre recombinase under the control of a promoter with a mutated estrogen receptor can be activated by addition of the estrogen antagonist tamoxifen and leads to deletion of exon 2 from the HIF-1α gene in the present model. The deletion of exon 2 raised the question whether a shortened version of the HIF-1α protein will be expressed - lacking exon 2 - or whether the protein is not produced at all. The analysis of the mRNA sequence and samples from HIF-1α$^{fl/fl}$Cre-ER$^{ki/wt}$ mice demonstrated, that deletion of exon 2 caused a frame shift of

the sequence. The theoretical amino acid sequence, which was expected by HIF-1α$^{fl/fl}$Cre-ER$^{ki/wt}$ mice according to the mRNA sequence, consists of only 16 amino acids followed by a stop codon. Therefore, the data indicate that the deletion of exon 2 leads to the complete absence of HIF-1α making it impossible to target the protein with antibodies. In line with our observation, the first report about HIF-1α$^{fl/fl}$Cre-ER$^{ki/wt}$ mice from Wang et al. demonstrated a complete deletion of HIF-1α in T lymphocytes according to WB data (Wang et al., 2011). In addition, complete absence of HIF-1α protein under hypoxic conditions was also observed in HIF-1α-null mouse embryonic fibroblasts generated by deletion of exon 2 (Ryan et al., 2000).

The use of Tam had side effects - male mice treated with Tam experienced scrotal swelling, possibly caused by residual estrogenic action of Tam. Other studies also reported scrotal swelling with histopathological changes in the testes and compromised fertility of the mice (Eissa et al., 2011; Patel et al., 2017; Reinert et al., 2012). Furthermore, another study reported tamoxifen-induced hernia development in the lower abdomen of the male mice that was caused by activation of MMP-2 and MMP-13 leading to decreased collage type II (Ma et al., 2015).

Another phenomenon was observed during genotyping – some of the animals demonstrated a deletion of exon 2 although they were not containing a Cre(ki) allele. Although these animals were excluded from the experiments, it is still important to understand how Cre(-) animals can bear an excision of exon 2. Remarkably, although only one or two animals per litter demonstrated the deletion, this phenomenon recurred in different breeds making it obvious that this phenomenon has a systemic and not random character. The most plausible reason is that some of the animals gained the allele with E2 excision during the cross-breeding and passed it on the progeny. This phenomenon was reported previously for other genes by several research groups (He et al., 2017; Kobayashi and Hensch, 2013; Zeller et al., 2008; Zhang et al., 2013b). The recent article of Song and Palmiter discussed the problems of using the Cre-loxP system highlighting the unexpected transient expression of Cre recombinase in the germline or during early development as a main reason for unwanted recombination events (Song and Palmiter, 2018). Another less likely reason may be an accidental contact of one parent animal with Tam, for example by food consumption. In conclusion, it is important for further Cre-loxP system experiments to validate the unexpected recombination in all experimental animals to avoid misinterpreting data.

5.4 *In vivo* effects of interaction between stromal and tumor cells with HIF-1α deficiency on tumor radiosensitivity

Tumor hypoxia with overexpression of HIF-1α is a driving factor for tumor growth and therapy resistance (Harada, 2011). Furthermore, the tumor microenvironment, including connective tissue, stromal and endothelial cells, is also involved in tumor progression and response towards radiotherapy (Garcia-Barros et al., 2003; Yoshimura et al., 2013). However, the connection between these two aspects remains largely undefined. Therefore, one of the aims of this study was the investigation of the effect tumor associated stromal cells may have on HIF-1α signaling and radioresistance of tumors.

The analysis of tumor growth with HIF-1α depleted LLC cells in the HIF-1α positive microenvironment of wt mice demonstrated that HIF-1α deficiency in tumors did not affect tumor growth. While irradiation clearly reduced the growth of HIF-1α depleted and control tumors and non-irradiated tumors grew more rapidly, tumor growth of HIF-1α depleted tumors did not differ from HIF-1α positive tumors. In addition, as demonstrated by qPCR and IHC, HIF-1α mRNA and protein levels were unchanged in the HIF-1α KD tumors as compared to controls. Literature reports have come to variable conclusions with respect to the function of HIF in *in vivo* models: Williams *et al.* showed prolonged tumor growth after radiotherapy in a xenograft model with a tumor line that is null for HIF-1β and therefore unable to render a HIF-1α response (Williams et al., 2005). In addition, the xenograft study with HepG2 tumor cells with a HIF-1α KD had a reduced growth rate; interestingly, tumors with HIF-2α KD demonstrated a more moderate, but still significant attenuation of tumor growth (Shneor et al., 2017). What all these studies had in common was the use of immunodeficient mice in xenograft models instead of immunocompetent mice in our model. On one hand, based on the results of present study it can be assumed that stromal cells may compensate for the effect of HIF-1α deletion in tumor cells by infiltration of the tumors. On the other hand, these data may indicate that the lentiviral knockdown of HIF-1α is not stable in LLC over the entire experimental period, which is in pronounced contrast to the situation in cell culture. The HIF-1α KD test in the LLC cells demonstrated that 10-20 % of all cells still remained HIF-1α positive. After 3 weeks of tumor development in the mice, the HIF-1α positive cells possibly have a selection advantage and proliferate faster than HIF-1α KD cells. As a result, the tumors are potentially composed mostly of HIF-1α positive cells.

This far, our lentiviral HIF-1α knockdown approach could not clarify whether the knockdown was efficient enough to generate a significant difference, or whether stromal cells had compensated the effect of HIF-1α deletion in tumor cells. For further investigation of the latter assumption an allograft mouse model with HIF-1α deficiency was used. Therefore, irradiation of tumors with a high dose of 15 Gy or a milder dose of 7.5 Gy was analyzed to investigate whether stromal cells can modify the hypoxic condition of tumor cells and enhance their radiation resistance. However, the tumor volume of the irradiated groups was not significantly changed regardless of HIF-1α deficiency in tumors cells and HIF-1α KO in the mice.

Interestingly, the non-irradiated groups demonstrated significant changes in tumor growth. Results of non-irradiated groups summarized from two independent experiments demonstrated that the mean volume of tumors with HIF-1α positive cells that grew in HIF-1α KO mice was significantly decreased compared to tumors with HIF-1α depleted cells that grew in HIF-1α positive mice. Thus, these data indicated that HIF-1α deficiency in tumor-infiltrating stromal cells could have more impact on tumor growth than HIF-1α deficiency in tumor cells. The mRNA levels of HIF-1α and its target genes VEGF, GLUT-1 and BNIP3 were not changed significantly. However, substantial variation inside the groups makes these data difficult to interpret. The impact of HIF-1α in stromal cells on the tumor growth is discussed very controversially in the literature. Targeted deletion of HIF-1α in malignant epithelial cells, endothelial cells or macrophages was shown to suppress tumor growth (Doedens et al., 2010; Liao et al., 2007; Tang et al., 2004). However, contradictory evidence was reported by Kim et al., 2012 who investigated tumor growth in a murine model of mammary cancer and found that deletion of HIF-1α or VEGF in tumor stromal fibroblasts enhances tumor growth and attenuates TAM infiltration (Kim et al., 2012).

Similarly to the *in vitro* data, the results from the allograft model experiments taken together with the previous reports indicated cell-specific and model-dependent effects of HIF-1α deficiency in tumor and stromal cells on tumor growth. Furthermore, additional work is needed to understand the effect of HIF-1α elimination on the radiosensitivity of tumors. While an acute hypoxic response was mainly mediated by HIF-1α activity, HIF-2α was also associated with chronic hypoxia (Koh et al., 2011). In contrast to HIF-1α, the significance of HIF-2α for radiotherapy is remarkably understudied. But there is evidence that inhibition of HIF-2α promotes tumor cell death and radiation responses *in vitro* (Bertout et al., 2009).

Because HIF-2α was present in the mice, this may have been a confounding factor in our study, which was focused on HIF-1α deletion.

The limitation of mouse experiments was the low number of animals at the end of the experiment. Although the theoretical amount of animals per group was calculated by statistical power analysis, the unexpected high rate of ulcerations dramatically decreased the number of animals at the end of the experiment. The significance analysis based on the low number of animals is difficult to interpret.

The *in vitro* investigation of this study uncovered a significant effect of HIF-1α deficiency on the IR-induced apoptosis and clonogenic potential. Furthermore, the observed increase of DNA damage and HR repair activity underlined the effectiveness of HIF-1α elimination for the radiosensitization of tumor cells. *In vivo* results are more controversial, although the data indicated an influence of HIF-1α deficiency in stromal cells on the tumor growth. However, this study does shed light on the complexity of HIF-1α-related network in tumor cells and surrounding tissue during irradiation that requires further in-depth investigation.

5.5 Future perspectives

HIF-1α is now accepted as a promising molecular target for the improvement of radiation therapy because of its involvement in the generation of tumor radioresistance. Further research and increased knowledge of the role of HIF-1α in tumor growth and induction of radioresistance may contribute to identification of improved diagnostic markers and development of more effective cancer treatments.

Certainly, *in vitro* models cannot reproduce all physiological events occurring during tumor progression and only mimic some part of it. The treatment of tumor cells with Hx exposes the whole population of cells to hypoxia – a situation, which is atypical for tumors. The nature of hypoxia is heterogeneous due to the proliferation of cancer cells and simultaneous growth of new blood vessels which supply tumors with oxygen. Therefore, the sub-population of HIF-1α expressing cells is surrounded by HIF-1α negative cells in tissues. Harrison et al., 2008 suggested an interesting *in vitro* model in which HIF-1α can be induced in a sub-population of cells, allowing the separation of effects of HIF-1α from other factors which are also involved in the response to hypoxia (Harrison et al., 2018). The use of this approach may

in the future be used for investigation of radioresistance in tumor cells and the role of HIF-1α in hypoxic and non-hypoxic areas of tumors.

Furthermore, in recent years the importance of three-dimensional tumor models that act as a bridge between monolayer *in vitro* and *in vivo* models has been recognized increasingly. These alternative experimental approaches, such as *in vitro* spheroid cultures or tissue engineered tumors, better recapitulate the dynamics and the heterogeneity of a tumor. Spheroids have many features of the tumor microenvironment, allow a higher throughput, and are easy to handle and less expensive. An interesting tool was engineered and presented by Rodenhizer et al., 2016 that allows analysis of cell metabolism and phenotype in a hypoxia gradient (Rodenhizer et al., 2016). The engineered tumor is assembled by rolling a single-biocomposite sheet and makes spatial mapping of cellular metabolism possible. This model can be used for further investigation of the present project for investigation of apoptosis and DNA damage in a gradient from mild to severe hypoxia in HIF-1α deficient cells.

Moreover, there is evidence that the regulation of some HIF-1α target proteins, such as VEGF and BNIP3, are not only HIF-1α-dependent (Choi et al., 2011; Namas et al., 2011). Thus, the analysis of further HIF-1α targets may contribute to a better understanding of the effects of HIF-1α deletion. Despite extensive optimization of the HIF-1α IHC it is still not sensitive enough for the analysis of HIF-1α expression und needs further improvement.

To clarify whether the HIF-1α knockdown was efficient enough to generate a significant difference, IHC with tumor tissue using GFP antibody can be performed. GFP-labeled cells contain shHIF-1α and therefore are HIF-1α deficient. Furthermore, as injected LLC cells are HIF-2α negative, but the stromal cells from the mice remains HIF-2α positive, the IHC with HIF-2α antibody may demonstrate the invading cells in the tumor tissue. Moreover, for the processing of tumors excised from HIF-1α KO mice the recent method called RNAScope assay is worth considering. It is based on *in situ* hybridization of double Z-shaped probes to target RNA molecules, followed by amplification the hybridization signals with label probes resulting in a punctate dot signal that can be visualized with a microscope. The major advantage of RNAScope over IHC is the use of probes designed to be highly specific for the target. This method can be used for analysis of RNA level of HIF-1α and is targets to validate and supplement IHC. A BaseScope assay is a modification of RNAScope that allows detection of short target sequences, such as specific detection of the exon deletion in tissue. For further investigation of this project, BaseScope probes could be customized to target

stromal cells harbouring a deletion of exon 2 in the tumor tissue, thus they could be distinguished from the injected tumor cells.

Another important aspect is the in-depth investigation of the stromal cells involved in the interaction in the present mouse allograft model. Using flow cytometry the differentiation and distribution of immune cells, fibroblasts and epithelial cells can be investigated. Furthermore, *ex vivo* co-culturing of separate stromal compartments with tumor cells under different hypoxic stages and irradiation doses can clarify the impact of stroma on the tumor growth and radioresistance.

Presumably, the investigation of other murine cell lines in an allograft model might contribute to unravel the demonstrated complex interactions of tumor and stromal cells with HIF-1α deficiency. Furthermore, use of the cell lines for tumor growth that are not proliferating as rapidly and aggressively as the LLC cells, is expected to solve the problem with ulcerations of tumors.

Taken together, data from previous studies and also results from this project demonstrated that although there is definitely an interplay between HIF-1α, DNA repair mechanisms, tumor growth and radioresponsiveness, the effects of HIF-1α are presumably tumor cell specific. This assumption bears the question whether HIF-1α is always a reasonable target for cancer therapy. Therefore, further investigation using other cell lines will be of particular importance. There is an urgent need to identify new tumor-specific biomarkers that affect the choice of therapy. Expanding the knowledge about special features of each cancer cell type due to the response to chemo- and radioresistance will allow improved application of customized therapeutic approaches to specifically target tumor cells and will be a further advancement for cancer therapy.

6 Summary

Poor prognosis of many solid tumors is often associated with hypoxic regions and an increased level of hypoxia-inducible factor-1α (HIF-1α). Previous findings indicate that HIF-1α expression is relevant for radiation resistance. Furthermore, there is evidence that the tumor microenvironment is also involved in protecting tumor cells from radiation induced cell death.

To clarify the role of HIF-1α deficiency in apoptosis, DNA damage repair and radiosensitization *in vitro*, murine Lewis Lung Carcinoma (LLC) cells with a doxycycline-inducible knockdown for HIF-1α were used. The data provided strong evidence that depletion of HIF-1α increased IR-induced apoptosis and impaired clonogenic potential of LLC cells and thus increased radiosensitivity of the cells. Furthermore, HIF-1α deficient LLC cells demonstrated an IR-induced increase of DNA damage measured by γH2AX foci and increased recruitment of RAD51, which suggests an alteration in homologous recombination repair. The level of 53BP1 IR-induced foci remained unchanged, as well as fast repair kinetics indicating that non-homologous end joining repair capacity was not affected. Next, this study investigated an *in vivo* effect of surrounding microenvironment on HIF-1α signaling in tumor cells and the effect of this interaction on the radiation sensitivity. The analysis of HIF-1α depletion in tumors in an allograft mouse model with wild-type C57BL/6 mice demonstrated unchanged tumor growth regardless of HIF-1α deficiency of the tumor cells. In addition, a murine allograft model with HIF-1α conditional knockout was used to elucidate whether HIF-1α simultaneous elimination in surrounding stroma cells and tumor cells affects radiosensitivity of the tumors. The tumor volume of the irradiated groups was not significantly changed regardless of HIF-1α deficiency in tumor cells and in the mice. However, the non-irradiated groups demonstrated that the volume of tumors with HIF-1α positive cells that grew in HIF-1α knockout mice was significantly decreased compared to tumors with HIF-1α depleted cells that grew in HIF-1α positive mice.

In vitro results of present study indicate that inactivation of HIF-1α leads to an enhanced radiation sensitivity of tumor cells. The *in vivo* results are more controversial, although the data indicated an influence of HIF-1α deficiency in stromal cells on tumor growth. The demonstrated complexity of HIF-1α-related networks in tumor cells and surrounding tissue during irradiation makes HIF-1α an attractive target for further investigation to enhance the outcome of radiation treatment.

7 Zusammenfassung

Hypoxische Bereiche mit einer erhöhten Expression des Hypoxie-induzierbaren Faktors 1α (HIF-1α) sind charakteristisch für viele solide Tumore. Frühere Studien haben gezeigt, dass die Expression von HIF-1α bei der Entwicklung einer Tumorresistenz während der Bestrahlungstherapie eine Rolle spielt. Außerdem wurde gezeigt, dass die Zellen aus der Mikroumgebung ebenfalls die Tumore vor der Bestrahlung schützen können.

Die murine Krebszelllinie Lewis-Lungenkarzinom (engl. Lewis Lung Carcinoma; LLC) Zellen mit einem Doxycyclin-induzierbaren Knockdown von HIF-1α wurde bezüglich der Rolle von HIF-1α-Inaktivierung in der Apoptose, DNA Schadensreparatur und Radiosensibilisierung untersucht. Die gezeigten Ergebnisse weisen auf eine erhöhte Apoptoserate und Verschlechterung des klonogenen Potentials, und somit auf eine erhöhte Radiosensitivität bei der HIF-1α-Inaktivierung in den LLC Zellen hin. Außerdem wurde in der Abwesenheit von HIF-1α die Erhöhung von γH2AX und vermehrte Rekrutierung von RAD51 gemessen, was auf eine erhöhte Anzahl an DNA Schäden und eine veränderte Reparatur durch homologe Rekombination hinweist. Allerdings wurden nach der Inaktivierung von HIF-1α keine Veränderungen bei der Reparaturkinetik und der 53BP1 Rekrutierung gemessen, was auf eine unveränderte Aktivität der nicht-homologen Endverknüpfung hinweist. Als Nächstes wurden die Effekte der Interaktion von umgebenden Stromazellen mit den HIF-1α inaktiven Tumorzellen auf die Radiosensibilisierung in einem Maus-Allotransplantations-Modell mit der Wildtyp C57BL/6-Maus untersucht. Diese Versuche zeigten keine Unterschiede bezüglich der HIF-1α-Inaktivierung. In einem Maus-Allotransplantations-Modell mit einem konditionalen HIF-1α-Knockout wurde gezeigt, dass die Tumorgröße nach der Bestrahlung nicht von der HIF-1α-Inaktivierung in den Stroma- und Tumorzellen beeinflusst wird. Bei den nicht bestrahlten Gruppen war das Tumorvolumen bei HIF-1α positiven Tumorzellen aus der HIF-1α Knockout-Maus geringer, als bei den HIF-1α inaktiven Tumoren aus der HIF-1α positiven Maus.

Insgesamt haben die *in vitro* Ergebnisse dieser Studie gezeigt, dass die Inaktivierung von HIF-1α die Radiosensibilisierung in Tumorzellen erhöht. *In vivo* Ergebnisse sind dagegen kontroverser, weisen allerdings auf den Einfluss von HIF-1α inaktiven Stromazellen auf das Tumorwachstum hin. Die gezeigte Komplexität des HIF-1α-abhängigen Netzwerkes in Stroma- und Tumorzellen während der Bestrahlung machen dieses Protein zum attraktiven Ziel der Forschung zur Verbesserung von Strahlentherapie.

8 References

Akakura, N., Kobayashi, M., Horiuchi, I., Suzuki, A., Wang, J., Chen, J., Niizeki, H., Kawamura, K., Hosokawa, M., and Asaka, M. (2001). Constitutive expression of hypoxia-inducible factor-1alpha renders pancreatic cancer cells resistant to apoptosis induced by hypoxia and nutrient deprivation. Cancer Res *61*, 6548-6554.

An, W.G., Kanekal, M., Simon, M.C., Maltepe, E., Blagosklonny, M.V., and Neckers, L.M. (1998). Stabilization of wild-type p53 by hypoxia-inducible factor 1alpha. Nature *392*, 405-408.

Bae, S.H., Jeong, J.W., Park, J.A., Kim, S.H., Bae, M.K., Choi, S.J., and Kim, K.W. (2004). Sumoylation increases HIF-1alpha stability and its transcriptional activity. Biochemical and biophysical research communications *324*, 394-400.

Bakr, A., Köcher, S., Volquardsen, J., Reimer, R., Borgmann, K., Dikomey, E., Rothkamm, K., and Mansour, W.Y. (2016). Functional crosstalk between DNA damage response proteins 53BP1 and BRCA1 regulates double strand break repair choice. Radiotherapy and Oncology *119*, 276-281.

Bao, S., Wu, Q., McLendon, R.E., Hao, Y., Shi, Q., Hjelmeland, A.B., Dewhirst, M.W., Bigner, D.D., and Rich, J.N. (2006). Glioma stem cells promote radioresistance by preferential activation of the DNA damage response. Nature *444*, 756-760.

Batty, D.P., and Wood, R.D. (2000). Damage recognition in nucleotide excision repair of DNA. Gene *241*, 193-204.

Bensaad, K., Favaro, E., Lewis, C.A., Peck, B., Lord, S., Collins, J.M., Pinnick, K.E., Wigfield, S., Buffa, F.M., Li, J.L., *et al.* (2014). Fatty acid uptake and lipid storage induced by HIF-1alpha contribute to cell growth and survival after hypoxia-reoxygenation. Cell Rep *9*, 349-365.

Berra, E., Benizri, E., Ginouves, A., Volmat, V., Roux, D., and Pouyssegur, J. (2003). HIF prolyl-hydroxylase 2 is the key oxygen sensor setting low steady-state levels of HIF-1alpha in normoxia. The EMBO journal *22*, 4082-4090.

Berra, E., Roux, D., Richard, D.E., and Pouyssegur, J. (2001). Hypoxia-inducible factor-1 alpha (HIF-1 alpha) escapes O(2)-driven proteasomal degradation irrespective of its subcellular localization: nucleus or cytoplasm. EMBO reports *2*, 615-620.

Berta, M.A., Mazure, N., Hattab, M., Pouyssegur, J., and Brahimi-Horn, M.C. (2007). SUMOylation of hypoxia-inducible factor-1alpha reduces its transcriptional activity. Biochemical and biophysical research communications *360*, 646-652.

Bertout, J.A., Majmundar, A.J., Gordan, J.D., Lam, J.C., Ditsworth, D., Keith, B., Brown, E.J., Nathanson, K.L., and Simon, M.C. (2009). HIF2alpha inhibition promotes p53 pathway activity, tumor cell death, and radiation responses. Proc Natl Acad Sci U S A *106*, 14391-14396.

Bertram, J.S., and Janik, P. (1980). Establishment of a cloned line of Lewis Lung Carcinoma cells adapted to cell culture. Cancer letters *11*, 63-73.

Bindra, R.S., Gibson, S.L., Meng, A., Westermark, U., Jasin, M., Pierce, A.J., Bristow, R.G., Classon, M.K., and Glazer, P.M. (2005). Hypoxia-induced down-regulation of BRCA1 expression by E2Fs. Cancer Res *65*, 11597-11604.

Bindra, R.S., Schaffer, P.J., Meng, A., Woo, J., Maseide, K., Roth, M.E., Lizardi, P., Hedley, D.W., Bristow, R.G., and Glazer, P.M. (2004). Down-regulation of Rad51 and decreased homologous recombination in hypoxic cancer cells. Mol Cell Biol *24*, 8504-8518.

Blanchard, K.L., Fandrey, J., Goldberg, M.A., and Bunn, H.F. (1993). Regulation of the erythropoietin gene. Stem cells (Dayton, Ohio) *11 Suppl 1*, 1-7.

Boulton, S.J. (2006). Cellular functions of the BRCA tumour-suppressor proteins. Biochemical Society transactions *34*, 633-645.

Bouquet, F., Ousset, M., Biard, D., Fallone, F., Dauvillier, S., Frit, P., Salles, B., and Muller, C. (2011). A DNA-dependent stress response involving DNA-PK occurs in hypoxic cells and contributes to cellular adaptation to hypoxia. Journal of cell science *124*, 1943-1951.

Box, A.H., and Demetrick, D.J. (2004). Cell cycle kinase inhibitor expression and hypoxia-induced cell cycle arrest in human cancer cell lines. Carcinogenesis *25*, 2325-2335.

Branco-Price, C., Zhang, N., Schnelle, M., Evans, C., Katschinski, Dörthe M., Liao, D., Ellies, L., and Johnson, Randall S. (2012). Endothelial Cell HIF-1α and HIF-2α Differentially Regulate Metastatic Success. Cancer cell *21*, 52-65.

Bray, F.N., Simmons, B.J., Wolfson, A.H., and Nouri, K. (2016). Acute and Chronic Cutaneous Reactions to Ionizing Radiation Therapy. Dermatology and Therapy *6*, 185-206.

Bristow, R.G., and Hill, R.P. (2008). Hypoxia and metabolism. Hypoxia, DNA repair and genetic instability. Nature reviews Cancer *8*, 180-192.

Brizel, D.M., Sibley, G.S., Prosnitz, L.R., Scher, R.L., and Dewhirst, M.W. (1997). Tumor hypoxia adversely affects the prognosis of carcinoma of the head and neck. International journal of radiation oncology, biology, physics *38*, 285-289.

Brown, J.M., and Giaccia, A.J. (1998). The unique physiology of solid tumors: opportunities (and problems) for cancer therapy. Cancer Res *58*, 1408-1416.

Bruick, R.K. (2000). Expression of the gene encoding the proapoptotic Nip3 protein is induced by hypoxia. Proc Natl Acad Sci U S A *97*, 9082-9087.

Bruning, U., Fitzpatrick, S.F., Frank, T., Birtwistle, M., Taylor, C.T., and Cheong, A. (2012). NFkappaB and HIF display synergistic behaviour during hypoxic inflammation. Cellular and molecular life sciences : CMLS *69*, 1319-1329.

Bunn, H.F., and Poyton, R.O. (1996). Oxygen sensing and molecular adaptation to hypoxia. Physiological reviews *76*, 839-885.

Bunting, S.F., Callén, E., Wong, N., Chen, H.-T., Polato, F., Gunn, A., Bothmer, A., Feldhahn, N., Fernandez-Capetillo, O., Cao, L., *et al.* (2010). 53BP1 Inhibits Homologous Recombination in Brca1-Deficient Cells by Blocking Resection of DNA Breaks. Cell *141*, 243-254.

Cam, H., Easton, J.B., High, A., and Houghton, P.J. (2010). mTORC1 signaling under hypoxic conditions is controlled by ATM-dependent phosphorylation of HIF-1alpha. Mol Cell *40*, 509-520.

Capp, J.P., Boudsocq, F., Bertrand, P., Laroche-Clary, A., Pourquier, P., Lopez, B.S., Cazaux, C., Hoffmann, J.S., and Canitrot, Y. (2006). The DNA polymerase lambda is required for the repair of non-compatible DNA double strand breaks by NHEJ in mammalian cells. Nucleic Acids Res *34*, 2998-3007.

Capp, J.P., Boudsocq, F., Besnard, A.G., Lopez, B.S., Cazaux, C., Hoffmann, J.S., and Canitrot, Y. (2007). Involvement of DNA polymerase mu in the repair of a specific subset of DNA double-strand breaks in mammalian cells. Nucleic Acids Res *35*, 3551-3560.

Carbia-Nagashima, A., Gerez, J., Perez-Castro, C., Paez-Pereda, M., Silberstein, S., Stalla, G.K., Holsboer, F., and Arzt, E. (2007). RSUME, a small RWD-containing protein, enhances SUMO conjugation and stabilizes HIF-1alpha during hypoxia. Cell *131*, 309-323.

Carmeliet, P., Dor, Y., Herbert, J.M., Fukumura, D., Brusselmans, K., Dewerchin, M., Neeman, M., Bono, F., Abramovitch, R., Maxwell, P., *et al.* (1998). Role of HIF-1alpha in hypoxia-mediated apoptosis, cell proliferation and tumour angiogenesis. Nature *394*, 485-490.

Ceradini, D.J., Kulkarni, A.R., Callaghan, M.J., Tepper, O.M., Bastidas, N., Kleinman, M.E., Capla, J.M., Galiano, R.D., Levine, J.P., and Gurtner, G.C. (2004). Progenitor cell trafficking is regulated by hypoxic gradients through HIF-1 induction of SDF-1. Nature medicine *10*, 858-864.

Chaitanya, G.V., Alexander, J.S., and Babu, P.P. (2010). PARP-1 cleavage fragments: signatures of cell-death proteases in neurodegeneration. Cell Communication and Signaling : CCS *8*, 31-31.

Chan, N., Koritzinsky, M., Zhao, H., Bindra, R., Glazer, P.M., Powell, S., Belmaaza, A., Wouters, B., and Bristow, R.G. (2008). Chronic hypoxia decreases synthesis of homologous recombination proteins to offset chemoresistance and radioresistance. Cancer Res *68*, 605-614.

Chen, J., Li, Y., Yu, T.-S., McKay, R.M., Burns, D.K., Kernie, S.G., and Parada, L.F. (2012). A restricted cell population propagates glioblastoma growth following chemotherapy. Nature *488*, 522-526.

Chen, Y.-Q., Zhao, C.-L., and Li, W. (2009). Effect of hypoxia-inducible factor-1α on transcription of survivin in non-small cell lung cancer. Journal of Experimental & Clinical Cancer Research *28*, 29.

Cheng, J., Kang, X., Zhang, S., and Yeh, E.T.H. (2007). SUMO-Specific Protease 1 Is Essential for Stabilization of HIF1α during Hypoxia. Cell *131*, 584-595.

Chi, P., Van Komen, S., Sehorn, M.G., Sigurdsson, S., and Sung, P. (2006). Roles of ATP binding and ATP hydrolysis in human Rad51 recombinase function. DNA Repair (Amst) *5*, 381-391.

Choi, S.B., Park, J.B., Song, T.J., and Choi, S.Y. (2011). Molecular mechanism of HIF-1-independent VEGF expression in a hepatocellular carcinoma cell line. International journal of molecular medicine *28*, 449-454.

Cockman, M.E., Masson, N., Mole, D.R., Jaakkola, P., Chang, G.W., Clifford, S.C., Maher, E.R., Pugh, C.W., Ratcliffe, P.J., and Maxwell, P.H. (2000). Hypoxia inducible factor-alpha binding and ubiquitylation by the von Hippel-Lindau tumor suppressor protein. J Biol Chem *275*, 25733-25741.

Condeelis, J., and Pollard, J.W. (2006). Macrophages: obligate partners for tumor cell migration, invasion, and metastasis. Cell *124*, 263-266.

Corzo, C.A., Condamine, T., Lu, L., Cotter, M.J., Youn, J.I., Cheng, P., Cho, H.I., Celis, E., Quiceno, D.G., Padhya, T., *et al.* (2010). HIF-1alpha regulates function and differentiation of myeloid-derived suppressor cells in the tumor microenvironment. J Exp Med *207*, 2439-2453.

D'Ignazio, L., Batie, M., and Rocha, S. (2017). Hypoxia and Inflammation in Cancer, Focus on HIF and NF-κB. Biomedicines *5*, 21.

Dang, E.V., Barbi, J., Yang, H.Y., Jinasena, D., Yu, H., Zheng, Y., Bordman, Z., Fu, J., Kim, Y., Yen, H.R., *et al.* (2011). Control of T(H)17/T(reg) balance by hypoxia-inducible factor 1. Cell *146*, 772-784.

David, S.S., O'Shea, V.L., and Kundu, S. (2007). Base-excision repair of oxidative DNA damage. Nature *447*, 941-950.

de Fraipont, F., Nicholson, A.C., Feige, J.J., and Van Meir, E.G. (2001). Thrombospondins and tumor angiogenesis. Trends in molecular medicine *7*, 401-407.

Dimitrova, N., Chen, Y.C., Spector, D.L., and de Lange, T. (2008). 53BP1 promotes non-homologous end joining of telomeres by increasing chromatin mobility. Nature *456*, 524-528.

Dimova, E.Y., Michiels, C., and Kietzmann, T. (2009). Kinases as upstream regulators of the HIF system: their emerging potential as anti-cancer drug targets. Current pharmaceutical design *15*, 3867-3877.

Doedens, A.L., Stockmann, C., Rubinstein, M.P., Liao, D., Zhang, N., DeNardo, D.G., Coussens, L.M., Karin, M., Goldrath, A.W., and Johnson, R.S. (2010). Macrophage expression of hypoxia-inducible factor-1 alpha suppresses T-cell function and promotes tumor progression. Cancer Res *70*, 7465-7475.

Duan, D.R., Pause, A., Burgess, W.H., Aso, T., Chen, D.Y., Garrett, K.P., Conaway, R.C., Conaway, J.W., Linehan, W.M., and Klausner, R.D. (1995). Inhibition of transcription elongation by the VHL tumor suppressor protein. Science *269*, 1402-1406.

Dunn, G.P., Bruce, A.T., Ikeda, H., Old, L.J., and Schreiber, R.D. (2002). Cancer immunoediting: from immunosurveillance to tumor escape. Nature immunology *3*, 991-998.

Dunn, J.O., Mythen, M.G., and Grocott, M.P. (2016). Physiology of oxygen transport. BJA Education *16*, 341-348.

Durant, S.T., and Nickoloff, J.A. (2005). Good timing in the cell cycle for precise DNA repair by BRCA1. Cell Cycle *4*, 1216-1222.

Ebert, B.L., Firth, J.D., and Ratcliffe, P.J. (1995). Hypoxia and mitochondrial inhibitors regulate expression of glucose transporter-1 via distinct Cis-acting sequences. J Biol Chem *270*, 29083-29089.

Eissa, M.M., Amer, E.I., and El Sawy, S.M. (2011). Leishmania major: activity of tamoxifen against experimental cutaneous leishmaniasis. Experimental parasitology *128*, 382-390.

Ema, M., Taya, S., Yokotani, N., Sogawa, K., Matsuda, Y., and Fujii-Kuriyama, Y. (1997). A novel bHLH-PAS factor with close sequence similarity to hypoxia-inducible factor 1alpha regulates the VEGF expression and is potentially involved in lung and vascular development. Proc Natl Acad Sci U S A *94*, 4273-4278.

Epstein, A.C.R., Gleadle, J.M., McNeill, L.A., Hewitson, K.S., O'Rourke, J., Mole, D.R., Mukherji, M., Metzen, E., Wilson, M.I., Dhanda, A., *et al.* (2001). C. elegans EGL-9 and Mammalian Homologs Define a Family of Dioxygenases that Regulate HIF by Prolyl Hydroxylation. Cell *107*, 43-54.

Erler, J.T., Cawthorne, C.J., Williams, K.J., Koritzinsky, M., Wouters, B.G., Wilson, C., Miller, C., Demonacos, C., Stratford, I.J., and Dive, C. (2004). Hypoxia-mediated down-regulation of Bid and Bax in tumors occurs via hypoxia-inducible factor 1-dependent and -independent mechanisms and contributes to drug resistance. Mol Cell Biol *24*, 2875-2889.

Esashi, F., Christ, N., Gannon, J., Liu, Y., Hunt, T., Jasin, M., and West, S.C. (2005). CDK-dependent phosphorylation of BRCA2 as a regulatory mechanism for recombinational repair. Nature *434*, 598-604.

Falck, J., Forment, J.V., Coates, J., Mistrik, M., Lukas, J., Bartek, J., and Jackson, S.P. (2012). CDK targeting of NBS1 promotes DNA-end resection, replication restart and homologous recombination. EMBO reports *13*, 561-568.

Fanelli, M.F., Chinen, L.T., Begnami, M.D., Costa, W.L., Jr., Fregnami, J.H., Soares, F.A., and Montagnini, A.L. (2012). The influence of transforming growth factor-alpha, cyclooxygenase-2, matrix metalloproteinase (MMP)-7, MMP-9 and CXCR4 proteins involved in epithelial-mesenchymal transition on overall survival of patients with gastric cancer. Histopathology *61*, 153-161.

Farrall, A.L., and Whitelaw, M.L. (2009). The HIF1alpha-inducible pro-cell death gene BNIP3 is a novel target of SIM2s repression through cross-talk on the hypoxia response element. Oncogene *28*, 3671-3680.

Firth, J.D., Ebert, B.L., and Ratcliffe, P.J. (1995). Hypoxic Regulation of Lactate-Dehydrogenase-a - Interaction between Hypoxia-Inducible Factor-1 and Camp Response Elements. J Biol Chem *270*, 21021-21027.

Flier, J.S., Mueckler, M.M., Usher, P., and Lodish, H.F. (1987). Elevated levels of glucose transport and transporter messenger RNA are induced by ras or src oncogenes. Science *235*, 1492-1495.

Forsythe, J.A., Jiang, B.H., Iyer, N.V., Agani, F., Leung, S.W., Koos, R.D., and Semenza, G.L. (1996). Activation of vascular endothelial growth factor gene transcription by hypoxia-inducible factor 1. Mol Cell Biol *16*, 4604-4613.

Frankenberg-Schwager, M., Gebauer, A., Koppe, C., Wolf, H., Pralle, E., and Frankenberg, D. (2009). Single-strand annealing, conservative homologous recombination, nonhomologous DNA end joining, and the cell cycle-dependent repair of DNA double-strand breaks induced by sparsely or densely ionizing radiation. Radiation research *171*, 265-273.

Freiberg, R.A., Krieg, A.J., Giaccia, A.J., and Hammond, E.M. (2006). Checking in on hypoxia/reoxygenation. Cell Cycle *5*, 1304-1307.

Fukuda, R., Zhang, H., Kim, J.W., Shimoda, L., Dang, C.V., and Semenza, G.L. (2007). HIF-1 regulates cytochrome oxidase subunits to optimize efficiency of respiration in hypoxic cells. Cell *129*, 111-122.

Garcia-Barros, M., Paris, F., Cordon-Cardo, C., Lyden, D., Rafii, S., Haimovitz-Friedman, A., Fuks, Z., and Kolesnick, R. (2003). Tumor Response to Radiotherapy Regulated by Endothelial Cell Apoptosis. Science *300*, 1155-1159.

Garcia-Calvo, M., Peterson, E.P., Rasper, D.M., Vaillancourt, J.P., Zamboni, R., Nicholson, D.W., and Thornberry, N.A. (1999). Purification and catalytic properties of human caspase family members. Cell death and differentiation *6*, 362-369.

Gardner, L.B., Li, Q., Park, M.S., Flanagan, W.M., Semenza, G.L., and Dang, C.V. (2001). Hypoxia inhibits G1/S transition through regulation of p27 expression. J Biol Chem *276*, 7919-7926.

Gatenby, R.A., and Gillies, R.J. (2004). Why do cancers have high aerobic glycolysis? Nature reviews Cancer *4*, 891-899.

Goda, N., Ryan, H.E., Khadivi, B., McNulty, W., Rickert, R.C., and Johnson, R.S. (2003). Hypoxia-inducible factor 1alpha is essential for cell cycle arrest during hypoxia. Mol Cell Biol *23*, 359-369.

Gómez-Cuadrado, L., Tracey, N., Ma, R., Qian, B., and Brunton, V.G. (2017). Mouse models of metastasis: progress and prospects. Disease Models & Mechanisms *10*, 1061-1074.

Goodarzi, A.A., Yu, Y., Riballo, E., Douglas, P., Walker, S.A., Ye, R., Harer, C., Marchetti, C., Morrice, N., Jeggo, P.A., *et al.* (2006). DNA-PK autophosphorylation facilitates Artemis endonuclease activity. The EMBO journal *25*, 3880-3889.

Gorski, D.H., Beckett, M.A., Jaskowiak, N.T., Calvin, D.P., Mauceri, H.J., Salloum, R.M., Seetharam, S., Koons, A., Hari, D.M., Kufe, D.W., *et al.* (1999). Blockage of the vascular endothelial growth factor stress response increases the antitumor effects of ionizing radiation. Cancer Res *59*, 3374-3378.

Grawunder, U., Wilm, M., Wu, X., Kulesza, P., Wilson, T.E., Mann, M., and Lieber, M.R. (1997). Activity of DNA ligase IV stimulated by complex formation with XRCC4 protein in mammalian cells. Nature *388*, 492-495.

Gray, L.H., Conger, A.D., Ebert, M., Hornsey, S., and Scott, O.C. (1953). The concentration of oxygen dissolved in tissues at the time of irradiation as a factor in radiotherapy. The British journal of radiology *26*, 638-648.

Gu, Y.Z., Moran, S.M., Hogenesch, J.B., Wartman, L., and Bradfield, C.A. (1998). Molecular characterization and chromosomal localization of a third alpha-class hypoxia inducible factor subunit, HIF3alpha. Gene expression *7*, 205-213.

Gunaratnam, L., Morley, M., Franovic, A., de Paulsen, N., Mekhail, K., Parolin, D.A., Nakamura, E., Lorimer, I.A., and Lee, S. (2003). Hypoxia inducible factor activates the transforming growth factor-alpha/epidermal growth factor receptor growth stimulatory pathway in VHL(-/-) renal cell carcinoma cells. J Biol Chem *278*, 44966-44974.

Gunnett, C.A., Lund, D.D., McDowell, A.K., Faraci, F.M., and Heistad, D.D. (2005). Mechanisms of inducible nitric oxide synthase-mediated vascular dysfunction. Arteriosclerosis, thrombosis, and vascular biology *25*, 1617-1622.

Gwak, G.Y., Yoon, J.H., Kim, K.M., Lee, H.S., Chung, J.W., and Gores, G.J. (2005). Hypoxia stimulates proliferation of human hepatoma cells through the induction of hexokinase II expression. Journal of hepatology *42*, 358-364.

Haaf, T., Golub, E.I., Reddy, G., Radding, C.M., and Ward, D.C. (1995). Nuclear foci of mammalian Rad51 recombination protein in somatic cells after DNA damage and its localization in synaptonemal complexes. Proc Natl Acad Sci U S A *92*, 2298-2302.

Hall, E.J., and Giaccia, A.J. (2012). Radiobiology for the Radiologist. Wolters Kluwer, Lippincott Williams & Wilkins *7th edition*.

Hamaguchi, T., Iizuka, N., Tsunedomi, R., Hamamoto, Y., Miyamoto, T., Iida, M., Tokuhisa, Y., Sakamoto, K., Takashima, M., Tamesa, T., *et al.* (2008). Glycolysis module activated by hypoxia-inducible factor 1alpha is related to the aggressive phenotype of hepatocellular carcinoma. International journal of oncology *33*, 725-731.

Hammond, E.M., Denko, N.C., Dorie, M.J., Abraham, R.T., and Giaccia, A.J. (2002). Hypoxia links ATR and p53 through replication arrest. Mol Cell Biol *22*, 1834-1843.

Hammond, E.M., Dorie, M.J., and Giaccia, A.J. (2003). ATR/ATM targets are phosphorylated by ATR in response to hypoxia and ATM in response to reoxygenation. J Biol Chem *278*, 12207-12213.

Hanahan, D., and Weinberg, R.A. (2000). The hallmarks of cancer. Cell *100*, 57-70.

Hanahan, D., and Weinberg, R.A. (2011). Hallmarks of cancer: the next generation. Cell *144*, 646-674.

Harada, H. (2011). How can we overcome tumor hypoxia in radiation therapy? Journal of radiation research *52*, 545-556.

Harada, H. (2016). Hypoxia-inducible factor 1–mediated characteristic features of cancer cells for tumor radioresistance. Journal of radiation research *57*, i99-i105.

Harada, H., Inoue, M., Itasaka, S., Hirota, K., Morinibu, A., Shinomiya, K., Zeng, L., Ou, G., Zhu, Y., Yoshimura, M., *et al.* (2012). Cancer cells that survive radiation therapy acquire HIF-1 activity and translocate towards tumour blood vessels. Nature Communications *3*, 783.

Harada, H., Itasaka, S., Kizaka-Kondoh, S., Shibuya, K., Morinibu, A., Shinomiya, K., and Hiraoka, M. (2009). The Akt/mTOR pathway assures the synthesis of HIF-1alpha protein in a glucose- and reoxygenation-dependent manner in irradiated tumors. J Biol Chem *284*, 5332-5342.

Harris, A.L. (2002). Hypoxia — a key regulatory factor in tumour growth. Nature Reviews Cancer *2*, 38.

Harrison, H., Pegg, H.J., Thompson, J., Bates, C., and Shore, P. (2018). HIF1-alpha expressing cells induce a hypoxic-like response in neighbouring cancer cells. BMC cancer *18*, 674.

Hauth, F., Toulany, M., Zips, D., and Menegakis, A. (2017). Cell-line dependent effects of hypoxia prior to irradiation in squamous cell carcinoma lines. Clinical and translational radiation oncology *5*, 12-19.

Hayashi, M., Yoo, Y.Y., Christensen, J., and Huang, L.E. (2011). Requirement of evading apoptosis for HIF-1alpha-induced malignant progression in mouse cells. Cell Cycle *10*, 2364-2372.

He, Y., Sun, X., Wang, L., Mishina, Y., Guan, J.L., and Liu, F. (2017). Male germline recombination of a conditional allele by the widely used Dermo1-cre (Twist2-cre) transgene. Genesis *55*.

Helmlinger, G., Yuan, F., Dellian, M., and Jain, R.K. (1997). Interstitial pH and pO2 gradients in solid tumors in vivo: high-resolution measurements reveal a lack of correlation. Nature medicine *3*, 177-182.

Henning, W., and Stürzbecher, H.-W. (2003). Homologous recombination and cell cycle checkpoints: Rad51 in tumour progression and therapy resistance. Toxicology *193*, 91-109.

Hu, C.-J., Wang, L.-Y., Chodosh, L.A., Keith, B., and Simon, M.C. (2003). Differential Roles of Hypoxia-Inducible Factor 1α (HIF-1α) and HIF-2α in Hypoxic Gene Regulation. Molecular and Cellular Biology *23*, 9361-9374.

Huang, L.E., Gu, J., Schau, M., and Bunn, H.F. (1998). Regulation of hypoxia-inducible factor 1alpha is mediated by an O2-dependent degradation domain via the ubiquitin-proteasome pathway. Proc Natl Acad Sci U S A *95*, 7987-7992.

Hurst, J.H. (2016). William Kaelin, Peter Ratcliffe, and Gregg Semenza receive the 2016 Albert Lasker Basic Medical Research Award. The Journal of clinical investigation *126*, 3628-3638.

Hussain, S.A., Ganesan, R., Reynolds, G., Gross, L., Stevens, A., Pastorek, J., Murray, P.G., Perunovic, B., Anwar, M.S., Billingham, L., *et al.* (2007). Hypoxia-regulated carbonic

anhydrase IX expression is associated with poor survival in patients with invasive breast cancer. Br J Cancer *96*, 104-109.

Iijima, K., Ohara, M., Seki, R., and Tauchi, H. (2008). Dancing on damaged chromatin: functions of ATM and the RAD50/MRE11/NBS1 complex in cellular responses to DNA damage. Journal of radiation research *49*, 451-464.

Iliakis, G., Murmann, T., and Soni, A. (2015). Alternative end-joining repair pathways are the ultimate backup for abrogated classical non-homologous end-joining and homologous recombination repair: Implications for the formation of chromosome translocations. Mutation research Genetic toxicology and environmental mutagenesis *793*, 166-175.

Isono, M., Niimi, A., Oike, T., Hagiwara, Y., Sato, H., Sekine, R., Yoshida, Y., Isobe, S.-Y., Obuse, C., Nishi, R., *et al.* (2017). BRCA1 Directs the Repair Pathway to Homologous Recombination by Promoting 53BP1 Dephosphorylation. Cell Reports *18*, 520-532.

Ivan, M., Kondo, K., Yang, H., Kim, W., Valiando, J., Ohh, M., Salic, A., Asara, J.M., Lane, W.S., and Kaelin, W.G., Jr. (2001). HIFalpha targeted for VHL-mediated destruction by proline hydroxylation: implications for O2 sensing. Science *292*, 464-468.

Iyer, N.V., Kotch, L.E., Agani, F., Leung, S.W., Laughner, E., Wenger, R.H., Gassmann, M., Gearhart, J.D., Lawler, A.M., Yu, A.Y., *et al.* (1998). Cellular and developmental control of O2 homeostasis by hypoxia-inducible factor 1 alpha. Genes Dev *12*, 149-162.

Jaakkola, P., Mole, D.R., Tian, Y.M., Wilson, M.I., Gielbert, J., Gaskell, S.J., von Kriegsheim, A., Hebestreit, H.F., Mukherji, M., Schofield, C.J., *et al.* (2001). Targeting of HIF-alpha to the von Hippel-Lindau ubiquitylation complex by O2-regulated prolyl hydroxylation. Science *292*, 468-472.

Jantsch, J., Chakravortty, D., Turza, N., Prechtel, A.T., Buchholz, B., Gerlach, R.G., Volke, M., Glasner, J., Warnecke, C., Wiesener, M.S., *et al.* (2008). Hypoxia and hypoxia-inducible factor-1 alpha modulate lipopolysaccharide-induced dendritic cell activation and function. Journal of immunology (Baltimore, Md : 1950) *180*, 4697-4705.

Jeong, J.W., Bae, M.K., Ahn, M.Y., Kim, S.H., Sohn, T.K., Bae, M.H., Yoo, M.A., Song, E.J., Lee, K.J., and Kim, K.W. (2002). Regulation and destabilization of HIF-1alpha by ARD1-mediated acetylation. Cell *111*, 709-720.

Jiang, B.H., Zheng, J.Z., Leung, S.W., Roe, R., and Semenza, G.L. (1997). Transactivation and inhibitory domains of hypoxia-inducible factor 1alpha. Modulation of transcriptional activity by oxygen tension. J Biol Chem *272*, 19253-19260.

Jiao, M., and Nan, K.J. (2012). Activation of PI3 kinase/Akt/HIF-1alpha pathway contributes to hypoxia-induced epithelial-mesenchymal transition and chemoresistance in hepatocellular carcinoma. International journal of oncology *40*, 461-468.

Jiricny, J. (2006). The multifaceted mismatch-repair system. Nat Rev Mol Cell Biol *7*, 335-346.

Johnson, A.B., Denko, N., and Barton, M.C. (2008). Hypoxia induces a novel signature of chromatin modifications and global repression of transcription. Mutation research *640*, 174-179.

Joyce, J.A., and Pollard, J.W. (2009). Microenvironmental regulation of metastasis. Nature reviews Cancer *9*, 239-252.

Kaelin, W.G., Jr., and Ratcliffe, P.J. (2008). Oxygen sensing by metazoans: the central role of the HIF hydroxylase pathway. Mol Cell *30*, 393-402.

Kamura, T., Sato, S., Iwai, K., Czyzyk-Krzeska, M., Conaway, R.C., and Conaway, J.W. (2000). Activation of HIF1alpha ubiquitination by a reconstituted von Hippel-Lindau (VHL) tumor suppressor complex. Proc Natl Acad Sci U S A *97*, 10430-10435.

Kang, M.J., Jung, S.M., Kim, M.J., Bae, J.H., Kim, H.B., Kim, J.Y., Park, S.J., Song, H.S., Kim, D.W., Kang, C.D., *et al.* (2008). DNA-dependent protein kinase is involved in heat shock protein-mediated accumulation of hypoxia-inducible factor-1alpha in hypoxic preconditioned HepG2 cells. The FEBS journal *275*, 5969-5981.

Karar, J., and Maity, A. (2009). Modulating the tumor microenvironment to increase radiation responsiveness. Cancer biology & therapy *8*, 1994-2001.

Kashiwagi, S., Izumi, Y., Gohongi, T., Demou, Z.N., Xu, L., Huang, P.L., Buerk, D.G., Munn, L.L., Jain, R.K., and Fukumura, D. (2005). NO mediates mural cell recruitment and vessel morphogenesis in murine melanomas and tissue-engineered blood vessels. The Journal of clinical investigation *115*, 1816-1827.

Keith, B., and Simon, M.C. (2007). Hypoxia Inducible Factors, stem cells and cancer. Cell *129*, 465-472.

Kelly, B.D., Hackett, S.F., Hirota, K., Oshima, Y., Cai, Z., Berg-Dixon, S., Rowan, A., Yan, Z., Campochiaro, P.A., and Semenza, G.L. (2003). Cell type-specific regulation of angiogenic growth factor gene expression and induction of angiogenesis in nonischemic tissue by a constitutively active form of hypoxia-inducible factor 1. Circulation research *93*, 1074-1081.

Kietzmann, T., Mennerich, D., and Dimova, E.Y. (2016). Hypoxia-Inducible Factors (HIFs) and Phosphorylation: Impact on Stability, Localization, and Transactivity. Frontiers in Cell and Developmental Biology *4*, 11.

Kim, J.W., Evans, C., Weidemann, A., Takeda, N., Lee, Y.S., Stockmann, C., Branco-Price, C., Brandberg, F., Leone, G., Ostrowski, M.C., *et al.* (2012). Loss of fibroblast HIF-1alpha accelerates tumorigenesis. Cancer Res *72*, 3187-3195.

Kobayashi, J. (2004). Molecular mechanism of the recruitment of NBS1/hMRE11/hRAD50 complex to DNA double-strand breaks: NBS1 binds to gamma-H2AX through FHA/BRCT domain. Journal of radiation research *45*, 473-478.

Kobayashi, Y., and Hensch, T.K. (2013). Germline recombination by conditional gene targeting with Parvalbumin-Cre lines. Frontiers in neural circuits *7*, 168.

Koh, M.Y., Lemos, R., Jr., Liu, X., and Powis, G. (2011). The hypoxia-associated factor switches cells from HIF-1alpha- to HIF-2alpha-dependent signaling promoting stem cell characteristics, aggressive tumor growth and invasion. Cancer Res *71*, 4015-4027.

Koshiji, M., Kageyama, Y., Pete, E.A., Horikawa, I., Barrett, J.C., and Huang, L.E. (2004). HIF-1alpha induces cell cycle arrest by functionally counteracting Myc. The EMBO journal *23*, 1949-1956.

Krishnamachary, B., Zagzag, D., Nagasawa, H., Rainey, K., Okuyama, H., Baek, J.H., and Semenza, G.L. (2006). Hypoxia-inducible factor-1-dependent repression of E-cadherin in von Hippel-Lindau tumor suppressor-null renal cell carcinoma mediated by TCF3, ZFHX1A, and ZFHX1B. Cancer Res *66*, 2725-2731.

Kumar, H., and Choi, D.-K. (2015). Hypoxia Inducible Factor Pathway and Physiological Adaptation: A Cell Survival Pathway? Mediators of Inflammation *2015*, 11.

Kumar, V., and Gabrilovich, D.I. (2014). Hypoxia-inducible factors in regulation of immune responses in tumour microenvironment. Immunology *143*, 512-519.

Kvietikova, I., Wenger, R.H., Marti, H.H., and Gassmann, M. (1995). The transcription factors ATF-1 and CREB-1 bind constitutively to the hypoxia-inducible factor-1 (HIF-1) DNA recognition site. Nucleic Acids Research *23*, 4542-4550.

Lamouille, S., Xu, J., and Derynck, R. (2014). Molecular mechanisms of epithelial-mesenchymal transition. Nat Rev Mol Cell Biol *15*, 178-196.

Lan, J., Lu, H., Samanta, D., Salman, S., Lu, Y., and Semenza, G.L. (2018). Hypoxia-inducible factor 1-dependent expression of adenosine receptor 2B promotes breast cancer stem cell enrichment. Proc Natl Acad Sci U S A.

Lando, D., Peet, D.J., Whelan, D.A., Gorman, J.J., and Whitelaw, M.L. (2002). Asparagine hydroxylation of the HIF transactivation domain a hypoxic switch. Science *295*, 858-861.

Laughner, E., Taghavi, P., Chiles, K., Mahon, P.C., and Semenza, G.L. (2001). HER2 (neu) signaling increases the rate of hypoxia-inducible factor 1alpha (HIF-1alpha) synthesis: novel mechanism for HIF-1-mediated vascular endothelial growth factor expression. Mol Cell Biol *21*, 3995-4004.

Leach, R.M., and Treacher, D.F. (1992). The pulmonary physician and critical care. 6. Oxygen transport: the relation between oxygen delivery and consumption. Thorax *47*, 971-978.

Levine, B., and Klionsky, D.J. (2004). Development by self-digestion: molecular mechanisms and biological functions of autophagy. Developmental cell *6*, 463-477.

Li, F., Sonveaux, P., Rabbani, Z.N., Liu, S., Yan, B., Huang, Q., Vujaskovic, Z., Dewhirst, M.W., and Li, C.-Y. (2007). Regulation of HIF-1α Stability through S-nitrosylation. Molecular cell *26*, 63-74.

Liang, D., Ma, Y., Liu, J., Trope, C.G., Holm, R., Nesland, J.M., and Suo, Z. (2012). The hypoxic microenvironment upgrades stem-like properties of ovarian cancer cells. BMC cancer *12*, 201.

Liao, D., Corle, C., Seagroves, T.N., and Johnson, R.S. (2007). Hypoxia-inducible factor-1alpha is a key regulator of metastasis in a transgenic model of cancer initiation and progression. Cancer Res *67*, 563-572.

Livak, K.J., and Schmittgen, T.D. (2001). Analysis of relative gene expression data using real-time quantitative PCR and the 2(-Delta Delta C(T)) Method. Methods (San Diego, Calif) *25*, 402-408.

Lonergan, K.M., Iliopoulos, O., Ohh, M., Kamura, T., Conaway, R.C., Conaway, J.W., and Kaelin, W.G. (1998). Regulation of Hypoxia-Inducible mRNAs by the von Hippel-Lindau Tumor Suppressor Protein Requires Binding to Complexes Containing Elongins B/C and Cul2. Molecular and Cellular Biology *18*, 732-741.

Lukashev, D., Klebanov, B., Kojima, H., Grinberg, A., Ohta, A., Berenfeld, L., Wenger, R.H., Ohta, A., and Sitkovsky, M. (2006). Cutting edge: hypoxia-inducible factor 1alpha and its activation-inducible short isoform I.1 negatively regulate functions of CD4+ and CD8+ T lymphocytes. Journal of immunology (Baltimore, Md : 1950) *177*, 4962-4965.

Ma, X., Liu, Y., Wang, Q., Chen, Y., Liu, M., Li, X., Xiang, R., Wei, Y., Duan, Y., and Han, J. (2015). Tamoxifen induces the development of hernia in mice by activating MMP-2 and MMP-13 expression. Biochimica et Biophysica Acta (BBA) - Molecular Basis of Disease *1852*, 1038-1048.

Ma, Y., Pannicke, U., Schwarz, K., and Lieber, M.R. (2002). Hairpin opening and overhang processing by an Artemis/DNA-dependent protein kinase complex in nonhomologous end joining and V(D)J recombination. Cell *108*, 781-794.

Makino, Y., Kanopka, A., Wilson, W.J., Tanaka, H., and Poellinger, L. (2002). Inhibitory PAS domain protein (IPAS) is a hypoxia-inducible splicing variant of the hypoxia-inducible factor-3alpha locus. J Biol Chem *277*, 32405-32408.

Mancini, M., Gariboldi, M.B., Taiana, E., Bonzi, M.C., Craparotta, I., Pagin, M., and Monti, E. (2014). Co-targeting the IGF system and HIF-1 inhibits migration and invasion by (triple-negative) breast cancer cells. British Journal of Cancer *110*, 2865-2873.

Mantovani, A., Allavena, P., Sica, A., and Balkwill, F. (2008). Cancer-related inflammation. Nature *454*, 436-444.

Martinez-Outschoorn, U.E., Lisanti, M.P., and Sotgia, F. (2014). Catabolic cancer-associated fibroblasts transfer energy and biomass to anabolic cancer cells, fueling tumor growth. Seminars in cancer biology *25*, 47-60.

Masson, N., Willam, C., Maxwell, P.H., Pugh, C.W., and Ratcliffe, P.J. (2001). Independent function of two destruction domains in hypoxia-inducible factor-alpha chains activated by prolyl hydroxylation. The EMBO journal *20*, 5197-5206.

Mathupala, S.P., Rempel, A., and Pedersen, P.L. (2001). Glucose catabolism in cancer cells: identification and characterization of a marked activation response of the type II hexokinase gene to hypoxic conditions. J Biol Chem *276*, 43407-43412.

Matsumoto, K., Akazawa, S., Ishibashi, M., Trocino, R.A., Matsuo, H., Yamasaki, H., Yamaguchi, Y., Nagamatsu, S., and Nagataki, S. (1995). Abundant expression of GLUT1 and GLUT3 in rat embryo during the early organogenesis period. Biochemical and biophysical research communications *209*, 95-102.

Matsuzaki, Y., Umemoto, T., Tanaka, Y., Okano, T., and Yamato, M. (2015). β2-Microglobulin is an appropriate reference gene for RT-PCR-based gene expression analysis of hematopoietic stem cells. Regenerative Therapy *1*, 91-97.

Maxwell, P.H., Dachs, G.U., Gleadle, J.M., Nicholls, L.G., Harris, A.L., Stratford, I.J., Hankinson, O., Pugh, C.W., and Ratcliffe, P.J. (1997). Hypoxia-inducible factor-1 modulates gene expression in solid tumors and influences both angiogenesis and tumor growth. Proc Natl Acad Sci U S A *94*, 8104-8109.

Maxwell, P.H., Wiesener, M.S., Chang, G.W., Clifford, S.C., Vaux, E.C., Cockman, M.E., Wykoff, C.C., Pugh, C.W., Maher, E.R., and Ratcliffe, P.J. (1999). The tumour suppressor protein VHL targets hypoxia-inducible factors for oxygen-dependent proteolysis. Nature *399*, 271-275.

McKinnon, P.J. (2004). ATM and ataxia telangiectasia. EMBO reports *5*, 772-776.

Meng, A.X., Jalali, F., Cuddihy, A., Chan, N., Bindra, R.S., Glazer, P.M., and Bristow, R.G. (2005). Hypoxia down-regulates DNA double strand break repair gene expression in prostate cancer cells. Radiother Oncol *76*, 168-176.

Mersch, E. (2015). Die Bedeutung des Hypoxia-inducible Factor-1α in Tumorzellen für die strahlentherapeutische Behandlung maligner Tumore.

Metzen, E., Berchner-Pfannschmidt, U., Stengel, P., Marxsen, J.H., Stolze, I., Klinger, M., Huang, W.Q., Wotzlaw, C., Hellwig-Burgel, T., Jelkmann, W., *et al.* (2003). Intracellular localisation of human HIF-1 alpha hydroxylases: implications for oxygen sensing. Journal of cell science *116*, 1319-1326.

Mimeault, M., and Batra, S.K. (2013). Hypoxia-inducing factors as master regulators of stemness properties and altered metabolism of cancer- and metastasis-initiating cells. Journal of cellular and molecular medicine *17*, 30-54.

Moeller, B.J., Cao, Y., Li, C.Y., and Dewhirst, M.W. (2004). Radiation activates HIF-1 to regulate vascular radiosensitivity in tumors: role of reoxygenation, free radicals, and stress granules. Cancer cell *5*, 429-441.

Moeller, B.J., and Dewhirst, M.W. (2006). HIF-1 and tumour radiosensitivity. British Journal Of Cancer *95*, 1.

Moeller, B.J., Dreher, M.R., Rabbani, Z.N., Schroeder, T., Cao, Y., Li, C.Y., and Dewhirst, M.W. (2005). Pleiotropic effects of HIF-1 blockade on tumor radiosensitivity. Cancer cell *8*, 99-110.

Mole, D.R., Blancher, C., Copley, R.R., Pollard, P.J., Gleadle, J.M., Ragoussis, J., and Ratcliffe, P.J. (2009). Genome-wide association of hypoxia-inducible factor (HIF)-1alpha and HIF-2alpha DNA binding with expression profiling of hypoxia-inducible transcripts. J Biol Chem *284*, 16767-16775.

Murre, C., Bain, G., van Dijk, M.A., Engel, I., Furnari, B.A., Massari, M.E., Matthews, J.R., Quong, M.W., Rivera, R.R., and Stuiver, M.H. (1994). Structure and function of helix-loop-helix proteins. Biochimica et biophysica acta *1218*, 129-135.

Namas, R.A., Metukuri, M.R., Dhupar, R., Velosa, C., Jefferson, B.S., Myer, E., Constantine, G.M., Billiar, T.R., Vodovotz, Y., and Zamora, R. (2011). Hypoxia-induced overexpression of BNIP3 is not dependent on hypoxia-inducible factor 1alpha in mouse hepatocytes. Shock (Augusta, Ga) *36*, 196-202.

Nambu, J.R., Lewis, J.O., Wharton, K.A., Jr., and Crews, S.T. (1991). The Drosophila single-minded gene encodes a helix-loop-helix protein that acts as a master regulator of CNS midline development. Cell *67*, 1157-1167.

Noman, M.Z., Buart, S., Van Pelt, J., Richon, C., Hasmim, M., Leleu, N., Suchorska, W.M., Jalil, A., Lecluse, Y., El Hage, F., *et al.* (2009). The Cooperative Induction of Hypoxia-Inducible Factor-1α and STAT3 during Hypoxia Induced an Impairment of Tumor Susceptibility to CTL-Mediated Cell Lysis. The Journal of Immunology *182*, 3510-3521.

O'Rourke, J.F., Pugh, C.W., Bartlett, S.M., and Ratcliffe, P.J. (1996). Identification of hypoxically inducible mRNAs in HeLa cells using differential-display PCR. Role of hypoxia-inducible factor-1. European journal of biochemistry *241*, 403-410.

Ohh, M., Park, C.W., Ivan, M., Hoffman, M.A., Kim, T.Y., Huang, L.E., Pavletich, N., Chau, V., and Kaelin, W.G. (2000). Ubiquitination of hypoxia-inducible factor requires direct binding to the beta-domain of the von Hippel-Lindau protein. Nature cell biology *2*, 423-427.

Patel, S.H., O'Hara, L., Atanassova, N., Smith, S.E., Curley, M.K., Rebourcet, D., Darbey, A.L., Gannon, A.-L., Sharpe, R.M., and Smith, L.B. (2017). Low-dose tamoxifen treatment in juvenile males has long-term adverse effects on the reproductive system: implications for inducible transgenics. Scientific Reports *7*, 8991.

Peet, D., and Linke, S. (2006). Regulation of HIF: asparaginyl hydroxylation. Novartis Foundation symposium *272*, 37-49; discussion 49-53, 131-140.

Petrova, V., Annicchiarico-Petruzzelli, M., Melino, G., and Amelio, I. (2018). The hypoxic tumour microenvironment. Oncogenesis *7*, 10.

Piret, J.P., Cosse, J.P., Ninane, N., Raes, M., and Michiels, C. (2006). Hypoxia protects HepG2 cells against etoposide-induced apoptosis via a HIF-1-independent pathway. Experimental cell research *312*, 2908-2920.

Potter, C., and Harris, A.L. (2004). Hypoxia inducible carbonic anhydrase IX, marker of tumour hypoxia, survival pathway and therapy target. Cell Cycle *3*, 164-167.

Prakash, R., Zhang, Y., Feng, W., and Jasin, M. (2015). Homologous recombination and human health: the roles of BRCA1, BRCA2, and associated proteins. Cold Spring Harb Perspect Biol *7*, a016600.

Racker, E., Resnick, R.J., and Feldman, R. (1985). Glycolysis and methylaminoisobutyrate uptake in rat-1 cells transfected with ras or myc oncogenes. Proc Natl Acad Sci U S A *82*, 3535-3538.

Ravi, R., Mookerjee, B., Bhujwalla, Z.M., Sutter, C.H., Artemov, D., Zeng, Q., Dillehay, L.E., Madan, A., Semenza, G.L., and Bedi, A. (2000). Regulation of tumor angiogenesis by p53-induced degradation of hypoxia-inducible factor 1alpha. Genes Dev *14*, 34-44.

Reddy, P., Jacquier, A.C., Abovich, N., Petersen, G., and Rosbash, M. (1986). The period clock locus of D. melanogaster codes for a proteoglycan. Cell *46*, 53-61.

Reinert, R.B., Kantz, J., Misfeldt, A.A., Poffenberger, G., Gannon, M., Brissova, M., and Powers, A.C. (2012). Tamoxifen-Induced Cre-loxP Recombination Is Prolonged in Pancreatic Islets of Adult Mice. PLoS ONE *7*, e33529.

Ren, Y., Hao, P., Dutta, B., Cheow, E.S., Sim, K.H., Gan, C.S., Lim, S.K., and Sze, S.K. (2013). Hypoxia modulates A431 cellular pathways association to tumor radioresistance and enhanced migration revealed by comprehensive proteomic and functional studies. Molecular & cellular proteomics : MCP *12*, 485-498.

Richard, D.E., Berra, E., Gothie, E., Roux, D., and Pouyssegur, J. (1999). p42/p44 mitogen-activated protein kinases phosphorylate hypoxia-inducible factor 1alpha (HIF-1alpha) and enhance the transcriptional activity of HIF-1. J Biol Chem *274*, 32631-32637.

Richardson, A.E., Hamilton, N., Davis, W., Brito, C., and De León, D. (2011). Insulin-like Growth Factor-2 (IGF-2) Activates Estrogen Receptor-α and -β via the IGF-1 and the Insulin Receptors in Breast Cancer Cells. Growth factors (Chur, Switzerland) *29*, 82-93.

Rodenhizer, D., Gaude, E., Cojocari, D., Mahadevan, R., Frezza, C., Wouters, B.G., and McGuigan, A.P. (2016). A three-dimensional engineered tumour for spatial snapshot analysis of cell metabolism and phenotype in hypoxic gradients. Nature materials *15*, 227-234.

Rofstad, E.K., Gaustad, J.V., Egeland, T.A., Mathiesen, B., and Galappathi, K. (2010). Tumors exposed to acute cyclic hypoxic stress show enhanced angiogenesis, perfusion and metastatic dissemination. International journal of cancer *127*, 1535-1546.

Rogakou, E.P., Pilch, D.R., Orr, A.H., Ivanova, V.S., and Bonner, W.M. (1998). DNA double-stranded breaks induce histone H2AX phosphorylation on serine 139. J Biol Chem *273*, 5858-5868.

Rohwer, N., Zasada, C., Kempa, S., and Cramer, T. (2013). The growing complexity of HIF-1alpha's role in tumorigenesis: DNA repair and beyond. Oncogene *32*, 3569-3576.

Rothkamm, K., Kruger, I., Thompson, L.H., and Lobrich, M. (2003). Pathways of DNA double-strand break repair during the mammalian cell cycle. Mol Cell Biol *23*, 5706-5715.

Rowlands, J.C., and Gustafsson, J.A. (1997). Aryl hydrocarbon receptor-mediated signal transduction. Critical reviews in toxicology *27*, 109-134.

Ryan, H.E., Lo, J., and Johnson, R.S. (1998). HIF-1 alpha is required for solid tumor formation and embryonic vascularization. The EMBO journal *17*, 3005-3015.

Ryan, H.E., Poloni, M., McNulty, W., Elson, D., Gassmann, M., Arbeit, J.M., and Johnson, R.S. (2000). Hypoxia-inducible factor-1alpha is a positive factor in solid tumor growth. Cancer Res *60*, 4010-4015.

Schay, G., Borka, B., Kernya, L., Bulyaki, E., Kardos, J., Fekete, M., and Fidy, J. (2016). Without Binding ATP, Human Rad51 Does Not Form Helical Filaments on ssDNA. The journal of physical chemistry B *120*, 2165-2178.

Schofield, C.J., and Ratcliffe, P.J. (2004). Oxygen sensing by HIF hydroxylases. Nat Rev Mol Cell Biol *5*, 343-354.

Seagroves, T.N., Ryan, H.E., Lu, H., Wouters, B.G., Knapp, M., Thibault, P., Laderoute, K., and Johnson, R.S. (2001). Transcription factor HIF-1 is a necessary mediator of the pasteur effect in mammalian cells. Mol Cell Biol *21*, 3436-3444.

Seibler, J., Zevnik, B., Kuter-Luks, B., Andreas, S., Kern, H., Hennek, T., Rode, A., Heimann, C., Faust, N., Kauselmann, G., *et al.* (2003). Rapid generation of inducible mouse mutants. Nucleic Acids Res *31*, e12.

Semenza, G.L. (2003). Targeting HIF-1 for cancer therapy. Nature reviews Cancer *3*, 721-732.

Semenza, G.L. (2007a). Hypoxia-inducible factor 1 (HIF-1) pathway. Science's STKE : signal transduction knowledge environment *2007*, cm8.

Semenza, G.L. (2007b). Life with oxygen. Science *318*, 62-64.

Semenza, G.L., Jiang, B.H., Leung, S.W., Passantino, R., Concordet, J.P., Maire, P., and Giallongo, A. (1996). Hypoxia response elements in the aldolase A, enolase 1, and lactate dehydrogenase A gene promoters contain essential binding sites for hypoxia-inducible factor 1. J Biol Chem *271*, 32529-32537.

Semenza, G.L., Roth, P.H., Fang, H.M., and Wang, G.L. (1994). Transcriptional Regulation of Genes Encoding Glycolytic-Enzymes by Hypoxia-Inducible Factor-1. J Biol Chem *269*, 23757-23763.

Semenza, G.L., and Wang, G.L. (1992). A nuclear factor induced by hypoxia via de novo protein synthesis binds to the human erythropoietin gene enhancer at a site required for transcriptional activation. Molecular and Cellular Biology *12*, 5447-5454.

Shibata, A., Conrad, S., Birraux, J., Geuting, V., Barton, O., Ismail, A., Kakarougkas, A., Meek, K., Taucher-Scholz, G., Lobrich, M., *et al.* (2011). Factors determining DNA double-strand break repair pathway choice in G2 phase. The EMBO journal *30*, 1079-1092.

Shneor, D., Folberg, R., Pe'er, J., Honigman, A., and Frenkel, S. (2017). Stable knockdown of CREB, HIF-1 and HIF-2 by replication-competent retroviruses abrogates the responses to hypoxia in hepatocellular carcinoma. Cancer Gene Therapy *24*, 64-74.

Shweiki, D., Itin, A., Soffer, D., and Keshet, E. (1992). Vascular endothelial growth factor induced by hypoxia may mediate hypoxia-initiated angiogenesis. Nature *359*, 843-845.

Singleton, B.K., Torres-Arzayus, M.I., Rottinghaus, S.T., Taccioli, G.E., and Jeggo, P.A. (1999). The C terminus of Ku80 activates the DNA-dependent protein kinase catalytic subunit. Mol Cell Biol *19*, 3267-3277.

Song, A.J., and Palmiter, R.D. (2018). Detecting and Avoiding Problems When Using the Cre-lox System. Trends in genetics : TIG *34*, 333-340.

Soucek, L., Lawlor, E.R., Soto, D., Shchors, K., Swigart, L.B., and Evan, G.I. (2007). Mast cells are required for angiogenesis and macroscopic expansion of Myc-induced pancreatic islet tumors. Nature medicine *13*, 1211-1218.

Sowter, H.M., Ratcliffe, P.J., Watson, P., Greenberg, A.H., and Harris, A.L. (2001). HIF-1-dependent regulation of hypoxic induction of the cell death factors BNIP3 and NIX in human tumors. Cancer Res *61*, 6669-6673.

Sparmann, A., and Bar-Sagi, D. (2004). Ras-induced interleukin-8 expression plays a critical role in tumor growth and angiogenesis. Cancer cell *6*, 447-458.

Sprong, D., Janssen, H.L., Vens, C., and Begg, A.C. (2006). Resistance of hypoxic cells to ionizing radiation is influenced by homologous recombination status. International journal of radiation oncology, biology, physics *64*, 562-572.

Stebbins, C.E., Kaelin, W.G., Jr., and Pavletich, N.P. (1999). Structure of the VHL-ElonginC-ElonginB complex: implications for VHL tumor suppressor function. Science *284*, 455-461.

Stegeman, H., Span, P.N., Peeters, W.J.M., Verheijen, M.M.G., Grénman, R., Meijer, T.W.H., Kaanders, J.H.A.M., and Bussink, J. (2016). Interaction between hypoxia, AKT and HIF-1 signaling in HNSCC and NSCLC: implications for future treatment strategies. Future Science OA *2*, FSO84.

Stiff, T., O'Driscoll, M., Rief, N., Iwabuchi, K., Lobrich, M., and Jeggo, P.A. (2004). ATM and DNA-PK function redundantly to phosphorylate H2AX after exposure to ionizing radiation. Cancer Res *64*, 2390-2396.

Stiff, T., Walker, S.A., Cerosaletti, K., Goodarzi, A.A., Petermann, E., Concannon, P., O'Driscoll, M., and Jeggo, P.A. (2006). ATR-dependent phosphorylation and activation of ATM in response to UV treatment or replication fork stalling. The EMBO journal *25*, 5775-5782.

Sugrue, T., Lowndes, N.F., and Ceredig, R. (2014). Hypoxia enhances the radioresistance of mouse mesenchymal stromal cells. Stem cells (Dayton, Ohio) *32*, 2188-2200.

Sun, X.P., Dong, X., Lin, L., Jiang, X., Wei, Z., Zhai, B., Sun, B., Zhang, Q., Wang, X., Jiang, H., *et al.* (2014). Up-regulation of survivin by AKT and hypoxia-inducible factor 1alpha contributes to cisplatin resistance in gastric cancer. The FEBS journal *281*, 115-128.

Suzuki, H., Tomida, A., and Tsuruo, T. (2001). Dephosphorylated hypoxia-inducible factor 1alpha as a mediator of p53-dependent apoptosis during hypoxia. Oncogene *20*, 5779-5788.

Swann, J.B., and Smyth, M.J. (2007). Immune surveillance of tumors. Journal of Clinical Investigation *117*, 1137-1146.

Swanson, H.I., and Bradfield, C.A. (1993). The AH-receptor: genetics, structure and function. Pharmacogenetics *3*, 213-230.

Takasaki, C., Kobayashi, M., Ishibashi, H., Akashi, T., and Okubo, K. (2016). Expression of hypoxia-inducible factor-1alpha affects tumor proliferation and antiapoptosis in surgically resected lung cancer. Molecular and clinical oncology *5*, 295-300.

Talks, K.L., Turley, H., Gatter, K.C., Maxwell, P.H., Pugh, C.W., Ratcliffe, P.J., and Harris, A.L. (2000). The expression and distribution of the hypoxia-inducible factors HIF-1alpha and HIF-2alpha in normal human tissues, cancers, and tumor-associated macrophages. The American journal of pathology *157*, 411-421.

Tang, N., Wang, L., Esko, J., Giordano, F.J., Huang, Y., Gerber, H.P., Ferrara, N., and Johnson, R.S. (2004). Loss of HIF-1alpha in endothelial cells disrupts a hypoxia-driven VEGF autocrine loop necessary for tumorigenesis. Cancer cell *6*, 485-495.

Tanimoto, K., Makino, Y., Pereira, T., and Poellinger, L. (2000). Mechanism of regulation of the hypoxia-inducible factor-1 alpha by the von Hippel-Lindau tumor suppressor protein. The EMBO journal *19*, 4298-4309.

Tarhini, A.A., Lin, Y., Yeku, O., LaFramboise, W.A., Ashraf, M., Sander, C., Lee, S., and Kirkwood, J.M. (2014). A four-marker signature of TNF-RII, TGF-alpha, TIMP-1 and CRP is prognostic of worse survival in high-risk surgically resected melanoma. Journal of translational medicine *12*, 19.

Thiery, J.P., Acloque, H., Huang, R.Y., and Nieto, M.A. (2009). Epithelial-mesenchymal transitions in development and disease. Cell *139*, 871-890.

Thiry, A., Dogne, J.M., Masereel, B., and Supuran, C.T. (2006). Targeting tumor-associated carbonic anhydrase IX in cancer therapy. Trends in pharmacological sciences *27*, 566-573.

Tian, H., McKnight, S.L., and Russell, D.W. (1997). Endothelial PAS domain protein 1 (EPAS1), a transcription factor selectively expressed in endothelial cells. Genes Dev *11*, 72-82.

To, K.K., Sedelnikova, O.A., Samons, M., Bonner, W.M., and Huang, L.E. (2006). The phosphorylation status of PAS-B distinguishes HIF-1alpha from HIF-2alpha in NBS1 repression. The EMBO journal *25*, 4784-4794.

Um, J.H., Kang, C.D., Bae, J.H., Shin, G.G., Kim, D.W., Kim, D.W., Chung, B.S., and Kim, S.H. (2004). Association of DNA-dependent protein kinase with hypoxia inducible factor-1 and its implication in resistance to anticancer drugs in hypoxic tumor cells. Experimental & molecular medicine *36*, 233-242.

van der Groep, P., Bouter, A., Menko, F.H., van der Wall, E., and van Diest, P.J. (2008). High frequency of HIF-1alpha overexpression in BRCA1 related breast cancer. Breast cancer research and treatment *111*, 475-480.

Vande Velde, C., Cizeau, J., Dubik, D., Alimonti, J., Brown, T., Israels, S., Hakem, R., and Greenberg, A.H. (2000). BNIP3 and genetic control of necrosis-like cell death through the mitochondrial permeability transition pore. Mol Cell Biol *20*, 5454-5468.

Vander Heiden, M.G., Cantley, L.C., and Thompson, C.B. (2009). Understanding the Warburg effect: the metabolic requirements of cell proliferation. Science *324*, 1029-1033.

Varia, M.A., Calkins-Adams, D.P., Rinker, L.H., Kennedy, A.S., Novotny, D.B., Fowler, W.C., Jr., and Raleigh, J.A. (1998). Pimonidazole: a novel hypoxia marker for complementary study of tumor hypoxia and cell proliferation in cervical carcinoma. Gynecologic oncology *71*, 270-277.

Vaupel, P., Briest, S., and Hockel, M. (2002). Hypoxia in breast cancer: pathogenesis, characterization and biological/therapeutic implications. Wiener medizinische Wochenschrift (1946) *152*, 334-342.

Vaupel, P., Thews, O., and Hoeckel, M. (2001). Treatment resistance of solid tumors: role of hypoxia and anemia. Medical oncology (Northwood, London, England) *18*, 243-259.

Voss, M.J., Moller, M.F., Powe, D.G., Niggemann, B., Zanker, K.S., and Entschladen, F. (2011). Luminal and basal-like breast cancer cells show increased migration induced by hypoxia, mediated by an autocrine mechanism. BMC cancer *11*, 158.

Walker, J.R., Corpina, R.A., and Goldberg, J. (2001). Structure of the Ku heterodimer bound to DNA and its implications for double-strand break repair. Nature *412*, 607-614.

Wang, G.L., Jiang, B.H., Rue, E.A., and Semenza, G.L. (1995). Hypoxia-inducible factor 1 is a basic-helix-loop-helix-PAS heterodimer regulated by cellular O2 tension. Proceedings of the National Academy of Sciences *92*, 5510-5514.

Wang, G.L., and Semenza, G.L. (1993a). Characterization of hypoxia-inducible factor 1 and regulation of DNA binding activity by hypoxia. J Biol Chem *268*, 21513-21518.

Wang, G.L., and Semenza, G.L. (1993b). General involvement of hypoxia-inducible factor 1 in transcriptional response to hypoxia. Proceedings of the National Academy of Sciences of the United States of America *90*, 4304-4308.

Wang, G.L., and Semenza, G.L. (1995). Purification and characterization of hypoxia-inducible factor 1. J Biol Chem *270*, 1230-1237.

Wang, R., Dillon, C.P., Shi, L.Z., Milasta, S., Carter, R., Finkelstein, D., McCormick, L.L., Fitzgerald, P., Chi, H., Munger, J., *et al.* (2011). The transcription factor Myc controls metabolic reprogramming upon T lymphocyte activation. Immunity *35*, 871-882.

Wang, Y.G., Nnakwe, C., Lane, W.S., Modesti, M., and Frank, K.M. (2004). Phosphorylation and regulation of DNA ligase IV stability by DNA-dependent protein kinase. J Biol Chem *279*, 37282-37290.

Warburg, O. (1956). On the origin of cancer cells. Science *123*, 309-314.

West, S.C. (2003). Molecular views of recombination proteins and their control. Nat Rev Mol Cell Biol *4*, 435-445.

Wiesener, M.S., Jurgensen, J.S., Rosenberger, C., Scholze, C.K., Horstrup, J.H., Warnecke, C., Mandriota, S., Bechmann, I., Frei, U.A., Pugh, C.W., *et al.* (2003). Widespread hypoxia-inducible expression of HIF-2alpha in distinct cell populations of different organs. FASEB journal : official publication of the Federation of American Societies for Experimental Biology *17*, 271-273.

Williams, K.J., Telfer, B.A., Xenaki, D., Sheridan, M.R., Desbaillets, I., Peters, H.J., Honess, D., Harris, A.L., Dachs, G.U., van der Kogel, A., *et al.* (2005). Enhanced response to radiotherapy in tumours deficient in the function of hypoxia-inducible factor-1. Radiother Oncol *75*, 89-98.

Williams, R.S., Williams, J.S., and Tainer, J.A. (2007). Mre11-Rad50-Nbs1 is a keystone complex connecting DNA repair machinery, double-strand break signaling, and the chromatin template. Biochemistry and cell biology = Biochimie et biologie cellulaire *85*, 509-520.

Wirthner, R., Wrann, S., Balamurugan, K., Wenger, R.H., and Stiehl, D.P. (2008). Impaired DNA double-strand break repair contributes to chemoresistance in HIF-1 alpha-deficient mouse embryonic fibroblasts. Carcinogenesis *29*, 2306-2316.

Wold, M.S. (1997). Replication protein A: a heterotrimeric, single-stranded DNA-binding protein required for eukaryotic DNA metabolism. Annual review of biochemistry *66*, 61-92.

Xia, X., Lemieux, M.E., Li, W., Carroll, J.S., Brown, M., Liu, X.S., and Kung, A.L. (2009). Integrative analysis of HIF binding and transactivation reveals its role in maintaining histone methylation homeostasis. Proc Natl Acad Sci U S A *106*, 4260-4265.

Xia, Y., Jiang, L., and Zhong, T. (2018). The role of HIF-1α in chemo-/radioresistant tumors. OncoTargets and therapy *11*, 3003-3011.

Xu, D., Yao, Y., Lu, L., Costa, M., and Dai, W. (2010). Plk3 functions as an essential component of the hypoxia regulatory pathway by direct phosphorylation of HIF-1alpha. J Biol Chem *285*, 38944-38950.

Yamashita, S. (2007). Heat-induced antigen retrieval: Mechanisms and application to histochemistry. Progress in Histochemistry and Cytochemistry *41*, 141-200.

Yang, M.H., Wu, M.Z., Chiou, S.H., Chen, P.M., Chang, S.Y., Liu, C.J., Teng, S.C., and Wu, K.J. (2008). Direct regulation of TWIST by HIF-1alpha promotes metastasis. Nature cell biology *10*, 295-305.

Yano, K., Morotomi-Yano, K., Wang, S.Y., Uematsu, N., Lee, K.J., Asaithamby, A., Weterings, E., and Chen, D.J. (2008). Ku recruits XLF to DNA double-strand breaks. EMBO reports *9*, 91-96.

Yasinska, I.M., and Sumbayev, V.V. (2003). S-nitrosation of Cys-800 of HIF-1alpha protein activates its interaction with p300 and stimulates its transcriptional activity. FEBS Lett *549*, 105-109.

Yoo, Y.G., Christensen, J., and Huang, L.E. (2011). HIF-1alpha confers aggressive malignant traits on human tumor cells independent of its canonical transcriptional function. Cancer Res *71*, 1244-1252.

Yoshimura, M., Itasaka, S., Harada, H., and Hiraoka, M. (2013). Microenvironment and radiation therapy. BioMed research international *2013*, 685308.

Younes, M., Lechago, L.V., Somoano, J.R., Mosharaf, M., and Lechago, J. (1996). Wide expression of the human erythrocyte glucose transporter Glut1 in human cancers. Cancer Res *56*, 1164-1167.

Yu, X., and Chen, J. (2004). DNA damage-induced cell cycle checkpoint control requires CtIP, a phosphorylation-dependent binding partner of BRCA1 C-terminal domains. Mol Cell Biol *24*, 9478-9486.

Zeller, A., Crestani, F., Camenisch, I., Iwasato, T., Itohara, S., Fritschy, J.M., and Rudolph, U. (2008). Cortical Glutamatergic Neurons Mediate the Motor Sedative Action of Diazepam. Molecular Pharmacology *73*, 282-291.

Zelzer, E., Wappner, P., and Shilo, B.Z. (1997). The PAS domain confers target gene specificity of Drosophila bHLH/PAS proteins. Genes Dev *11*, 2079-2089.

Zhang, H., Bosch-Marce, M., Shimoda, L.A., Tan, Y.S., Baek, J.H., Wesley, J.B., Gonzalez, F.J., and Semenza, G.L. (2008). Mitochondrial autophagy is an HIF-1-dependent adaptive metabolic response to hypoxia. J Biol Chem *283*, 10892-10903.

Zhang, J., Cheng, Q., Zhou, Y., Wang, Y., and Chen, X. (2013a). Slug is a key mediator of hypoxia induced cadherin switch in HNSCC: correlations with poor prognosis. Oral oncology *49*, 1043-1050.

Zhang, J., Dublin, P., Griemsmann, S., Klein, A., Brehm, R., Bedner, P., Fleischmann, B.K., Steinhauser, C., and Theis, M. (2013b). Germ-line recombination activity of the widely used hGFAP-Cre and nestin-Cre transgenes. PLoS One *8*, e82818.

Zhao, Q., Tan, B.B., Li, Y., Fan, L.Q., Yang, P.G., and Tian, Y. (2016). Enhancement of Drug Sensitivity by Knockdown of HIF-1alpha in Gastric Carcinoma Cells. Oncology research *23*, 129-136.

Zhou, C.-H., Zhang, X.-P., Liu, F., and Wang, W. (2015). Modeling the interplay between the HIF-1 and p53 pathways in hypoxia. Scientific Reports *5*, 13834.

Zhu, G.H., Huang, C., Feng, Z.Z., Lv, X.H., and Qiu, Z.J. (2013). Hypoxia-induced snail expression through transcriptional regulation by HIF-1alpha in pancreatic cancer cells. Digestive diseases and sciences *58*, 3503-3515.

9 Appendix

9.1 Abbreviations

53BP1	p53 binding protein 1
ACK	ammonium-chloride-potassium
ADRP	adipophilin
Akt	protein kinase-B
ALDOA	aldolase A
alt-NHEJ	alternative-NHEJ
ANGPT2	angiopoietin 2
ANOVA	analysis of variance
APS	ammonium persulfate
ARD1	arrest-defective-1
ARG1	arginase 1
ARNT	aryl hydrocarbon receptor nuclear translocator
ATM	ataxia telangiectasia mutated kinase
ATP	adenosine 5´-triphosphate
ATR	ataxia telangiectasia and Rad3-related kinase
B2M	ß2-microglobuline
BAX	B-cell lymphoma 2 (Bcl-2)-associated X protein
BCA	bicinchoninic acid
Bcl-2	B-cell lymphoma 2
BER	base excision repair
bHLH	basic-helix-loop-helix
BMDM	bone-marrow derived macrophages
BNIP3	Bcl2/adenovirus E1B 19-kDa interacting protein 3
BRCA1	breast cancer protein 1
BSA	bovine serum albumin
CAFs	cancer associated fibroblasts
CAIX	carbon anhydrase isoform IX
CBP	cAMP response element-binding (CREB)-binding protein
CDK	cyclin-dependent kinase
cDNA	complementary DNA
CHAPS	3-[(3-Cholamidopropyl)dimethylammonio]-1-propane-sulfonate
COX-2	cyclooxygenase 2
COX4-1	cytochrome c oxidase subunit 4-1
Cre(-)	HIF-1$\alpha^{fl/fl}$Cre-ER$^{wt/wt}$
Cre(ki)	HIF-1$\alpha^{fl/fl}$Cre-ER$^{ki/wt}$
CSC	cancer stem cells
CTAD	C-terminal transactivation domain
CtIP	C-terminal binding protein-interacting protein
DAB	diaminobenzidine
DCs	dendritic cells

DDR	DNA damage repair
DEPC	diethyl pyrocarbonate
DEQ	dose equivalent
DEVD-AMC	Asp-Glu-Val-Asp-7-amino-4-methylcoumarin
DMEM	Dulbecco´s modified eagle medium
DMSO	dimethylsulfoxide
DNA-PK	DNA-dependent protein kinase
Dox	doxycycline
DSB	double-strand break
DTT	dithiothreitol
E2	exon 2
EC	endothelial cell
EDTA	ethylenediaminetetraacetic acid
EMT	epithelial-mesenchymal transition
ENO1	enolase 1
EPAS1	endothelial PAS protein 1
Epo	erythropoietin
ESR1	estrogen receptor
FABP	fatty acid binding protein
FACS	fluorescence-activated cell sorting
FBS	fetal bovine serum
FIH-1	factor inhibiting HIF-1
gDNA	genomic DNA
GFP	green fluorescent protein
GLUT	glucose transporter
GPI	glucose phosphate isomerase
HCT	human colorectal carcinoma
HEK	human embryonic kidney
HEPES	4-(2-hydroxyethyl)-1-piperazineethanesulfonic acid
HIF-1	hypoxia-inducible factor 1
HK2	hexokinase 2
HR	homologous recombination
HRE	hypoxia-responsive element
HRP	horseradisch peroxidase
Hx	hypoxia
ID	inhibitory domain
IF	immunofluorescence staining
IGF-2	insulin growth factor-2
IgG	immunoglobulin G
IHC	immunohistochemistry
IL-6	interleukin 6
iNOS	inducible nitric oxide synthase
IPAS	inhibitory PER-ARNT-SIM domain
IR	ionizing radiation

IRIF	irradiation-induced foci
KD	knockdown
ki	knock-in
KO	knockout
LDH-A	lactate dehydrogenase-A
LIG4	DNA Ligase 4
LLC	Lewis lung carcnoma
MAPK	mitogen-activated protein kinase
MDC1	mediator of DNA damage checkpoint
MDM2	mouse double minute 2 homolog
MDSCs	myeloid-derived suppressor cells
MMP-9	matrix metalloprotease 9
MMR	mismatch repair
MOPS	3-(N-morpholine)propanesulfonic acid
MRN	Mre11-Rad50-NBS1 complex
mRNA	messenger RNA
MW	molecular weight
N	asparagine
NADH	reduced form of nicotinamide adenine dinucleotide
NADPH	reduced nicotinamide adenine dinucleotide phosphate
NBS1	Nijmegen breakage syndrome protein 1
NER	nucleotide excision repair
NF-κB	nuclear factor kappa B
NHEJ	non-homologous end joining
NO	nitric oxide
NTAD	N-terminal transactivation domain
Oct4	octamer-binding transcription factor 4
ODD	oxygen-dependent degradation domain
P	proline
p300	300-kilodalton coactivator protein
PARP-1	poly [ADP-ribose] polymerase 1
PAS	PER-ARNT-SIM
PBS	phosphate-buffered saline
PCR	Polymerase chain reaction
PDGFB	platelet-derived growth factor B
PDH	pyruvate dehydrogenase
PDK1	pyruvate dehydrogenase kinase isozyme 1
PE	phycoerythrin
PER	*D. melanogaster* period clock protein
PFA	paraformaldehyde
PFGE	pulsed-field gel electrophoresis
PFKFB4	6-phosphofructo-2-kinase/fructose-2,6-bisphosphatase 4
PGAM1	phosphoglycerate mutase 1
PGF	placental growth factor

PGK1	phosphoglycerate kinase 1
PHD	prolyl hydroxylase domain protein
PI	propidium iodide
PI3K	phosphatidylinositol 3-kinase
PKM2	pyruvate kinase isozyme M2
Plk3	polo-like kinase 3
pO_2	oxygen tension
PTEN	phosphatase and tensin homolog
PVDF	polyvinylidene fluoride
pVHL	von Hippel-Lindau protein
qPCR	quantitative polymerase chain reaction
RIPA	radioimmunoprecipitation assay buffer
ROS	reactive oxygen species
RPA	replication protein A
RTA	ready-to-assemble
S	serine
SCF	stem cell factor
SD	standard deviation
SDF1	stromal derived factor 1
SDS	sodium dodecyl sulfate
SENP1	SUMO-specific protease 1
shHIF-1α	shRNA that targeted HIF-1α
shRNA	short hairpin RNA
shscr	shscrambled RNA
SIM	*D. melanogaster* single-minded locus
SSA	single-strand annealing
SSB	single-strand break
SSBR	single-strand break repair
ssDNA	single-stranded DNA
SUMO-1	small ubiquitin-related modifier-1
Tam	tamoxifen
TAMs	tumor-associated macrophages
TBS	Tris-buffered saline
TCA	tricarboxylic acid
TEMED	tetramethylethylenediamine
Tet-On	tetracycline-inducible
TGF-α	transforming growth factor alpha
TILs	tumor infiltrating lymphoid cells
TME	tumor microenvironment
T_{reg}	regulatory T cell
TSP	thrombospondin
VEGF	vascular endothelial growth factor
WB	Western blot
wt	wild-type

x *g*	times gravity
XRCC4	X-ray cross complementing 4
ZEB1	zinc finger E-box binding homeobox 1
γH2AX	phosphorylated histone protein H2AX

9.2 List of Figures

9.3 List of Tables

9.4 Acknowledgements

Die Durchführung dieser Arbeit wäre nicht möglich gewesen ohne Unterstützung vieler Personen, bei denen ich mich aufs Herzlichste bedanken möchte.

Ein großer Dank gilt meinem Betreuer Prof. Dr. Eric Metzen für seine fachliche Kompetenz und Unterstützung bei allen entstandenen Problemen. Zusätzlich danke ich den Gutachtern dieser Arbeit für die wissenschaftliche Auseinandersetzung mit diesem Projekt. Außerdem möchte ich mich bei Prof. Dr. Joachim Fandrey bedanken, dass er es mir ermöglicht hat, die Arbeit am Institut für Physiologie anzufertigen. Bei den Organisatoren des Graduiertenkollegs GRK1739 möchte ich mich für das strukturierte Programm und Ermöglichung eines wissenschaftlichen Austausches bedanken. Zusätzlich bedanke ich mich bei Prof. Dr. George Iliakis und besonders bei Anna Broich für die Zusammenarbeit und Unterstützung bei der Durchführung der PFGE. Bei allen GRK Doktoranden möchte ich mich für gute Tipps, aufbauende Worte und die schöne Zeit bedanken. Meinem GRK Mentor Prof. Dr. Alexander Schramm danke ich für seine kritische Auseinandersetzung mit meinem Thema.

Bei meinen Arbeitskollegen aus dem Institut für Physiologie, insbesondere bei allen ehemaligen und derzeitigen Kollegen aus der Arbeitsgruppe Metzen, bedanke ich mich für die tolle Zeit, die Freundlichkeit und Hilfsbereitschaft. Dr. Helena Riffkin und Dr. Ulf Brockmeier danke ich für die hilfreiche wissenschaftliche Beratung, stetige Unterstützung und tolle Gesprächsthemen. Bei Frau Melanie Baumann, Kirsten Göpelt und Jennifer Baumann bedanke ich mich für die exzellente technische Assistenz, wertvolle Tipps und fröhliche Stimmung im Labor. Zusätzlich will ich mich besonders bei allen fertigen und noch angehenden medizinischen Doktoranden für all die spaßigen Momente, humorvollen Umgang mit allen Niederlagen und gute Laune im Labor bedanken.

Darüber hinaus möchte ich mich bei meinen Freunden für aufbauende Worte und Momente der Entspannung bedanken. Ein besonderer Dank gilt meinen Eltern, die immer hinter mir standen. Zusätzlich gilt mein großer Dank meinen Großeltern, die immer bedingungslos an mich geglaubt haben. Meiner kleinen Schwester Leoni bin ich sehr dankbar dafür, dass sie Verständnis gezeigt hat, obwohl ich sie so selten besuchen konnte. Sie ist der Sonnenschein, der immer Freude und ein Lächeln in mir weckte. Zuletzt danke ich meinem Freund Jan Claudius für seine Geduld und Verständnis, seine fachliche und emotionale Unterstützung und seine besondere Fähigkeit, mich immer zum Lachen zu bringen.

9.5 Publication list

Kranz, P., Neumann, F., **Wolf, A.**, Classen, F., Pompsch, M., Ocklenburg, T., Baumann, J., Janke, K., Baumann, M., Goepelt, K., Riffkin, H., Metzen, E., Brockmeier, U. (2017). PDI is an essential redox-sensitive activator of PERK during the unfolded protein response (UPR). Cell death & disease 8, e2986.

Classen, F., Kranz, P., Riffkin, H., Pompsch, M., **Wolf, A.**, Göpelt, K., Baumann, M., Baumann, J., Brockmeier, U., Metzen, E. (2018). Autophagy induced by ionizing radiation promotes cell death over survival in human colorectal cancer cells. Exp. Cell Res

Wolf, A., Kranz, P., Riffkin, H., Mersch, E., Baumann, J., Baumann, M., Göpelt, K., Broich, A., Iliakis, G., Brockmeier, U., Metzen, E. (in preparation). HIF-1α knockdown increases radiation sensitivity and DNA damage of LLC cells.

Bernardini, A., **Wolf, A.**, Brockmeier, U., Riffkin, H., Metzen, E., Acker-Palmer, A., Acker, H., Fandrey, J. (in preparation). Flavoprotein and Pin1 mediated oxygen sensing pathways: redox ratio microscopy of Type I cells within the mouse carotid body ex vivo.

9.6 Curriculum vitae

Der Lebenslauf ist in der Online-Version aus Gründen des Datenschutzes nicht enthalten.

9.7 Declarations

Erklärung:

Hiermit erkläre ich, gem. § 7 Abs. (2) d) +f) der Promotionsordnung der Fakultät für Biologie zur Erlangung des Dr. rer. nat., dass ich die vorliegende Dissertation selbstständig verfasst und mich keiner anderen als der angegebenen Hilfsmittel bedient, bei der Abfassung der Dissertation nur die angegebenen Hilfsmittel benutzt und alle wörtlich oder inhaltlich übernommenen Stellen als solche gekennzeichnet habe.

Essen, den _____ _____

Alexandra Wolf

Erklärung:

Hiermit erkläre ich, gem. § 7 Abs. (2) e) +g) der Promotionsordnung der Fakultät für Biologie zur Erlangung des Dr. rer. nat., dass ich keine anderen Promotionen bzw. Promotionsversuche in der Vergangenheit durchgeführt habe und dass diese Arbeit von keiner anderen Fakultät/Fachbereich abgelehnt worden ist.

Essen, den _____ _____

Alexandra Wolf

Erklärung:

Hiermit erkläre ich, gem. § 6 Abs. (2) g) der Promotionsordnung der Fakultät für Biologie zur Erlangung des Dr. rer. nat., dass ich das Arbeitsgebiet, dem das Thema „*Effect of HIF-1α deficiency in tumor cells and murine tumor stroma on radiation sensitivity and growth of tumors*“ zuzuordnen ist, in Forschung und Lehre vertrete und den Antrag von Alexandra Wolf befürworte und die Betreuung auch im Falle eines Weggangs, wenn nicht wichtige Gründe dem entgegenstehen, weiterführen werde.

_____

Name des Mitglieds der Universität Duisburg-Essen in Druckbuchstaben

Essen, den _____ _____

Prof. Dr. Eric Metzen